Development of Finite Volume Solver for Dilute Gas-Droplet Flows with Evaporation

By
Mrunalini B
Roll No. ME10M04
M.Tech II Yr.-Thermofluids

A Thesis Submitted
in Partial Fulfillment of the Requirements
for the Degree of
Master of Technology

Department Of Mechanical Engineering
Indian Institute Of Technology Hyderabad

JULY 2012

Declaration

I declare that this written submission represents my ideas in my own words, and where ideas and words of others have been included, I have adequately cited and referenced the original sources. I also declare that I have adhered to all principles of academic honesty and integrity and have not misinterpreted or fabricated or falsified any idea/data/fact/source in my submission. I understand that any violation of the above will be a cause for disciplinary action by the Institute and can also evoke penal action from the sources that have thus not been properly cited, or from whom proper permission has not been taken when needed.

(Signature)

MRUNALINI.B

(Student Name)

ME10M04

(Roll No.)

Approval Sheet

This thesis entitled "Development of Finite Volume Solver for Dilute Gas Droplet flows with Evaporation" by Mrunalini B is approved for the degree of Master of Technology from IIT Hyderabad.

(Dr. Raja Banerjee) Examiner
Dept. of Mechanical Engg.
IITH

(Dr. K. Venkatasubbaiah) Examiner
Dept. of Mechanical Engg.
IITH

(Prof. Vinayak Eswaran) Adviser
Dept. of Mechanical Engg.
IITH

(Prof. Kolluru V.L. Subramaniam) Chairman
Dept. of Civil Engg.
IITH

Acknowledgements

I express my sincere gratitude to my thesis adviser Prof. Vinayak Eswaran for his valuable guidance, timely suggestions and constant encouragement. His interest and confidence in me has helped immensely for the successful completion of this work. I am thankful to Narendra Gajbiye for guiding me through the basics of Anupravaha solver and constantly helping and clearing my doubts. I am also grateful to Praveen Throvagunta for helping me with the code. I would also like to thank Sumer Dirbude for his friendly support and encouragement.

I would also like to express my sincere gratitude to Dr. Raja Banerjee, Assistant Professor, Dept. of Mechanical Engineering, IIT Hyderabad for lending me books which enabled me to gain more understanding. A special note of thanks to my classmates Amit, Prakash, Ravi and Raja Jai Singh for inspiring me by doing their best always. I would also like to thank Jancy, Revathy, Sravanti, Tanima, Yogita and all my friends in IIT Hyderbad for making my stay at IIT Hyderabad, memorable and enjoyable.

I would like to make a special mention of the excellent computational facilities provided by Professor Eswaran. I would also like to thank the staff and fellow students in CAE lab for creating a conducive environment to work in.

Finally, I would like to thank my family for their constant support and encouragement. Their faith in me has enabled me to do my best.

Mrunalini B

To my family ...

Abstract

An algorithm is implemented for dilute gas-droplet flows with evaporation in a general purpose CFD solver, *IITK-DAE ANUPRAVAHA SOLVER*. Modules for Gas-Particle flows and Gas-Droplet flows with evaporation were implemented by Adhiraj Dasgupts [2] and Shashwat Swami Jaiswal [33]. But these modules had shortcomings as they were not able to give a converged solution for particles/diameters of smaller size. These issues are addressed in this thesis and a new algorithm and with modified governing equations are developed to solve the issues.

The finite volume method with non-staggered grid arrangement has been used along with a fully implicit and semi-coupled algorithm to numerically solve the set of governing equations. A two-way coupling has been incorporated between the two phases by including source terms in the governing equations. A classical model for droplet evaporation has been implemented in the solver and extensively verified against the available literature for low evaporation rate conditions. The solver has been successfully verified against the results of gas-particle flow and gas-droplet channel flow with evaporation against the results of the commercial software ANSYS Fluent. The numerical problems associated with the earlier modules have been largely overcome, with particles as small as a few microns being simulated by the present algorithm.

Contents

List of Figures

List of Tables

Nomenclature

u_g, v_g, w_g	Gas-phase velocity components (m/s)
u_d, v_d, w_d	Droplet-phase velocity components (m/s)
P	Pressure (N/m^2)
ρ_g	Density of gas-phase (kg/m^3)
μ	Molecular viscosity of gas-phase$(kg/m \cdot s)$
ν	Kinematic viscosity of gas-phase (m^2/s)
ρ_d	Material Density of droplet-phase (kg/m^3)
ϑ_d	Volume fraction of droplet-phase
Θ_d	Normalized volume fraction of droplet-phase
C_d	Drag coefficient
τ	Shear stress (N/m^2)
τ_w	Wall shear stress(N/m^2)
ΔV_p	Volume of the cell with centroid P
$\mathbf{S}$	Surface area vector
F_{gf}	Volume flux gas-phase at face f
F_{df}	Volume flux droplet-phase at face f
F_{Mgf}	Momentum flux gas-phase at face f
F_{Mdf}	Momentum flux droplet-phase at face f
$F_{d\phi f}$	Diffusion flux of variable ϕ
Re	Flow Reynolds number
Re_d	Droplet Reynolds number
d_d	Particle diameter
$\mathbf{f_d}$	Drag force per unit volume (N/m^3)
β	Exchange coefficient for interphase drag
n	Number density of droplet-phase $(1/m^3)$
$\dot{m}_v$	Evaporation rate for a single droplet (kg/s)
g_x, g_y, g_z	Components of acceleration due to gravity (m/s^2)
C_{pc}	Specific heat at constant pressure of pure gas $(J/kg\,K)$
C_{pg}	Specific heat at constant pressure of gas-phase $(J/kg\,K)$
C_{vd}	Specific heat at constant pressure of evaporated fuel vapour $(J/kg\,K)$
C_{ld}	Specific heat for liquid droplet $(J/kg\,K)$
L	Latent heat of vaporization of liquid drop (J/kg)
k_g	Thermal conductivity of gas-phase $(W/m\,K)$
k_c	Thermal conductivity of pure gas $(W/m\,K)$
k_v	Thermal conductivity of evaporated fuel vapour$(W/m\,K)$
T_g	Gas-phase temperature (K)

T_d	Droplet-phase temperature (K)
T_s	Droplet surface temperature (K)
α	Thermal diffusivity for gas-phase$\left(\equiv \frac{k}{\rho C_p}\right)$ (m^2/s)
D	Diffusion coefficient of fuel vapour in gas (m^2/s)
λ_{st}	Steady-state evaporation rate (mm^2/s)
R	Universal gas constant $(J/kmol\,K)$
Y_F	Fuel mass fraction
Y_{F_S}	Fuel mass fraction at the droplet surface
Y_{F_∞}	Fuel mass fraction at free stream
B_M	Spalding mass transfer number
B_T	Spalding heat transfer number
M_A	Molecular weight of gas $(kg/kmole)$
M_F	Molecular weight of fuel $(kg/kmole)$
h	Heat transfer coefficient $(W/m^2\,K)$
Q	Heat transfer from gas to a single drop (J/s)
Q_e	Heat used in vaporization of fuel (J/s)
Nu	Nusselt number
Pr	Prandtl number $\left(\equiv \frac{\nu}{\alpha}\right)$
Sc	Schmidt number $\left(\equiv \frac{\nu}{D}\right)$
Le	Lewis number$\left(\equiv \frac{\alpha}{D}\right)$

Chapter 1

Introduction

Many natural processes like formation and motion of rain drops, sand dunes formation etc., and industrial processes like flows in boilers and evaporators, heat exchangers, internal combustion engines etc., involve the interaction between matter existing in different states. The interaction between the various phases or states of matter may be in terms of mass and/or momentum and/or energy transfer. Such flows are termed as Multi-phase flows. Multi-phase flows can be quite complex and may involve various phases interacting simultaneously.

The simplest of all multi-phase flows are *two-phase* flows. In this work, mathematical modeling of two-phase flows involving gas and evaporating liquid droplets is attempted considering certain assumptions. The development of accurate mathematical models of two-phase flows is important for optimum design and control of various industrial systems. Mathematical modeling of two-phase flows poses several challenges as the problem involves rapidly changing and/or moving interfaces and continuous interaction between the phases which affect the behavior of each of the interacting phases. In this work, we numerically solve dilute dispersed two-phase flows using the three fundamental principles that govern any fluid flow: (i) mass conservation, (ii) momentum conservation and (iii) energy conservation. A brief introduction to two-phase flows is given below.

Two phase flows, in general, can be characterized both by the combination of interacting phases and also by the interface structures. Classification based on the state of the constituents of the flow is as follows:

1. Gas-Solid flows (Particle laden flows, fluidized beds)

2. Gas-Liquid flows (Bubbly flows, slug flows, gas-droplet flows)

3. Liquid-Solid flows (Slurry flows, sediment transport)

4. Immiscible-liquid flows

The second classification, based on the geometry of the interface between the interacting phases is as follows:

1. Separated flow/Free surface flows in which the two phases are separated by a distinct interface.

2. Dispersed flows in which both the phases are thoroughly mixed with each other.

3. Transitional/Mixed flow where the transition from separated to dispersed flows occurs.

Dispersed flows are further divided into three regimes by considering the phase of dispersion as follows:

1. Bubbly flows

2. Droplet or mist flows

3. Particle flows

This thesis involves numerical modeling of *dilute dispersed gas-droplet* flows involving gas and evaporating liquid droplets. *Dilute gas-particle* flows are considered as a special case of gas-droplet flows without evaporation. Droplets/Particles are called as the *disperse* phase and the fluid in which the droplets move is called as *continuous* phase.

In this work, dilute droplet flows with and without evaporation in a gas phase is being mathematically modelled as a part of IITK-DAE Anupravaha Solver. Tracking of interface between the various phases is a major component of separated flow algorithms, which usually is not attempted for disperse phase flows. For dispersed flows, the mixture is characterized by *volume-fraction*, without making reference to the shape of the actual interfaces between the phases. This procedure is described elaborately in Section 1.4.3. A brief introduction about IITK-DAE Anupravaha solver is given in the following Section 1.1 first.

1.1 IITK-DAE Anupravaha Solver

IITK-DAE Anupravaha Solver is a multi-block finite volume based solver capable of solving Navier-Stokes, energy and other scalar equations for solving flow and heat transfer problems of engineering applications. It uses non-orthogonal hexahedral structured grids and is coded using 'C' programming language. Anupravaha solver can be used on 2D, 2D Axis-symmetric and 3D structured grids. This solver is written using CGNS(CFD General Notation System) format and hence reads grids in CGNS format, solves the required equations and generates results in CGNS files which can be read and displayed by any post-processing software. The solver uses dynamic memory allocation and user choices for grid, equations, variables, boundary conditions, type of algorithm, type of time-stepping schemes, type of convective schemes etc., are made directly using the compiled code. There is also a provision for incorporating user-defined functions for various physical properties. A variable density approach has been completely integrated in the solver. The following modules are available in the solver

1. Conjugate Heat Transfer module
2. Various Turbulence models
3. Solidification and Melting module
4. Combustion module
5. Two-Phase module
6. Flow field coupled with Electric Field
7. Liquid Metal Magneto-Hydro Dynamics
8. Radiation

1.2 Gas Droplet Flows with Evaporation

Gas droplet flows are encountered in many engineering applications like IC engines, gas turbine systems, heat exchangers etc.. Gas-droplet flows may be dilute or dense. In dense gas droplet flow, the interaction between the droplets is of prime importance. Therefore, phenomena such as droplet-collision, droplet break-up, the effect of adjacent drop on transport rate etc., have to be modeled in dense gas-droplet flows. This involves

a three-way coupling for modeling the effect of droplets on gas, the effect of gas on droplets and the effect of neighboring droplets on each other. On the other hand, dilute gas-droplet flow does not require the consideration of droplet-droplet interaction. In such a case, depending on the droplet concentration, a one-way or two-way coupling would suffice.

A one-way coupling indicates that the droplets are affected by the fluid flow, but not vice-versa; in two-way coupling the two phases influence each other. It follows therefore that for very low particle concentrations a one-way coupling is sometimes enough to model the interactions, whereas for somewhat denser flows a two-way coupling must be considered. The governing equations for a two-phase flows are considerably more complex than for single phase flows due to this reason. In this work, a two-way coupling is employed to take into account the mass, momentum and energy transfer between the droplet and the surrounding gas.

1.3 Literature survey

The problem of two-phase flows involving particles or droplets in a gas stream has garnered a lot of attention from researchers owing to their practical applications. Considerable amount of work has been done in this subject from the early 1950s. The fundamental concepts of two-phase flows, its classification and solution strategies are discussed in detail in the book by Ishii-Hibiki [22]. In the early years of research, motion of particles/droplets in a gas stream and the evaporation characteristics have been addressed independently. Numerical approaches for solving the motion of particles using Eulerian-Lagrangian model have been extensively discussed by Loth [15]. An extensive review on the various modelling approaches for droplet vaporization is given by Sazhin et al. [32].

Gas-droplet flows with evaporation involve simultaneous heat and mass transfer. The physics of the mass and heat transfer involved in gas-droplet flows is explained in detail in the book by Koichi Asano [3]. The governing equations used for both the phases in two-continua formulation is given in book by Sirignano [34]. Previous research on two-fluid modeling is reported by Crowe et al. [5], Darwish [7] and Guo et al. [18]. The parameters used in the study such as volume fraction, number density are described in detail, with various averaging procedures, in Crowe et al. [5]. The evaporation model

used in this work is based on the Spalding model analyzed extensively by Chin and Lefebvre. [4]

The simplest model for droplet evaporation was first suggested by Maxwell in 1877 [16]. According to this model, the rate of evaporation is controlled exclusively by the diffusion process. His model ignores the effect of the convective flow of the mixture of gas and fuel vapor away from the surface of the droplet. The classical d^2-law of evaporation is formulated by Godsave [17] and Spalding [35] for a single isolated droplet evaporating in a quiescent environment. To take into account the effect of the convective flow of the surrounding gas, which enhances the heat and mass transfer between the droplet and the gas phase, many researchers have given correction factors for the basic models. In a comprehensive theoretical and experimental study, Frossling [14] first showed that effects of convection on heat and mass transfer rates could be accommodated by a correction factor that is a function of the Reynolds number and the Schmidt (or Prandtl) number. This correlation was later modified by Ranz and Marshall [29]. Later, Faeth [11] analyzed the available data on convective effects and proposed a synthesized correlation. The present study uses the correlation given by Ranz and Marshall [29].

The evaporation model used in the present study is essentially the classical model of Spalding [35]. The model used is described in the book by Lefebvre [23]. In the present study, the 'rapid mixing model' for the liquid droplet described in Faeth [11] is used. This simplifies the analysis by assuming infinite conductivity of the liquid. However, this may lead to small error in the solution. For the liquid droplet phase analysis, Abramzon et al.[1] used effective conductivity model. Expressions for the variation of properties of gases and liquids used in this study are taken from Perry [27] and Reid [30]. Hubbard et al. [19] studied the effect of transient and variable properties on drop evaporation rate, and showed that the '1/3' rule worked well as a mixing rule used. In the present evaporation model this rule is used for the calculation of the properties at droplet surface based on average temperature and composition.

In the literature, there are many experimental studies dealing with droplet evaporation. However, there are only few studies that come to the basic and ideal case of a single droplet evaporation in a quiescent or convective environment. A large number of studies consider multi-component droplets in turbulent evaporating sprays, jets with different classes of droplets where each class refers to a group of droplets of same

diameters having their own volume fraction, mass flow rates. Therefore we compare our results with experimental results of Downing [8], Ranz and Marshall [29] and the numerical results of Chin and Lefebvre [4], Kolaitis [20] and Miller et al. [24]. For the study of laminar gas-droplet flows in one of the cases we have assumed the initial droplet temperature is the saturation temperature, to simplify the analysis as discussed in Mongia et al.[25] and Elghobashi et al.[10].

1.4 Solution Methods

Models for two-phase flows can be categorized into two different groups. In the first group, there are models that track the interface between the two phases. These are ideal for separated flows. In the second group, there are models where the exact position of the interface is not followed specifically. Dispersed flows are usually modeled using models from this second group. The number of interfaces between the two phases in dispersed flow is too high for interface tracking methods to be suitable, at least with today's computing capacity. To model this type of flows, another strategy is employed in which the dispersed phase is assumed to be composed of spherical particles/droplets/bubbles. This assumption negates the need for interface tracking. Based on this strategy, there are two approaches commonly used for modeling gas-disperse phase flows: Eulerian-Eulerian approach and the Eulerian-Lagrangian approach.

1.4.1 The Eulerian-Lagrangian Approach

The general idea in this approach is to follow each particle/droplet/bubble of the flow as they advect in the continuous phase. The carrier phase is treated as a continuum and is calculated in an Eulerian reference frame, while particles/droplets/bubbles of the disperse phase are tracked using a Lagrangian approach. In this approach, the inter-phase transfer terms are calculated for the disperse phase while tracking the particles/droplets/bubbles using Lagrangian framework and these are then used in the Eulerian form of the equations of the continuous phase. This kind of iterative solution of carrier and disperse phases inevitably requires strong relaxation of inter-phase source terms for improving the convergence behaviour. Hence, Eulerian-Lagrangian approach works well for few particles/droplets/bubbles but becomes computationally expensive for modeling a large number of particles/droplets/bubbles unless each tracked entity is assumed to be a proxy for many actual particles/droplets/bubbles. Eulerian-Lagrangian approach for simulating evaporating gas-droplet flows has been extensively

applied by Salman et al. [31].

1.4.2 The Eulerian-Eulerian Approach

Another approach to model dispersed flows is to treat both the phases as a continuum. This is generally referred to as Eulerian-Eulerian approach or two-fluid model, first discussed by Ishii [22]. In this case local instantaneous equation of mass, momentum and energy balance for both the phases are derived along with source terms for interaction between the phases. A very important concept in the Eulerian-Eulerian approach is that of *volume-fraction* or volume concentration which is defined in the Section 1.4.3.

The following modeling approaches are used within the purview of the Eulerian-Eulerian method based on the interaction between the two phases:

1. **Homogeneous Equilibrium Model:** In this model, flow is analyzed by treating it as an idealized 'mixture' fluid whose properties are determined based on the properties of its constituents and their proportions.

2. **Drift Flux Model:** Drift flux model is similar to the homogeneous equilibrium model but it takes into account for the 'slip' i.e., the differential motion between the phases, and so additional terms appear in the equations. The drift flux model and the homogeneous models are sometimes referred to as mixture models. They are simpler than the two-fluid model described below.

3. **Two Fluid Model:** In the two fluid model both the phases have their own velocity and temperature field equations and separate properties. The interaction between the two phases is taken care of by including exchange coefficients. This is the method adopted in this work[1]. Details are given in section 1.4.3. One drawback of this approach is implementation of exchange coefficients.

1.4.3 Two Fluid Model

In the present work, an Eulerian-Eulerian two-fluid model is used to simulate two-phase flows. The phases are treated as inter-penetrating continua and mass, momentum and energy equations are solved to obtain the velocity and temperature fields separately for the phases. Each dependent variable at any specific point is an instantaneous

[1]It must be noted that the detailed flow field *within* droplets are not obtained using this method. Rather, the average momentum of droplets are computed.

average value over a neighbourhood of that point that includes both phases. Therefore, properties of both carrier phase and disperse phase exist at a point, regardless of whether that point is actually in the carrier phase or in the disperse phase at that instant.

Hereafter, we will refer to the carrier phase as gas and disperse phase as liquid, although the formulation is general and will work for liquid (carrier phase)-solid (disperse phase) flows as well. This method is a two-continua approach since both a continuum of gas properties and a continuum of liquid properties are defined. Details of the governing equations are given in section 2.2.

We define the volume fraction of any phase *'p'* as the ratio of the volume occupied by that phase to the total volume in a small region around the point under consideration. Mathematically, we can write

$$\vartheta_p = \lim_{\Delta V \to 0} \frac{\Delta V_p}{\Delta V}$$

Here ϑ_p denotes the volume fraction of phase *'p'*, and ΔV_p is the volume occupied by that phase in the neighbourhood of the point of interest, whereas ΔV is the total volume occupied by the two phases in the neighborhood of the point. Defined in this way, ϑ becomes a function, with a value at each point. In the Eulerian-Eulerian framework ϑ is assumed to be a continuous variable and often transport equations are solved for it.

According to the conservation principle, the summation of the volume fractions must be unity, $\vartheta_g + \vartheta_d = 1$ where, ϑ_g is the volume fraction of the gas phase and ϑ_d is the volume fraction of the droplet phase. Another important parameter, number density is defined as the number of particles/droplets per unit volume, we can write

$$n = \lim_{\Delta V \to 0} \frac{\Delta N}{\Delta V}$$

also

$$n = \frac{6\vartheta_d}{\pi {d_d}^3} \tag{1.1}$$

where n denotes the number density of the disperse phase, and ΔN is the number of particles/droplets in unit volume and d_d is diameter of the particles/droplets (which are assumed to be spheres of the same size).

1.5 Previous Work

Dilute gas-particle flows and dilute gas-droplet flows problems were incorporated in IITK-DAE Anupravaha Solver by Adhiraj Dasgupta [2] and Shashwat Swami Jaiswal [33] respectively in 2008. But, the modules had convergence issues for smaller diameters of particles/droplets. The particle/droplet size and volume fraction limitations of the earlier algorithms is listed in Table 1.1. Also, in gas-droplet flow solver, the final

Table 1.1: Limitations of Previous two-phase flow solver

Solver	Maximum Inlet Volume Fraction	Minimum Inlet Diameter
Gas-Particle Flows	0.05%	80 $\mu\, m$
Gas-Droplet Flows	0.05%	$400\mu\, m$

diameter after evaporation was limited to $80\mu\, m$ by enforcing a constraint on the volume fraction. When the constraint was relaxed, it lead to convergence issues. Apart from the above mentioned short-comings, volume increase due to the evaporated droplet vapours was also not considered in the gas-droplet flow solver. This was due to the divergence-free velocity condition imposed for continuity which is not compatible with volume changes (say, due to evaporation in the flow).

Convergence problems in the previous solvers were due to two reasons:

1. Momentum equations for dispersed phase were used to solve for the specific momentum $\mathbf{V}_d$ of the particles/droplets, defined as $\mathbf{V}_d = \rho_d \vartheta_d \, \mathbf{u}_d$. The velocity field was then obtained by dividing the specific momentum with $\rho_d \vartheta_d$. Since, we are dealing with dilute flows, ϑ_d is a very small number and convergence for such small numbers was proving to be a difficulty. For droplets with smaller diameters, evaporation occurs rapidly and hence, the volume fraction decreases to an even smaller value within a few milliseconds. Division by such small numbers for obtaining the velocity field was leading to round-off errors. Since, the governing equations of both phases are tightly coupled, the above mentioned difficulty lead to over-all convergence of the solution.

2. In gas-droplet flow solver, a convective equation was solved for the number density (n) of droplets in order to apply a constraint on thee total evaporation rate. For

the considered volume-fraction of the dispersed phase, the number density values were very large. For example, the number density for $100\mu\,m$ droplets at inlet with inlet volume fraction of 0.0005, is $9.5454545e^8$. Such large values lead to convergence issues and since n was incorporated in the source terms of all the equations, it lead to difficulties in the over-all convergence of the solution.

1.6 Objectives of the Present Work

1. To develop a robust algorithm to solve dilute gas-droplet flows with evaporation using an Eulerian-Eulerian framework. The code developed for this purpose will be the module for solving 'disperse phase flows' in IIK-DAE Anupravaha solver.

2. To modify the governing equations of gas-particle flows such that converged solution is obtained for smaller diameters.

3. To implement and validate the 'evaporation model' for use with the module for solving droplet phase flows.

4. To validate the solver by comparing the results with those obtained using analytical solutions, or the commercial package Fluent.

1.7 Thesis Organization

The thesis is organized in the following way. Chapter 2 deals with the assumptions, governing equations and boundary conditions. Chapter 3 includes the discretization procedure and the solution algorithm. Chapter 4 presents the results.

Chapter 2

Governing Equations and Assumptions

2.1 Assumptions

An Eulerian two-fluid model is employed in the present study employing two-way coupling between the two phases,using governing equations derived based on the following assumptions:

1. The spray is assumed to be *dilute* ($\vartheta_d < 0.1\%$) . Under this assumption droplet collisions are ignored and the effect of adjacent drops on drop transport rates are neglected. Also viscous stresses, and temperature and pressure variation *within* the dispersed phase are neglected.

2. At each location of the flow field, droplet-phase and gas -phase co-exist and inter-penetrate with each other, each having its own velocity and temperature.

3. The flow around the droplet is assumed to be quasi-steady, that means the flow immediately adjusts to the local boundary conditions. This allows the use of drag coefficient formulations to represent the inter-phase forces on the droplets.

4. The droplets are assumed to be spherical and mono-sized.

5. The radial velocity of the liquid surface due to the evaporation of the liquid is neglected.

6. Effects of drag and forced convection are represented by empirical relations.

7. It is assumed that the only significant inter-phase force is due to drag. This is largely true for droplet-to-gas density ratios $(\rho_d/\rho_g) > 600$.

8. During the evaporation process, droplets do not break-up; chemical reaction is also neglected.

9. The gas phase Lewis number is assumed to be unity. This assumption implies that thermal diffusivity and molecular diffusivity are equal hence enabling us to use gas-phase properties while calculating the evaporation rate of a droplet without the need to find the molecular diffusivity of the droplets in the gas phase.

2.2 The Governing Equations

2.2.1 Gas-Phase

The governing equations for the gas phase are the Navier-Stokes equations, energy equation and mass fraction equation with extra source terms that reflects the contribution of the droplet phase on the gas phase. In cartesian coordinates, the equations are as below. All symbols are explained at the end of this sub-section.

Continuity: A source term for mass transfer due to evaporation is incorporated in the continuity equation. The continuity equation is as follows

$$\frac{\partial\, \vartheta_g \rho_g}{\partial\, t} + \frac{\partial\, \vartheta_g \rho_g\, U_{g,j}}{\partial\, x_j} = n\, \dot{m}_v \tag{2.1}$$

Writing in vector notation, it is

$$\frac{\partial\, \vartheta_g \rho_g}{\partial\, t} + \nabla \cdot (\vartheta_g \rho_g\, \mathbf{u}_g) = n\, \dot{m}_v \tag{2.2}$$

Momentum: Apart from the drag force between the dispersed and the continuous phase, momentum transfer also occurs due to evaporation.

$$\begin{aligned}\frac{\partial\, (\vartheta_g \rho_g\, U_{g,i})}{\partial\, t} + \frac{\partial\, (\vartheta_g \rho_g\, U_{g,i}\, U_{g,j})}{\partial\, x_j} = \frac{\partial}{\partial\, x_i}(\frac{\vartheta_g \mu_g\, \partial U_{g,i}}{\partial\, x_j}) - \vartheta_g \frac{\partial\, P}{\partial\, x_i} + \\ \vartheta_g \rho_g\, g_i + n\, \dot{m}_v U_{d,i} - \vartheta_d\, f_{d,i}\end{aligned} \tag{2.3}$$

Writing in vector notation,

$$\begin{aligned}\frac{\partial\, (\vartheta_g \rho_g\, \mathbf{u}_g)}{\partial\, t} + \nabla \cdot (\vartheta_g \rho_g\, \mathbf{u}_g\, \mathbf{u}_g) = \nabla \cdot (\mu_g\, \vartheta_g \nabla \mathbf{u}_g) - \vartheta_g \nabla P + \\ \vartheta_g \rho_g\, \mathbf{g} + n\, \dot{m}_v \mathbf{u}_d - \vartheta_d\, \boldsymbol{f}_d\end{aligned} \tag{2.4}$$

Energy: Evaporation process differs from other mass transfer in the fact that energy is also transferred simultaneously with mass. The heat transfer from the continuous phase to the dispersed phase should hence be considered while computing the temperature of the continuous phase.

$$\frac{\partial\,(\vartheta_g \rho_g\, C_{pg}\, T_g)}{\partial\, t} + \frac{\partial\,(\vartheta_g \rho_g C_{pg}\, T_g\, U_{g,j})}{\partial\, x_j} = \frac{\partial}{\partial\, x_i}(\vartheta_g\, k_g\, \frac{\partial\, T_g}{\partial\, x_j}) + n\, \dot{m}_v\, C_{vd}\, T_d - n\, Q \tag{2.5}$$

Writing in vector notation, it is

$$\frac{\partial\,(\vartheta_g \rho_g\, C_{pg}\, T_g)}{\partial\, t} + \nabla \cdot (\vartheta_g \rho_g C_{pg}\, T_g\, \mathbf{u}_g) = \nabla \cdot (\vartheta_g k_g\, \nabla\, T_g) + n\, \dot{m}_v\, C_{vd}\, T_d - n\, Q \tag{2.6}$$

Species Mass Fraction: As evaporation from the droplets is also considered, it is assumed that the evaporated vapour is of a different species (say, fuel) than the ambient gas. Therefore, an equation for the species Y_F is also solved:

$$\frac{\partial\,(\vartheta_g \rho_g\, Y_F)}{\partial\, t} + \frac{\partial\,(\vartheta_g \rho_g\, Y_F\, U_{g,j})}{\partial\, x_j} = \frac{\partial}{\partial\, x_i}(\vartheta_g \rho_g\, D\, \frac{\partial\, Y_F}{\partial\, x_j}) + n\, \dot{m}_v \tag{2.7}$$

Writing in Vector notation,

$$\frac{\partial\,(\vartheta_g \rho_g\, Y_F)}{\partial\, t} + \nabla \cdot (\vartheta_g \rho_g\, Y_F\, \mathbf{u}_g) = \nabla \cdot (\vartheta_g \rho_g\, D\, \nabla Y_F) + n\, \dot{m}_v \tag{2.8}$$

where ρ_g is the density of the gas phase, $\mathbf{u}_g$ and T_g are velocities and temperature of the gas phase respectively. The subscripts g and d refer to the gas and droplet phases respectively. Y_F is the evaporated fuel mass fraction, μ is viscosity, C_{pg} is the specific heat at constant pressure, k_g is thermal conductivity of the gas phase, $\mathbf{g}$ is acceleration due to gravity. $\dot{m}_v$ is the evaporation rate for a single droplet, n is the number density of droplets per unit volume of flow, C_{vd} is the specific heat of the *vapour* phase of the liquid in the droplet, T_d is droplet temperature, D is the diffusion coefficient of fuel vapour in gas and Q is heat transfer from the gas to a single drop, $\boldsymbol{f}_d$ the drag force acting on the droplet per unit volume. This is described in next section, 2.2.2.

2.2.2 Droplet-Phase

The governing equations for the droplet phase are derived as follows:

Continuity: due to evaporation, some amount of mass is transfered from the droplet phase to the gas phase. It is accounted by incorporating a negative source term in the continuity equation of the droplet phase.

$$\frac{\partial\,(\rho_d\, \vartheta_d)}{\partial\, t} + \frac{\partial\,(\rho_d\, \vartheta_d\, U_{d,i})}{\partial\, x_i} = -n\dot{m}_v \tag{2.9}$$

Writing in vector notation,

$$\frac{\partial\,(\rho_d\,\vartheta_d)}{\partial\,t} + \nabla\cdot(\rho_d\,\vartheta_d\,\mathbf{u}_d) = -n\dot{m}_v \tag{2.10}$$

Momentum: An equal and opposite amount of momentum is exchanged from the gas phase to the droplet phase so that the total momentum of the system remains constant.

$$\frac{\partial\,\rho_d\,\vartheta_d\,U_{di}}{\partial\,t} + \frac{\partial\,(\rho_d\,\vartheta_d\,U_{di}\,U_{dj})}{\partial\,x_i} = -\vartheta_d\frac{\partial\,P}{\partial\,x_i} + \vartheta_d\,\rho_d\,g_i - n\,\dot{m}_v\,U_{di} + \vartheta_d\,f_{di} \tag{2.11}$$

Writing in Vector notation,

$$\frac{\partial\,\rho_d\,\vartheta_d\,\mathbf{u}_d}{\partial\,t} + \nabla\cdot(\rho_d\,\vartheta_d\,\mathbf{u}_d\,\mathbf{u}_d) = -\vartheta_d\nabla\,P + \vartheta_d\,\rho_d\,\mathbf{g} - n\,\dot{m}_v\,\mathbf{u}_d + \vartheta_d\,\boldsymbol{f}_d \tag{2.12}$$

where ϑ_d is the volume fraction, ρ_d is the material density of the droplet phase and $\mathbf{u}_d$ is local velocity of the droplets. The term $(\vartheta_d\,\boldsymbol{f}_d)$ in equations 2.4 and 2.12 is the drag force acting on the droplet phase per unit volume and is given by (Kolev [21]):

$$\boldsymbol{f}_d = \rho_g\,\frac{1}{\left(\frac{4}{3}\,\pi\,\{\frac{d_d}{2}\}^3\right)}\,\frac{1}{2}C_d\,|\mathbf{u}_g - \mathbf{u}_d|\,(\mathbf{u}_g - \mathbf{u}_d)\left(\frac{\pi}{4}d_d^2\right) = \beta\,(\mathbf{u}_g - \mathbf{u}_d)$$

where d_d is the diameter of the droplets and C_d is the drag coefficient which is given by (Kolev [21]):

$$C_d\;=\;\begin{cases}\frac{24}{Re_d} & \text{if } Re_d \le 1\\ \frac{24}{Re_d}\,(1+0.15\,{Re_d}^{0.687}) & \text{if } 1 \le Re_d \le 1000\end{cases}$$

where Re_d is the *droplet Reynolds number*, defined as (Miller et al. [24])

$$Re_d = \frac{\rho_g\,|\mathbf{u}_g - \mathbf{u}_d|\,d_d}{\mu_g}$$

Energy:

$$\frac{\partial\,[\rho_d\,\vartheta_d\,C_{ld}\,T_d]}{\partial\,t} + \nabla\cdot(\rho_d\,\vartheta_d\,C_{ld}\,T_d\,\mathbf{u}_d) = -n\,\dot{m}_v\,C_{ld}\,T_d - n\,\dot{m}_v\,L + n\,Q \tag{2.13}$$

where T_d is droplet temperature and L is the latent heat of vaporization of the liquid droplet at the droplet temperature.

2.3 Solution form of the governing equations

2.3.1 Gas-Phase

Continuity:

The continuity equation for the gas phase, Eqn. (2.2) may be written as: Since $\vartheta_g =$

$1 - \vartheta_d \simeq 1$, we take it out of the derivatives and get,

$$\frac{\partial \rho_g}{\partial t} + \nabla \cdot (\rho_g \, \mathbf{u}_g) = \frac{1}{\vartheta_g} n \, \dot{m}_v \tag{2.14}$$

or

$$\frac{\partial \rho_g}{\partial t} + \mathbf{u_g} \cdot \nabla \rho_g + \rho_g \nabla \cdot \mathbf{u_g} = \frac{1}{\vartheta_g} n \, \dot{m}_v \tag{2.15}$$

or,

$$\frac{D \, \rho_g}{D t} + \rho_g \nabla \cdot \mathbf{u_g} = \frac{1}{\vartheta_g} n \, \dot{m}_v \tag{2.16}$$

Momentum:

The momentum Eqn. (2.4) can be simplified further as,

$$\begin{aligned} \frac{\partial \, \mathbf{u}_g}{\partial \, t} + \nabla \cdot (\mathbf{u}_g \, \mathbf{u}_g) - \frac{1}{\rho_g} \left[\nabla \cdot (\mu_g \nabla \mathbf{u}_g) \right] = -\frac{1}{\rho_g} \nabla P + \mathbf{g} \; - \frac{1}{\vartheta_g \rho_g} \left[n \, \dot{m}_v \, \mathbf{u}_g \right] \\ + \frac{1}{\vartheta_g \rho_g} \left[n \, \dot{m}_v \, \mathbf{u}_d \right] - \frac{\vartheta_d}{\vartheta_g \rho_g} \boldsymbol{f}_d + \mathbf{u}_g \left[\nabla \cdot \mathbf{u}_g \right] \end{aligned} \tag{2.17}$$

Energy:

The energy equation of carrier phase Eqn. (2.6) can be further simplified as,

$$\begin{aligned} \frac{\partial \left(C_{pg} \, T_g \right)}{\partial \, t} + \nabla \cdot (C_{pg} \, T_g \, \mathbf{u}_g) = \frac{1}{\rho_g} \left[\nabla \cdot (k_g \nabla \, T_g) \right] + \frac{1}{\vartheta_g \rho_g} \left[n \, \dot{m}_v \, C_{vd} \, T_d \right] \\ - \frac{1}{\vartheta_g \rho_g} \left[n \, \dot{m}_v \, C_{pg} \, T_g \right] - \frac{n \, Q}{\vartheta_g \rho_g} + C_{pg} \, T_g \left[\nabla \cdot \mathbf{u}_g \right] \end{aligned} \tag{2.18}$$

where, it may be noted, the gas density ρ_g has been taken out of the partial differentials by using Eqn. 2.14. In the above equations, gas phase specific heat C_{pg} and thermal conductivity k_g are computed by mixing laws as a mass fraction average of pure species specific heat and thermal conductivity as follows,

$$C_{pg} = Y_F \, C_{vd} + (1 - Y_F) \, C_{pc} \quad \text{and} \quad k_g = Y_F \, k_{vd} + (1 - Y_F) \, k_c \tag{2.19}$$

where C_{pc} and k_c are the specific heat and thermal conductivity for pure gas respectively, while the subscripts vd refer to the corresponding qualities for the evaporated vapour from the droplets.

Species Mass Fraction:

$$\frac{\partial \left(Y_F \right)}{\partial \, t} + \nabla \cdot (Y_F \, \mathbf{u}_g) = \frac{1}{\rho_g} \nabla \cdot (\rho_g D \, \nabla Y_F) + \frac{1}{\vartheta_g \rho_g} n \, \dot{m}_v (1 - Y_F) + Y_F [\nabla \cdot \mathbf{u}_g] \tag{2.20}$$

2.3.2 Droplet-Phase

The continuity equation for the droplet phase is written as,

$$\frac{\partial\,(\rho_d \vartheta_d)}{\partial\, t} + \nabla \cdot (\rho_d\, \vartheta_d\, \mathbf{u}_d) = -n\dot{m}_v \tag{2.21}$$

For dilute two-phase flows, $\vartheta_d < 0.1\%$. Hence, for computational ease, we normalize the volume fraction equation by considering the initial volume fraction as ϑ_0 and define the normalized volume fraction of the dispersed phase as Θ_d.

$$\Theta_d \equiv \frac{\vartheta_d}{\vartheta_o}$$

Writing Eq(2.9) in vector notation, we get

$$\frac{\partial\,(\rho_d\, \Theta_d \vartheta_0)}{\partial\, t} + \nabla \cdot (\rho_d\, \Theta_d \vartheta_0\, \mathbf{u}_d) = -n\dot{m}_v \tag{2.22}$$

On simplifying it further we get,

$$\frac{d\,\Theta_d}{dt} + \nabla \cdot (\Theta_d \mathbf{u_d}) = -\frac{n\,\dot{m}_v}{\rho_d \vartheta_0} \tag{2.23}$$

Momentum: The droplet phase momentum equation, Eqn. (2.11) can be simplified as follows:

$$\frac{\partial\, \mathbf{u}_d}{\partial\, t} + \nabla \cdot (\mathbf{u}_d \mathbf{u}_d) = -\frac{1}{\rho_d} \nabla\, P + \mathbf{g} + \frac{1}{\rho_d}\, \boldsymbol{f}_d + \mathbf{u}_g\, [\, \nabla \cdot \mathbf{u}_g\,] \tag{2.24}$$

Substituting Eqn. (2.9), the momentum equation can be simplified as

$$\frac{\partial\, U_{d,i}}{\partial\, t} + U_{d,j}\, \frac{\partial\,(U_{d,i})}{\partial\, x_j} = -\frac{1}{\rho_d} \frac{\partial\, P}{\partial\, x_i} + g_i + \frac{1}{\rho_d} f_{di} \tag{2.25}$$

Writing in vector form,

$$\frac{\partial\, \mathbf{u}_d}{\partial\, t} + \nabla \cdot (\mathbf{u}_d \mathbf{u}_d) = -\frac{1}{\rho_d} \nabla\, P + \mathbf{g} + \frac{1}{\rho_d}\, \boldsymbol{f}_d + \mathbf{u}_d\, [\, \nabla \cdot \mathbf{u}_d\,] \tag{2.26}$$

Energy:

$$\frac{\partial\, C_{ld}\, T_d}{\partial\, t} + \nabla \cdot (C_{ld}\, T_d \mathbf{u}_d) = -\frac{n\dot{m}_v L}{\rho_d \vartheta_d} + \frac{n\, Q}{\rho_d \vartheta_d} + C_{ld}\, T_d\, [\nabla \cdot \mathbf{u}_d] \tag{2.27}$$

2.4 Boundary Conditions

2.4.1 At Solid Boundaries

At solid boundaries a no-slip condition is specified for the gas phase. Hence at the solid boundaries,

$$u_g = 0, \qquad v_g = 0, \qquad w_g = 0.$$

For pressure, it is usual to specify a homogeneous Neumann boundary condition, that is

$$\frac{\partial P}{\partial n} = 0$$

where n is the coordinate normal to the wall.
For the droplet phase a free-slip boundary condition is assumed at the wall. Hence we have

$$u_{d,n} = 0$$
$$\frac{\partial u_{d,t}}{\partial n} = 0$$

where n, t is the wall normal and tangential component of velocity, respectively. For volume fraction, fuel mass fraction and droplet temperature a homogeneous Neumann boundary condition is specified at the walls.

$$\frac{\partial \phi}{\partial n} = 0$$

where ϕ is ϑ_d, Y_F and T_d.

2.4.2 Inlet

At the inlet, all variables other than pressure are specified using Dirichlett condition:

$$\phi = \phi_{in}$$

where ϕ is any variable except pressure. The boundary condition for pressure is once again assumed to be of homogeneous Neumann type,

$$\frac{\partial P}{\partial n} = 0$$

2.4.3 Outlet

At the outlet a homogeneous Neumann condition is assumed for all flow variables except pressure.

$$\frac{\partial \phi}{\partial n} = 0$$

where ϕ is any variable except pressure. For pressure, any constant value may be specified, because it is only the pressure gradient that is important, and not the absolute pressure. It is convenient to specify a homogeneous Dirichlet condition for pressure at the outlet.

$$P = 0$$

2.5 Evaporation Model for Single Component Droplets

2.5.1 Classical D^2-Law

The classical D^2-law was formulated in the 1950s by Godsave [17] and Spalding [35]. It was derived for an isolated, pure-component droplet burning in a quiescent, oxidizing environment. This evaporation model is based on the following assumptions:

1. The drop is spherical.
2. The fuel is a pure liquid having a well-defined boiling point.
3. Radiation heat transfer is negligible.

It has since then been termed the D^2-law, because it predicts that the square of the droplet diameter decreases linearly with time. The model can be used both for the combustion and for the evaporation of a droplet. This model is explained in detail in [23].

A sketch of the droplet evaporation process is provided in Fig. 2.1, for the hypothetical case where a single-component drop is suddenly introduced into a gas at elevated temperature. At typical injection temperatures, the fuel vapour concentration at liquid surface is low which leads to negligible mass diffusion from the drop. Under these conditions, the droplet behaves like any cold body placed in a hot environment and utilizes the heat received to increase it temperature. In general, temperature is not

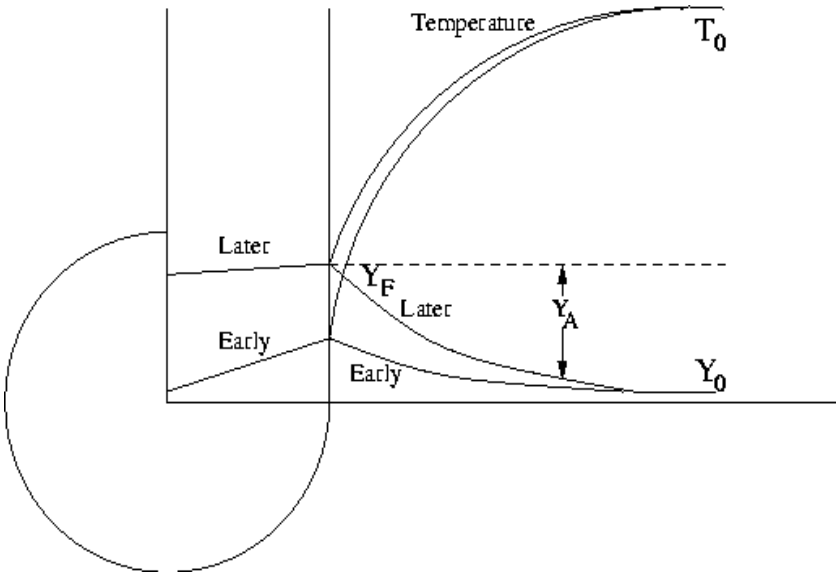

Figure 2.1: Variation of temperature and gas concentration during droplet evaporation (Faeth) [11].

uniform within the droplet but is lower at the center of the drop, with maximum liquid temperature at the surface. Initially, almost all of the heat supplied to the drop serves to raise its temperature. As the liquid temperature rises, the fuel vapour formed at the liquid surface has two effects i.e., an increasing portion of the energy reaching the drop surface is utilized for providing the heat of vaporization of the evaporating fuel, and the outward flow of the fuel vapour reduces the heat transfer to the droplet. This slows the rate of increase of the liquid surface temperature and therefore, later in the process, the temperature becomes relatively uniform in the droplet. Eventually, a stage is reached where all the heat reaching the surface is utilized for the heat of vaporization and the droplet stabilizes at a temperature called the "wet bulb temperature". The droplet attains its steady-state and the drop diameter diminishes with time according to the relationship ([35],[17])

$$d_0^2 - d^2 = \lambda_{st} t \tag{2.28}$$

Burning rate curves are shown in Fig. 2.2 for n-Heptane which for the studied case has $\lambda_{st} = 0.30\ mm^2/\text{s}$.

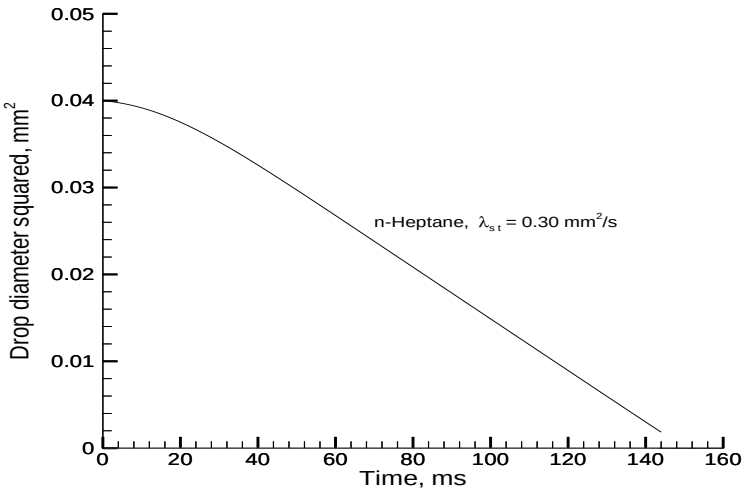

Figure 2.2: Burning rate curves for n-Heptane

2.5.2 Mathematical Formulation

Evaporation process is characterized by simultaneous mass and heat transfer. A measure of the mass transfer rate from the droplet to the surrounding gas and heat transfer rate from the ambient gas to the drop is hence required to analyze the rate of evaporation of the droplets. We use two parameters, mass transfer number (B_M) and heat transfer number (B_T) to quantitatively measure mass and heat transfer rates.

Mass transfer number

An expression for the mass transfer number, B_M and hence, the rate of evaporation of a single spherical fuel drop, $\dot{m}_v$ is derived by neglecting thermal diffusion and assuming that the driving force for species diffusion is a concentration gradient in the direction of the diffusion path, the following expression is obtained for an evaporating drop [23]:

$$\frac{dY_F}{dr} = -\frac{RT}{D_c P}\left(\dot{m}_v Y_A\right) \tag{2.29}$$

Y_F = fuel mass fraction
Y_A = air mass fraction
$\dot{m}_v$ = mass rate of diffusion per unit area
D_c = diffusion coefficient
P = gas pressure

r = radius ($r = 0$ at center of drop and $r = r_s$ at drop surface)

From continuity considerations, the mass rate of diffusion at the drop surface, $\dot{m}_{v_S}$ is given by

$$\dot{m}_{v_S}\, 4\pi r_s^2 = \dot{m}_v\, 4\pi r^2$$

Applying the following boundary conditions

$r = r_s$;	$T = T_s$;	$Y_F = Y_{F_S}$
$r = \infty$;	$T = T_\infty$;	$Y_F = Y_{F_\infty} = 0$

and integrating Eqn. 2.29 between $r = r_s$ and $r = \infty$ gives the mass transfer rate as

$$\dot{m}_v = 2\pi d_d \rho D_c \ln(1 - Y_{F_S}) \tag{2.30}$$

Assuming the Lewis number ($Le \equiv \frac{\alpha}{D}$) is equal to unity, the quantity ρD_c can be replaced by $(k/C_p)_g$, where k and C_p are the mean thermal conductivity and specific heat,respectively.
Defining

$$B_M = \frac{Y_{F_s} - Y_{F_\infty}}{(1 - Y_{F_S})} \tag{2.31}$$

Now substituting B_M in Eq. 2.30 gives [23]

$$\dot{m}_v = 2\pi d_d \left(\frac{k}{C_p}\right)_g \ln(1 + B_M) \tag{2.32}$$

This is the basic equation for the evaporation rate of a fuel drop of diameter d_d. Its accuracy is very much dependent on the choice of the values of k_g and C_{pg}. The reference temperature and composition for the evaluation of the average properties will be discussed later in this chapter.

Heat transfer number

Similar to the above analysis but based on the convective and conductive heat fluxes across a thin shell surrounding the evaporating drop, lead to the following expression for heat transfer number [35]:

$$B_T = \frac{C_{pg}(T_\infty - T_s)}{L} \tag{2.33}$$

where L is the latent heat of vaporization of fuel at droplet surface temperature T_s.

The number B_T denotes the ratio of the available enthalpy in the surrounding gas to the heat required to evaporate the fuel. In this case the rate of evaporation, for Lewis number of unity, is obtained as

$$\dot{m}_v = 2\pi d_d \left(\frac{k}{C_p}\right)_g \ln(1 + B_T) \tag{2.34}$$

Under the steady-state condition $B_M = B_T$ and either Eq. 2.32 or Eq. 2.34 may be used to calculate the rate of evaporation. The advantage of Eq. 2.32 is that it applies under all conditions, including the transient state of droplet heat-up, whereas Eq. 2.34 can only be used for steady-state evaporation. However, Eq.2.34 is usually easier to evaluate, since the magnitudes of various terms are either contained in the data of the problem or readily available in the literature. This is particularly true when the ambient gas temperature is significantly higher than the fuel surface temperature T_s, then T_s can be replaced by the boiling temperature of the fuel with little loss in accuracy.

2.5.3 Calculation of Steady-State Evaporation Rates

The stage in the drop evaporation process when the drop surface has attained its wet-bulb temperature is called as steady-state. At steady state, all the heat reaching the drop surface is utilized in providing the latent heat of evaporation. Hence, at steady-state $B_M = B_T$ which leads to the relation between Y_{F_s} and T_S as.

$$\frac{Y_{F_S}}{(1 - Y_{F_S})} = \frac{C_{pg}(T_\infty - T_s)}{L} \tag{2.35}$$

The fuel vapour mass fraction at the droplet surface is calculated by taking the partial pressure weighted average of molecular weights,

$$Y_{F_S} = \left[1 + \left(\frac{P}{P_{F_S}} - 1\right)\frac{M_A}{M_F}\right]^{-1} \tag{2.36}$$

where,

P_{F_S} = fuel vapour pressure at the drop surface
P = ambient pressure (sum of fuel vapour pressure and air partial pressure at the drop surface)
M_A = molecular weight of air
M_F = molecular weight of fuel

The quantitaive values of P, M_A, M_F, and T_∞ are usually known for any problem. Fuel vapour pressure is a functions of T_S and can be easily obtained using the following modified form of Clausius-Clapeyron equation for organic fuels [23]

$$P_{F_S} = exp\left(a - \frac{b}{T_s - 43}\right)\ kPa \tag{2.37}$$

Eqns. 2.35 and 2.37 form a set of equations for the two unknowns Y_{F_S} and T_S. Having obtained these values, the mass evaporation rate for the drop can be calculated from equation 2.32 or 2.34.

2.5.4 Evaporation Constant

It has been shown earlier that during the steady-state period of an evaporating drop its diameter at any instant may be related to its initial diameter by an expression

$$d_0^2 - d^2 = \lambda_{st}\, t \tag{2.38}$$

where λ is the evaporation constant as defined by Godsave [17]. Eqn. **??** is rewritten as

$$\lambda_{st} = \frac{d(d_d)^2}{dt} = 2\, d_d \frac{d(d_d)}{dt} \tag{2.39}$$

The value of λ_{st} may be used to determine the steady-state transfer number $B = B_M = B_T$. From Eq. 2.39 it can be shown that

$$\dot{m}_v = \frac{dm_v}{dt} = \frac{d}{dt}\{\rho_d \frac{4\pi}{3} \frac{{d_d}^3}{8}\} = \frac{\pi}{4}\rho_d d_d \lambda_{st} \tag{2.40}$$

Equating 2.32 and 2.40 gives

$$\lambda_{st} = \frac{8\, k_g \ln(1+B)}{C_{pg}\rho_d} \tag{2.41}$$

2.6 Unsteady-State Analysis

Even before the drop reaches its wet-bulb temperature, a very small amount of evaporation takes place owing to the diffusion of fuel vapors at the drop surface. This can be seen from Fig. 2.2 showing the relationship between droplet diameter squared and time. During most of the evaporation period, the slope of ${d_d}^2/t$ is seen to be constant but at the start it is almost zero. The slope then gradually increases with time until the droplet attains its wet-bulb temperature, after which it remains constant throughout its lifetime.

For the purpose of analysis, the vaporization process is divided into the transient or unsteady state and the steady state. The magnitude of the unsteady portion depends on many parameters such as properties of fuel, ambient pressure and temperature and initial temperature of the drop.

2.6.1 Calculation of drop surface temperature

If the rate of heat transfer to a drop per unit surface area per unit time is denoted by q, then

$$\dot{q} = \frac{\dot{m}_v \, L}{\pi \, {d_d}^2} \tag{2.42}$$

Substituting for $\dot{m}_v$ gives

$$\dot{q} = \frac{2(k/C_p)_g \, L \, \ln(1 + B_M)}{d_d} \tag{2.43}$$

A quasi-steady gas phase is assumed in which the boundary layer around the drop has the same characteristics as a steady boundary layer for the same conditions of drop size, velocity, surface temperature and ambient temperature. Nusselt number is then given by [23]

$$Nu = \frac{h \, d_d}{k_g} = \frac{\dot{q} \, d_d}{k_g(T_\infty - T_s)}$$

On substituting Eqn. (2.43) we have,

$$Nu = 2L \, \frac{\ln(1 + B_M)}{C_{pg}} = 2\frac{\ln(1 + B_M)}{B_M} = 2\frac{\ln(1 + B_M)}{B_M} \tag{2.44}$$

The heat transferred from the gas to the drop is then given by

$$\dot{Q} = \pi \, {d_d}^2 \, \dot{q} \tag{2.45}$$

or

$$\dot{Q} = 2 \, \pi \, d_d \, k_g \, (T_\infty - T_s) \, \frac{\ln(1 + B_M)}{B_M} \tag{2.46}$$

Now the heat used in vaporization of the fuel is

$$\dot{Q}_e = \dot{m}_v \, L = 2 \, \pi \, d_d \, (k/C_p)_g \, L \, \ln(1 + B_M) \tag{2.47}$$

The heat available for the heating up the drop is hence the difference between Q and Q_e

$$\dot{Q} - \dot{Q}_e = 2 \, \pi \, d_d \, k_g \, \ln(1 + B_T) \, \left(\frac{T_\infty - T_s}{B_M} - \frac{L}{C_{pg}} \right) \tag{2.48}$$

or

$$\dot{Q} - \dot{Q}_e = \dot{m}_v \, L \left(\frac{B_T}{B_M} - 1 \right) \tag{2.49}$$

It should be noted in Eq. 2.49 that when $B_T = B_M$ the value of $Q - Q_e$ becomes zero, denoting the end of the heat-up period. Now the rate of change of the drop surface temperature is given by

$$\frac{d\,T_s}{dt} = \frac{\dot{Q} - \dot{Q}_e}{C_{ld}\, m} = \frac{\dot{m}_v \, L}{C_{ld}\, m} \left(\frac{B_T}{B_M} - 1 \right) \tag{2.50}$$

where m = drop mass $=(\pi/6)\,\rho_F\, {d_d}^3$. The Eulerian form of the above equation, Eqn. (2.13) is used in the present study which has been discussed earlier in this chapter. Since, uniform temperature model is being considered for droplet phase, $T_d = T_s$. Also, the rate of change of diameter of droplet may be given by combining equations 2.39 and 2.41,

$$\frac{d\,d_d}{dt} = \frac{4\,k_g \, \ln(1 + B_M)}{C_{pg}\, \rho_d \, d_d} \tag{2.51}$$

Eqns (2.50) and (2.51) give the change of droplet surface temperature T_s and diameter d_d during the transient period. However, they can be used even after steady-state is reached then $T_s = T_{sat}$, as $B_M = B_T$, while Eqn (2.50) continues to give correct values for the change in diameter (as in Eqns 2.39-2.41) according to the D^2 model.

2.7 Drop analysis

Transport processes within the drop are treated in different ways by different models such as the thin skin model, uniform temperature model, uniform state model. In this study we will use the uniform temperature model also known as 'rapid mixing limit' or 'infinite conductivity model' which postulates infinite thermal diffusivity and assumes that the temperature within the droplet is spatially uniform although time varying. We also assume that the species concentration is uniform within the drop.

2.8 Convective effects on evaporation

For drop evaporation under quiescent conditions, the principal mode of heat transfer is conduction. But if relative motion exists between the droplet and the surrounding fluid, the rate of evaporation is enhanced. The gas-phase convective environment has a considerable impact on the droplet evaporation process, as both the heat and the

mass transfer process between the phases are enhanced by relative motion between them. In order to consider these phenomena, mass flux and energy transfer rates are corrected by implementing semi-empirical correlations for the calculation of both mass and heat transfer numbers. One of the first reliable correlations was given by Frossling [14]. He showed that the effect of convection on heat and mass transfer rates could be accommodated by a correction factor that is a function of Reynolds number and either Schmidt or Prandtl number. This correction factor has been later modified by Ranz and Marshall [29].

The correction factor when the diffusion rates are controlling the evaporation rate is

$$1 + 0.3\, Re_d^{0.5}\, Sc_g^{0.33} \tag{2.52}$$

And when the heat transfer rates are controlling the evaporation rate,

$$1 + 0.3\, Re_d^{0.5}\, Pr_g^{0.33} \tag{2.53}$$

Combining equations 2.32 and 2.53 yields the following equation for the rate of fuel evaporation under convective environment:

$$\dot{m}_v = 2\pi d_d \left(\frac{k}{C_p}\right)_g \ln(1 + B_M)\,(1 + 0.3\, Re_d^{0.5}\, Pr_g^{0.33}) \tag{2.54}$$

This equation gives the instantaneous rate of evaporation for a drop of diameter d_d. As described earlier heat transfer rates between the phases are also enhanced under convective environment. So the expression for rate of heat transferred from the gas to the drop Q (Eqn. 2.46) and the heat used in vaporization of the fuel Q_e (Eqn. 2.47) can also be modified using the correction factor as follows,

$$Q = 2\,\pi\, d_d\, k_g\,(T_\infty - T_s)\,\frac{\ln(1 + B_M)}{B_M}\,(1 + 0.3\, Re_d^{0.5}\, Pr_g^{0.33}) \tag{2.55}$$

and

$$Q_e = \dot{m}_v\, L = 2\,\pi\, d_d \left(\frac{k}{C_p}\right)_g L\, \ln(1 + B_M)\,(1 + 0.3\, Re_d^{0.5}\, Pr_g^{0.33}) \tag{2.56}$$

In the above expressions Re_d is the droplet Reynolds number. The definition of droplet Reynolds number is based on the relative velocity between the droplet and the surrounding gas, on the free stream density and the average gas film viscosity. Generally, most evaporation processes occur due to the temperature difference between the droplet phase and gas phase. So, in all such cases, heat transfer controls the evaporation process and Eqns. (2.54) through (2.56) are appropriate. If however, mass transfer is the controlling mechanism we replace Pr_g by Schmidt number Sc_g in these equations.

2.9 Property Evaluation

The evaporation model given by Spalding [35] is based on the assumption that the Lewis number within the gas phase is unity. From the definition of the Lewis number, $Le \equiv \alpha/D_c$, it can be seen that $\alpha = D_c$ for the present case, where $\alpha = k/(\rho C_p)$ is the thermal diffusivity. This implies that the rate of heat and mass transfer are of the same magnitude. This assumption provides simplification and as a consequence, the number of properties which has to be evaluated in order to solve the problem is reduced. This is true only for the steady-state analysis. The properties such as density and thermal conductivity of the evaporated liquid has to be evaluated at some mean film temperature and composition. In the literature several schemes have been proposed but many authors found that the scheme which they called the '1/3 rule' worked best. The rule used the following reference states for temperature and composition, designated with the subscript r:

$$T_r = T_S + \frac{T_\infty - T_S}{3} \tag{2.57}$$

$$Y_{F_r} = Y_{F_S} + \frac{Y_{F_\infty} - Y_{F_S}}{3} \tag{2.58}$$

where Y_F is mass fraction of the fuel vapour. Subscripts s and ∞ refer to the surface and ambient conditions. If the fuel concentration at an infinite distance from the droplet is assumed to be zero, Eqn. (2.58) becomes

$$Y_{F_r} = \frac{2}{3} Y_{F_S} \tag{2.59}$$

$$Y_{A_r} = 1 - Y_{F_r} = 1 - \frac{2}{3} Y_{F_S} \tag{2.60}$$

where Y_{A_r} is the reference mass fraction of air. The above equations are used in this study to calculate the reference values of the physical properties of the vapour-gas mixture that constitutes the environment of the evaporating drop. This means that the reference state is closer to the droplet surface than the mean film value. For example, the reference specific heat and thermal conductivity is obtained as,

$$C_{pg} = Y_{A_r} \left(C_{pA} \text{ at } T_r\right) + Y_{F_r} \left(C_{pv} \text{ at } T_r\right) \tag{2.61}$$

$$k_g = Y_{A_r} \left(k_A \text{ at } T_r\right) + Y_{F_r} \left(k_v \text{ at } T_r\right) \tag{2.62}$$

Chapter 3

Discretization Procedure and Solution Algorithm

3.1 Description of the Finite Volume Method

The Finite Volume method for solving the incompressible Navier Stokes equations has become very popular in recent years because of the following advantages

1. It is easy to implement on non-orthogonal curvilinear grids.
2. The solution can be obtained in the actual physical domain without transforming the governing equations.
3. It is easy to implement the boundary conditions.

When the primitive variable (e.g.velocity and pressure) approach is used, special treatment for pressure is required in the solution algorithm because the pressure does not have its own governing equation for incompressible flow. The continuity equation, having no explicit link to the pressure, is just an additional constraint on the velocity field that must be satisfied together with the momentum equations. It is an appropriate manipulation of that constraint which leads to an equation for the pressure.

In the present study, the Navier Stokes and Energy equations have been solved using the finite volume method. We have used non-staggered (collocated) grid arrangement, where the dependent variables are calculated at the centroid of the finite volume. But this arrangement can produce non-physical oscillations in the pressure field, the

so-called checker-board pressure distribution. When central differencing is used to represent both the pressure gradient term in the momentum equations and the cell-face velocity in the continuity equation, it then happens that the velocities depend on pressure at alternate nodes and not on adjacent ones and the pressure too depends on velocities at alternate nodes. This behavior is called velocity-pressure decoupling, Patankar [26].

To avoid this decoupling, the momentum interpolation method, first proposed by Rhie and Chow [28] has been used. In this approach, the cell-face velocity in the continuity equations are evaluated by linearly interpolating the so-called "mass" velocities computed without the pressure terms in the discretized equations while directly evaluating the pressure gradient using values at the adjacent cell centers. This results in a strong velocity-pressure coupling. The pressure gradient terms, appearing in the momentum equations, are still represented by central difference approximation.

3.2 Grid Generation

Grids used in this thesis are generated using *ANSYS ICEMCFD* software.The grids used in this thesis are structured grids with quadrilateral nodes. *ANSYS ICEMCFD* is a grid generation system combining various technologies such as computer aided geometric design, computational geometry and computer graphics, structured and unstructured grid generation algorithms.Grids generated in *ANSYS ICEMCFD* are saved in Version 2.4 CGNS format.

3.3 CGNS file format

CGNS (CFD General Notation System) originated in 1994 as a joint effort between Boeing and NASA, and has since grown to include many other contributing organizations worldwide. It is an effort to standardize CFD input and output, include grid (both structured and unstructured), flow solution, connectivity, boundary conditions (BCs), and auxiliary information. CGNS is also extensible, and allows for file-stamping and user-inserted-commenting. It employs ADF (Advanced Data Format), a system which reads a binary files that are portable across computer platforms. CGNS also includes a second layer of software known as the mid-level library, or API (Application Programming Interface), which eases the implementation of CGNS into existing codes.

A CGNS file is an entity that is organized (inside the file itself) into a set of *nodes* in a tree-like structure, in much the same way as directories are organized in the UNIX environment. The top-most node is referred to as the *root node*. Each node below the root node is defined by both a name and a label, and may or may not contain information data. Each node can also be a *parent* to one or more *child* nodes.

CGNS files are binary files and they cannot be viewed by user with standard UNIX ASCII- editing tools. The utility ADF was created to allow users to easily view CGNS files. For more detailed information, readers are suggested to see the CGNS website ***www.cgns.org*** (especially the User's Guide Section).

In the present work, CGNS version 2.4 file-format is used to store grids and flow solution. Post processing is done by *Tecplot 360*, which is also a CGNS compatible software.

3.4 Integral Form of Governing Equations

The three-dimensional Navier-Stokes equations can be expressed in the following general convection-diffusion-source integral form:

$$\frac{\partial}{\partial t}\int_V \rho dV + \int_S \rho \mathbf{u} \cdot \mathbf{dS} = 0 \tag{3.1}$$

$$\frac{\partial}{\partial t}\int_V \rho\phi dV + \int_S [\rho \mathbf{u}\phi - \mathbf{\Gamma}_\phi \nabla\phi] \cdot \mathbf{dS} = \int_V S_\phi dV \tag{3.2}$$

where ρ represents the fluid density, $\mathbf{u}$ is the fluid velocity, Γ_ϕ is the diffusion coefficient for the quantity ϕ (viscosity in case of momentum equations), ϕ stands for any vector component or scalar quantity, S_ϕ is the volumetric source term. If ϕ is other than velocity *i.e* temperature, scalar *etc.* then density (ρ) should be replaced by $(\rho C_p)_\phi$.

In this formulation we work with **Cartesian components** of velocity. So ϕ can be the three Cartesian component of velocity u, v, w as well as any scalar *e.g.*, temperature, species concentration, which needs to be determined.

3.5 Description of the Finite-Volume Method

We will now discuss the finite volume method applied to a general 3-D geometry. The entire solution domain is initially divided into zones and then zones are subdivided into a number of finite volumes defined by the coordinates of their eight vertices read from the CGNS grid file. We have used the collocated grid arrangement where all the dependent variables are defined at the centroid of the cell. The FVM method used in this work is explained in detail in BARC Report [9].

3.6 Discretization Procedure

The discretization of the transport equations is performed using the finite volume approach. All the transport equation can be represented in the following general form,

$$\frac{\partial}{\partial t}\int_V \rho\phi dV + \int_S [\rho\mathbf{u}\phi - \Gamma_\phi \nabla\phi]\cdot\mathbf{dS} = \int_V S_\phi dV \tag{3.3}$$

which consists of the rate of change of ϕ, convection diffusion fluxes and the source term. The rate of change and source terms are integrated over the cell volume, whereas the convection and diffusion terms sum fluxes through the CV faces.

3.6.1 Discretization of the General Convection-Diffusion Equation

(a) Rate of change: In the discretization of the unsteady term it has been assumed that the value of the dependent variable at the centroid is the average over the entire control volume. Thus

$$\frac{\partial}{\partial t}\int_V \rho\phi dV \approx \frac{(\rho\phi V)_P^{n+1} - (\rho\phi V)_P^n}{\Delta t} \approx V_P \frac{(\rho\phi)_P^{n+1} - (\rho\phi)_P^n}{\Delta t} \tag{3.4}$$

where V_P is the volume of the cell.

(b) Convection fluxes: The approximation of the surface integral over convection flux of variable ϕ has been done in the following way,

$$\int_S \rho\mathbf{u}\phi\cdot\mathbf{dS} \approx \sum_j \rho_j\phi_j(\mathbf{u}\cdot\mathbf{S})_\mathbf{j} = \sum F_j\phi_j \tag{3.5}$$

where ϕ_j is the value of ϕ at the center of the face j. In this work, the value of the ϕ_j is evaluated using upwind scheme or Center difference scheme(CDS).

The upwind scheme is based on the assumption that the convected cell face value is equal to that at the upstream cell along the same coordinate direction. Thus, the value ϕ_e at the east face is assigned the value ϕ_P if $u_e \geq 0$, *i.e.*, the flux F_e is positive, and the value ϕ_E if $u_e < 0$, *i.e.*, the flux F_e is negative. This can be conveniently summarized as

$$F_e\phi_e = \phi_P[|F_e, 0|] - \phi_E[|-F_e, 0|] \tag{3.6}$$

Here $[|p, q|]$ denotes the maximum of p and q. Similar expression can be written for the rest of the faces.

While using CDS, the value of ϕ_j is evaluated using center difference linear interpolation from the neighboring nodal values.

$$F_e\phi_e = F_e\left(\frac{V_E}{V_E + V_P}\phi_P + \frac{V_P}{V_E + V_P}\phi_E\right) \tag{3.7}$$

(c) Diffusion fluxes: The surface integral over diffusion flux of variable ϕ can be approximated as

$$\int_S \Gamma_\phi \nabla\phi \cdot \mathbf{dS} \approx \sum_{j=e,w,n,s,t,b} (\Gamma_\phi \nabla\phi \cdot \mathbf{S})_\mathbf{j} = \sum_j -F_j^d \tag{3.8}$$

For east face we can write,

$$F_e^d = -\Gamma_\phi(\alpha_1\frac{\phi_E - \phi_P}{\Delta x^1} + \alpha_2\frac{\phi_{se} - \phi_{ne}}{\Delta x^2} + \alpha_3\frac{\phi_{te} - \phi_{be}}{\Delta x^3}) \tag{3.9}$$

Calculation of $\alpha_1, \alpha_2, \alpha_3$, the edge center values appearing in cross derivative diffusion flux, special treatment of diffusion fluxes of corner cells and computation of spatial derivatives at cell-center of a non-orthogonal grid is elaborated in Barc Report [9].

(d) Source: The source term is integrated over the cell volume as follows:

$$\int_V S_\phi dV \approx (S_\phi)_p V_P \tag{3.10}$$

In the momentum equations, the pressure term is a source term, while in species transport equations chemical reaction could be a source term.

(e) Pressure Term: Its discretization is same as that of the ordinary diffusion flux and is given by

$$-\int_{V_P} \nabla p \mathbf{n}_i dV \approx -(\nabla p \cdot \mathbf{n}_i)_P V_P \tag{3.11}$$

where $\mathbf{n}_i$ is the unit vector in the direction of the velocity component, u_i. However, the Gauss divergence theorem can be used to convert the volume integral to a surface integral which can be discretized as

$$-\int_S p n_i \mathbf{dS} \approx -\sum_j p_j S_{ij} \tag{3.12}$$

p_j is the pressure at the j^{th} face center and S_{ij} is the i^{th} direction component of the surface vector for face j.

3.7 The Discretized Equations

3.7.1 Gas-Phase

We now present the discretized versions of the equations discussed in the previous chapter. **Continuity:**
The discretized form of Eqn. (2.14) is:

$$\Delta V_p \frac{{\rho_g}^{n+1} - \rho_g^n}{\Delta t} + \sum_f \rho_{gf}^{n+1} F_{gf}^{n+1} = \frac{1}{\vartheta_g^{n+1}} \Delta V_p \, (n \, \dot{m}_v)^n \tag{3.13}$$

Momentum:
The discretized form of Eqn. (2.17) is:

$$\begin{aligned} \Delta V_p \frac{u_g^{n+1} - u_g^n}{\Delta t} + \sum_f u_{gf}^m F_{gf}^m + \frac{1}{\rho_g^n} \sum_f F_{duf}^{n+1} + \frac{\Delta V_p}{\vartheta_g^n \rho_g^n} A^n u_g^{n+1} = \\ \frac{-1}{\rho_g^n} \sum_f P_f^{n+1} S_{fx} + \Delta V_p \, g_x \\ + \frac{\Delta V_p}{\vartheta_g^n \, \rho_g^n} \left(A^n \, u_d^n - \vartheta_d^n f_{dx}^n\right) + u_g^n \sum_f F_{gf}^m \end{aligned} \tag{3.14}$$

$$\Delta V_p \frac{v_g^{n+1} - v_g^n}{\Delta t} + \sum_f v_{gf}^m F_{gf}^m + \frac{1}{\rho_g^n} \sum_f F_{dvf}^{n+1} + \frac{\Delta V_p}{\vartheta_g^n \rho_g^n} A^n v_g^{n+1} = \frac{-1}{\rho_g^n} \sum_f P_f^{n+1} S_{fy} + \Delta V_p g_y + \frac{\Delta V_p}{\vartheta_g^n \rho_g^n} \left(A^n v_d^n - \vartheta_d^n f_{dy}^n \right) + v_g^n \sum_f F_{gf}^m \tag{3.15}$$

$$\Delta V_p \frac{w_g^{n+1} - w_g^n}{\Delta t} + \sum_f w_{gf}^m F_{gf}^m + \frac{1}{\rho_g^n} \sum_f F_{dwf}^{n+1} + \frac{\Delta V_p}{\vartheta_g^n \rho_g^n} A^n w_g^{n+1} = \frac{-1}{\rho_g^n} \sum_f P_f^{n+1} S_{fz} + \Delta V_p g_z + \frac{\Delta V_p}{\vartheta_g^n \rho_g^n} \left(A^n w_d^n - \vartheta_d^n f_{dz}^n \right) + w_g^n \sum_f F_{gf}^m \tag{3.16}$$

Energy:

The discretized form of Eqn. (2.18) is:

$$\Delta V_p C_{pg} \frac{T_g^{n+1} - T_g^n}{\Delta t} + \sum_f C_{pgf} T_{gf}^{n+1} F_{gf}^{n+1} + \frac{1}{\rho_g^{n+1}} \sum_f F_{dTf}^{n+1} + \frac{\Delta V_p}{\vartheta_g^{n+1} \rho_g^{n+1}} A^n C_{pg} T_g^{n+1} = \frac{\Delta V_p}{\vartheta_g^{n+1} \rho_g^{n+1}} A^n C_{vd} T_d^{n+1} - \frac{\Delta V_p}{\vartheta_g^{n+1} \rho_g^{n+1}} n^n Q^n + C_{pg} T_g^n \sum_f F_{gf}^{n+1} \tag{3.17}$$

Fuel Mass Fraction:

The discretized form of Eqn. (2.20) is:

$$\Delta V_p \frac{Y_F^{n+1} - Y_F^n}{\Delta t} + \sum_f Y_F^{n+1} F_{gf}^{n+1} + \frac{1}{\rho_g^{n+1}} \sum_f F_{dYf}^{n+1} = -\frac{\Delta V_p}{\vartheta_g^{n+1} \rho_g^{n+1}} A^n Y_F^{n+1} + Y_F^n \sum_f F_{gf}^{n+1} + \frac{\Delta V_p}{\vartheta_g^{n+1} \rho_g^{n+1}} A^n \tag{3.18}$$

In the equations 3.14 through 3.16, $m = n + 1$ for a fully implicit method and $m = n$ for a semi-implicit method. In the above equations, ΔV_p is the volume of the Finite Volume cell, u_g, v_g, w_g are the components of the gas phase velocity, u_d, v_d, w_d are the components of the droplet phase velocity, g_x, g_y, g_z are the components of acceleration due to gravity in X,Y, and Z directions respectively, $A^n \equiv n^n \dot{m}_v^n$ and

$$F_{gf} \equiv \mathbf{u}_{gf} \cdot \mathbf{S}_f$$

is the volume flux for the fluid phase, whereas

$$F_{d\phi f} \equiv -\mu \nabla \phi_{gf} \cdot \mathbf{S}_f; \qquad F_{dTf} \equiv -k_{gf} \nabla T_{gf} \cdot \mathbf{S}_f$$

and

$$F_{dYf} \equiv -(\rho_g D) \nabla Y_F \cdot \mathbf{S}_f$$

are the diffusion flux for the fluid (where $\phi = u, v, w$), diffusion flux for temperature and mass fraction respectively. Note that in the energy equation the value of C_{pg} is lagged by one time step.

3.7.2 Droplet-Phase

The discretized equations for the droplet phase are

Continuity:

The discretized form of Eqn. (2.23) is

$$\Delta V_p \left(\frac{\Theta_d^{n+1} - \Theta_d^n}{\Delta t}\right) + \sum_f \Theta_{df}^{n+1} F_{df}^{n+1} = -\frac{\Delta V_p}{\rho_d \vartheta_0} A^n \tag{3.19}$$

Momentum:

The discretized form of Eqn. (2.26) is

$$\begin{aligned} \Delta V_p \frac{u_d^{n+1} - u_d^n}{\Delta t} + \sum_f u_{df}^m F_{df}^m = &-\frac{1}{\rho_d^n} \sum_f P_f^{n+1} S_{fx} + \Delta V_p g_x \\ &+ \frac{\Delta V_p}{\rho_d^n} f_{dx}^n + u_d^n \sum_f F_{df}^m \end{aligned} \tag{3.20}$$

$$\begin{aligned} \Delta V_p \frac{v_d^{n+1} - v_d^n}{\Delta t} + \sum_f v_{df}^m F_{df}^m = &-\frac{1}{\rho_d^n} \sum_f P_f^{n+1} S_{fy} + \Delta V_p g_y \\ &+ \frac{\Delta V_p}{\rho_d^n} f_{dy}^n + v_d^n \sum_f F_{df}^m \end{aligned} \tag{3.21}$$

$$\begin{aligned} \Delta V_p \frac{w_d^{n+1} - w_d^n}{\Delta t} + \sum_f w_{df}^m F_{df}^m = &-\frac{1}{\rho_d^n} \sum_f P_f^{n+1} S_{fz} + \Delta V_p g_z \\ &+ \frac{\Delta V_p}{\rho_d^n} f_{dz}^n + w_d^n \sum_f F_{df}^m \end{aligned} \tag{3.22}$$

In the equations 3.20 through 3.22, $m = n + 1$ for a fully implicit method and $m = n$ for a semi-implicit method.

$$F_{df} \equiv \mathbf{u}_{df} \cdot \mathbf{S}_f$$

is the convective flux for the droplet phase.

Energy:

The discretized form of Eqn. (2.27) is

$$\Delta V_p \, C_{ld} \, \frac{T_d^{n+1} - T_d^n}{\Delta t} + C_{ld} \sum_f T_{gf}^{n+1} \, F_{df}^{n+1} = \frac{\Delta V_p}{\rho_d \, \vartheta_d^{n+1}} \left(n^n \, Q^n - A^n \, L \right) + C_{ld} \, T_d^n \sum_f F_{df}^{n+1} \tag{3.23}$$

3.8 The Solution Algorithm

We use a time-accurate time stepping method to solve the equations. The total evaporation rate per unit volume is represented by the parameter A and is given by

$$A^n = n^n \dot{m}_v^n \tag{3.24}$$

where, $\dot{m}_v$ is the rate of evaporation for a single droplet and has to be found from the evaporation model as described earlier. The number density of droplets per unit volume, n, is found for each cell by using the previous time step values of ϑ_d and d_d as

$$n^n = \frac{6 \, \vartheta_d^n}{\pi d_d^{3^n}} \tag{3.25}$$

The diameter of the droplets are updated by using the previous time-step's normalized volume fraction values as follows,

$$d_d = d_0 \left(\Theta_d^n \right)^{1/3} \tag{3.26}$$

We then calculate the source term due to drag by calculating C_d and β for each cell and storing the final drag value $\boldsymbol{f}_d{}^n$.

We use a fully implicit scheme for solving the momentum equations for the gas phase. Hence the discretized momentum equations become

$$\begin{aligned}\Delta V_p \frac{u_g^{n+1}-u_g^n}{\Delta t} + \sum_f u_{gf}^{n+1} F_{gf}^{n+1} + \frac{1}{\rho_g^n}\sum_f F_{duf}^{n+1} + C_v \frac{\Delta V_p}{\vartheta_g^n \rho_g^n} A^n u_g^{n+1} = \\ -\frac{1}{\rho_g^n}\sum_f P_f^{n+1} S_{fx} + \Delta V_p g_x \\ +C_v \frac{\Delta V_p}{\vartheta_g^n \rho_g^n}\left(A^n u_d^n - \vartheta_d^n f_{dx}^n\right) + u_g^n \sum_f F_{gf}^{n+1}\end{aligned} \tag{3.27}$$

$$\begin{aligned}\Delta V_p \frac{v_g^{n+1}-v_g^n}{\Delta t} + \sum_f v_{gf}^{n+1} F_{gf}^{n+1} + \frac{1}{\rho_g^n}\sum_f F_{dvf}^{n+1} + C_v \frac{\Delta V_p}{\vartheta_g^n \rho_g^n} A^n v_g^{n+1} = \\ -\frac{1}{\rho_g^n}\sum_f P_f^{n+1} S_{fy} + \Delta V_p g_y \\ +C_v \frac{\Delta V_p}{\vartheta_g^n \rho_g^n}\left(A^n v_d^n - \vartheta_d^n f_{dy}^n\right) + v_g^n \sum_f F_{gf}^{n+1}\end{aligned} \tag{3.28}$$

$$\begin{aligned}\Delta V_p \frac{w_g^{n+1}-w_g^n}{\Delta t} + \sum_f w_{gf}^{n+1} F_{gf}^{n+1} + \frac{1}{\rho_g^n}\sum_f F_{dwf}^{n+1} + C_v \frac{\Delta V_p}{\vartheta_g^n \rho_g^n} A^n w_g^{n+1} = \\ -\frac{1}{\rho_g^n}\sum_f P_f^{n+1} S_{fz} + \Delta V_p g_z \\ +C_v \frac{\Delta V_p}{\vartheta_g^n \rho_g^n}\left(A^n w_d^n - \vartheta_d^n f_{dz}^n\right) + w_g^n \sum_f F_{gf}^{n+1}\end{aligned} \tag{3.29}$$

We follow a two-step procedure to obtain the gas phase velocity components. The first step has two major loops - an inner loop (*) and an outer loop (**). In the inner loop, we first ignore the pressure completely and solve the Eqns.(3.30) through (3.32) for the so-called "mass" velocities u_g^*, v_g^* and w_g^*. The equations for mass velocity are

$$\begin{aligned}\Delta V_p \frac{u_g^*-u_g^n}{\Delta t} + \sum_f u_{gf}^* F_{gf}^{**} + \frac{1}{\rho_g^n}\sum_f F_{duf}^* + C_v \frac{\Delta V_p}{\vartheta_g^n \rho_g^n} A^n u_g^* = \\ \Delta V_p g_x + C_v \frac{\Delta V_p}{\vartheta_g^n \rho_g^n}\left(A^n u_d^n - \vartheta_d^n f_{dx}^n\right) \\ +u_g^n \sum_f F_{gf}^{**}\end{aligned} \tag{3.30}$$

$$\Delta V_p \frac{v_g^* - v_g^n}{\Delta t} + \sum_f v_{gf}^* F_{gf}^{**} + \frac{1}{\rho_g^n} \sum_f F_{dvf}^* + C_v \frac{\Delta V_p}{\vartheta_g^n \rho_g^n} A^n v_g^* = \Delta V_p g_y + C_v \frac{\Delta V_p}{\vartheta_g^n \rho_g^n} \left(A^n v_d^n - \vartheta_d^n f_{dy}^n \right) + v_g^n \sum_f F_{gf}^{**} \tag{3.31}$$

$$\Delta V_p \frac{w_g^* - w_g^n}{\Delta t} + \sum_f w_{gf}^* F_{gf}^{**} + \frac{1}{\rho_g^n} \sum_f F_{dwf}^* + C_v \frac{\Delta V_p}{\vartheta_g^n \rho_g^n} A^n w_g^* = \Delta V_p g_z + C_v \frac{\Delta V_p}{\vartheta_g^n \rho_g^n} \left(A^n w_d^n - \vartheta_d^n f_{dz}^n \right) + w_g^n \sum_f F_{gf}^{**} \tag{3.32}$$

Eqns. (3.30) through (3.32) are iterated to convergence within the inner loop [1]. We use a superscript $*$ for the diffusion term because the diffusion terms are calculated in terms of the mass velocities as they are being iterated in the inner loop. The superscript $**$ used in the convective flux F_{gf} which is evaluated in the outer loop of the first step, and is kept unchanged during the inner loop (*) iterations [2].

We then follow the same procedure for the momentum equations of the droplet phase. Hence, we have the fully-implicit discretized momentum equations as

$$\Delta V_p \frac{u_d^{n+1} - u_d^n}{\Delta t} + \sum_f u_{df}^{n+1} F_{df}^{n+1} = -\frac{1}{\rho_d^n} \sum_f P_f^{n+1} S_{fx} + \Delta V_p g_x + \frac{\Delta V_p}{\rho_d^n} f_{dx}^n + u_d^n \sum_f F_{df}^{n+1} \tag{3.33}$$

$$\Delta V_p \frac{v_d^{n+1} - v_d^n}{\Delta t} + \sum_f v_{df}^{n+1} F_{df}^{n+1} = -\frac{1}{\rho_d^n} \sum_f P_f^{n+1} S_{fy} + \Delta V_p g_y + \frac{\Delta V_p}{\rho_d^n} f_{dy}^n + v_d^n \sum_f F_{df}^{n+1} \tag{3.34}$$

[1] Actually, Eqns.(3.30) through (3.32) are calculated in three separate subloops within the inner loop.

[2] A single $*$ indicated quantities that are computed using the inner loop of the first step, whereas the $**$ indicates quantities calculated in the outer loop.

$$\Delta V_p \frac{w_d^{n+1} - w_d^n}{\Delta t} + \sum_f w_{df}^{n+1} F_{df}^{n+1} = -\frac{1}{\rho_d^n} \sum_f P_f^{n+1} S_{fz} + \Delta V_p g_z + \frac{\Delta V_p}{\rho_d^n} f_{dz}^n + w_d^n \sum_f F_{df}^{n+1} \tag{3.35}$$

The discretized equations for droplet "mass" velocities is as follow

$$\Delta V_p \frac{u_d^* - u_d^n}{\Delta t} + \sum_f u_{df}^* F_{df}^{**} = \Delta V_p g_x + \frac{\Delta V_p}{\rho_d^n} f_{dx}^n + u_d^n \sum_f F_{df}^{**} \tag{3.36}$$

$$\Delta V_p \frac{v_d^* - v_d^n}{\Delta t} + \sum_f v_{df}^* F_{df}^{**} = \Delta V_p g_y + \frac{\Delta V_p}{\rho_d^n} f_{dy}^n + v_d^n \sum_f F_{df}^{**} \tag{3.37}$$

$$\Delta V_p \frac{w_d^* - w_d^n}{\Delta t} + \sum_f w_{df}^* F_{df}^{**} = \Delta V_p g_z + \frac{\Delta V_p}{\rho_d^n} f_{dz}^n + w_d^n \sum_f F_{df}^{**} \tag{3.38}$$

Eqns. (3.36) through (3.38) too are iterated to convergence in three separate sub-loops in the inner loop of the first step. During any pass through the droplet "mass" velocity loop, we hold the convective fluxes F_{df}^{**} fixed and iterate for the mass velocities. Once the gas and droplet "mass" velocities are obtained, we update the pressure and the fluxes in the outer loop and return to the inner loop and use the updated fluxes for the next pass. This continues until the fluxes F_{gf}^{**} and F_{df}^{**} converge in the outer loop, and henceforth, are taken as the final values, F_{gf}^{n+1} and F_{df}^{n+1}.

We now look into the outer loop calculations. Having obtained the tentative mass velocities we turn to the pressure Poisson equation. This is derived from the total mass conservation principle. By adding Eqn.(2.2) and Eqn.(2.10), we get

$$\frac{\partial\, \vartheta_g \rho_g}{\partial\, t} + \nabla \cdot (\vartheta_g \rho_g\, \mathbf{u}_g) + \frac{\partial\, \vartheta_d \rho_d}{\partial\, t} + \nabla \cdot (\vartheta_d \rho_d\, \mathbf{u}_d) = 0 \tag{3.39}$$

For steady state problems, the temporal derivative tends to zero. Hence, we can simplify Eqn.(3.39) as,

$$\nabla \cdot (\vartheta_g \rho_g\, \mathbf{u}_g) + \nabla \cdot (\vartheta_d \rho_d\, \mathbf{u}_d) = 0 \tag{3.40}$$

which is the continuity equation that should be applied at the (n+1)th time level. So, we get

$$\nabla \cdot (\vartheta_g \rho_g \, \mathbf{u}_g)^{n+1} + \nabla \cdot (\vartheta_d \rho_d \, \mathbf{u}_d)^{n+1} = 0 \tag{3.41}$$

By subtracting Eqn. (3.30) from Eqn. (3.27), Eqn. (3.31) from Eqn.(3.28) and Eqn. (3.32) from Eqn. (3.29)we get

$$\mathbf{u}_g^{n+1} - \mathbf{u}_g^* = -\frac{\Delta \, t}{\rho_g} \nabla \, P \tag{3.42}$$

Similar conclusion can be made for droplet phase as,

$$\mathbf{u}_d^{n+1} - \mathbf{u}_d^* = -\frac{\Delta \, t}{\rho_d} \nabla \, P \tag{3.43}$$

By multiplying Eqn.(3.42) and Eqn.(3.43) by $\rho_g \vartheta_g$ and $\rho_d \vartheta_d$ respectively and substituting in Eqn.(3.41), we get

$$\Delta \, t \, \nabla^2 \, P = \nabla \cdot (\vartheta_g \rho_g \mathbf{u}_g^*) + \nabla \cdot (\vartheta_d \rho_d \mathbf{u}_d^* \tag{3.44}$$

In the above equation, we have used the principle $\vartheta_g + \vartheta_d = 1$. Discretization of Eqn.(3.44) leads to

$$\sum_f \nabla P_f^{**} \cdot \mathbf{S}_f = \frac{1}{\Delta \, t} \sum_f \rho_g^n \vartheta_g^n \mathbf{u}_{gf}^* \cdot \mathbf{S}_f + \frac{1}{\Delta \, t} \sum_f \rho_d^n \vartheta_d^n \mathbf{u}_{df}^* \cdot \mathbf{S}_f \tag{3.45}$$

We can define the fluxes on the R.H.S of Eqn. (3.45) as

$$F_{Mgf}^{**} [= (\vartheta_{gf}^n \rho_{gf}^n \mathbf{u}_{gf}^*).\mathbf{S}_f] = (\vartheta_{gf}^n \rho_{gf}^n) F_{gf}^{**} \tag{3.46}$$

$$F_{Mdf}^{**} [= (\vartheta_{df}^n \rho_{df}^n \mathbf{u}_{df}^*).\mathbf{S}_f] = (\vartheta_{df}^n \rho_{df}^n) F_{gf}^{**} \tag{3.47}$$

Here the values of u_{gi}^* and u_{di}^* at the cell faces is obtained by a volume interpolation. The superscript $**$ is used for pressure because Eqn. (3.45) is now iterated to convergence in the outer loop of step one.

Having obtained the pressure field P^{**} from Eqn.(3.45) we update the fluxes F_{gf} and F_{df} using momentum interpolation

$$F_{gf}^{**} = \mathbf{u}_{gf}^* \cdot \mathbf{S}_f - \left(\frac{\Delta \, t}{\rho_g^n} \right) \nabla P_f^{**} \cdot \mathbf{S}_f \tag{3.48}$$

$$F_{df}^{**} = \mathbf{u}_{df}^* \cdot \mathbf{S}_f - \left(\frac{\Delta \, t}{\rho_d^n} \right) \nabla P_f^{**} \cdot \mathbf{S}_f \tag{3.49}$$

After updating the fluxes F_{gf}^{**} and F_{df}^{**} in the outer loop, we once again solve the inner loop for the "mass" velocities, followed by the pressure and update the fluxes. This cycle continues until the values of fluxes converge. At that point we accept that $F_{gf}^{n+1} = F_{gf}^{**}$, $F_{df}^{n+1} = F_{df}^{**}$ and $P^{n+1} = P^{**}$. We now iterate the full momentum Eqns.(3.27) through (3.29) and Eqns.(3.33) through (3.35) to convergence. This last part comprises step two of the two-step algorithm. We now have the $\mathbf{u}_g^{n+1}$ and $\mathbf{u}_d^{n+1}$ values.

Also in the second step, we next iterate to convergence the continuity equation of the droplet phase to obtain the normalized volume fraction using F_{df}^{n+1} obtained from the converged $\mathbf{u}_{df}^{n+1}$.

$$\Delta V_p(\frac{\Theta_d^{n+1} - \Theta_d^n}{\Delta t}) + \sum_f \Theta_{df}^{n+1} F_{df}^{n+1} = -C_v \frac{\Delta V_p}{\rho_d \vartheta_0} A^n \tag{3.50}$$

We next solve the continuity equation of gas phase for density using F_{gf}^{n+1} obtained from the converged $\mathbf{u}_{gf}^{n+1}$. The discretized form is iterated to convergence.

$$\Delta V_p \frac{{\rho_g}^{n+1} - \rho_g^n}{\Delta t} + \sum_f \rho_{gf}^{n+1} F_{gf}^{n+1} = C_v \frac{1}{(1 - \vartheta_d^{n+1})} \Delta V_p (n \dot{m}_v)^n \tag{3.51}$$

Next, we solve the droplet temperature equation by iterating

$$\begin{aligned} \Delta V_p C_{ld} \frac{T_d^{n+1} - T_d^n}{\Delta t} + C_{ld} \sum_f T_{df}^{n+1} F_{df}^{n+1} = C_v \frac{\Delta V_p}{\rho_d \vartheta_d^{n+1}} (n^n Q^n - A^n L) \\ + C_{ld} T_d^n \sum_f F_{df}^{n+1} \end{aligned} \tag{3.52}$$

to convergence. We then solve the mass fraction equation and the energy equation of the gas phase.

$$\begin{aligned} \Delta V_p \frac{Y_F^{n+1} - Y_F^n}{\Delta t} + \sum_f Y_F^{n+1} F_{gf}^{n+1} + \frac{1}{\rho_g^{n+1}} \sum_f F_{dYf}^{n+1} \\ + C_v \frac{\Delta V_p}{\vartheta_g^{n+1} \rho_g^{n+1}} A^n Y_F^{n+1} = + Y_F^n \sum_f F_{gf}^{n+1} + C_v \frac{\Delta V_p}{\vartheta_g^{n+1} \rho_g^{n+1}} A^n \end{aligned} \tag{3.53}$$

$$\begin{aligned} \Delta V_p C_{pg} \frac{T_g^{n+1} - T_g^n}{\Delta t} + \sum_f C_{pgf} T_{gf}^{n+1} F_{gf}^{n+1} + \frac{1}{\rho_g^{n+1}} \sum_f F_{dTf}^{n+1} + \\ C_v \frac{\Delta V_p}{\vartheta_g^{n+1} \rho_g^{n+1}} A^n C_{vd} T_g^{n+1} = C_v \frac{\Delta V_p}{\vartheta_g^{n+1} \rho_g^{n+1}} A^n C_{vd} T_d^{n+1} \\ - C_v \frac{\Delta V_p}{\vartheta_g^{n+1} \rho_g^{n+1}} n^n Q^n + C_{pg} T_g^n \sum_f F_{gf}^{n+1} \end{aligned} \tag{3.54}$$

Note that the previous time step source term values are used in all the equations. The above steps are sequentially carried out at each time step. For all the equations of the droplet phase the convective terms are discretized by the first-order upwind scheme. This is specially helpful in avoiding negative or un-physical values of the volume fraction, however the inherent dissipation effects of the scheme reduces the sharp gradients in the solution.

3.9 Summary of the Algorithm

1. Initialize properties and fields for the carrier phase and the droplet phase, grids and other parameters.

2. Transfer $(n+1)^{th}$ time level values to n^{th} time level for all the solvable variables as volume fraction, velocity, density, temperature for the gas phase and droplet phase, fuel mass fraction and pressure.

3. Compute and store all the source terms with the previous time step values. Compute and store diameter d_d by using the following relation:

$$d_d = d_0(\Theta_d)^{1/3}$$

4. Solve for the "mass" velocity for the gas phase and droplet phase separately by iterating Eqns.(3.30) through (3.32) and (3.36) through (3.38)respectively with previous time step source term values.

5. Compute momentum fluxes, F^{**}_{Mgf} and F^{**}_{Mdf} using Eqn.(3.46) and Eqn.(3.47).

6. Solve for the pressure P^{**} by iterating Eqn. (3.45) to convergence.

7. Compute volume fluxes F^{**}_{gf} and F^{**}_{df} using Eqns. (3.48) and (3.49).

8. Repeat steps 4 to 7 until the fluxes, F^{**}_{gf} and F^{**}_{df} converge.

9. Accept $P^{n+1} = P^{**}$, $F^{n+1}_{gf} = F^{**}_{gf}$ and $F^{n+1}_{df} = F^{**}_{df}$

10. Iterate the full momentum equations for gas phase Eqns.(3.27) through (3.29) and full momentum equations for droplet phase (3.33) through (3.35)to convergence separately to obtain $\mathbf{u}^{n+1}_g$ and $\mathbf{u}^{n+1}_d$, respectively.

11. Solve the continuity equation of droplet phase Eqn(3.50) for normalized volume fraction of droplet, Θ_d^{n+1}. The volume fraction of the droplet phase is found using the relation $\vartheta_d = \vartheta_0 * \Theta_d$. Volume fraction of gas phase is obtained by using the relation $\vartheta_g = 1 - \vartheta_d$.

12. Solve the continuity equation of gas Eqn.(3.51) for obtaining gas phase density, ρ_g^{n+1}.

13. Solve the energy equation for the droplet phase Eqn.(3.52) for droplet temperature T_d^{n+1}.

14. Solve the evaporated fuel vapour mass fraction Eqn.(3.53) to obtain Y_F^{n+1}.

15. Solve the gas-phase energy Eqn.(3.54) to obtain T_g^{n+1}.

16. If the stopping criterion for the time stepping is not met return to step 2 and repeat steps 2 through 15 for the next time step and march forward in time.

3.10 Implementation of the Algorithm

The following limiters have been implemented for the algorithm to give converged solution for smaller particle/droplet diameters.

3.10.1 Limiter for Θ_d equation

If for a cell $\Theta_d^n < \epsilon$ ($\sim 1e-4$) we put $A^n = 0$ and $C_v = 0$. Otherwise, put $C_v = 1$ and compute and store A using n^{th} level variable values by the aforementioned relationship. The value of ϵ implies that we are not allowing the diameter of the droplet to fall below a certain value which depends on the droplet initial diameter and volume fraction. The value of C_v used in the equations becomes zero when the diameter of the droplet reaches this particular value. When $C_v = 0$, all the inter-phase mass, momentum and energy transfer terms go to zero resulting in only the convection of the smallest droplets by the gas.

3.10.2 Enforcing gas-phase and droplet-phase velocity equality

When very small particles/droplets are released in a moving gas stream, they acquire the velocity of the carrier-phase in a matter of few milli-seconds. We enforce this condition when the volume fraction of the droplet phase reduces to such a small value that the droplet diameter is only a few microns. Therefore, for a cell if $\Theta_d^n < \epsilon$ then we put $\mathbf{u}_d^n = \mathbf{u}_g^n$. This also enforces the condition that drag force, $\boldsymbol{f}_d{}^n = 0$ in those cells.

3.10.3 Enforcing T_d is constant after heat-up period

Once the temperature of the droplet reaches the saturation temperature (wet-bulb temperature), the heat provided to the droplet from the gas phase is utilized completely in providing the heat of vaporization. In other words, $\dot{Q} = \dot{Q}_e$ making the source term in Eqn.(2.13) zero. But, in actual numerical implementation, it is seen that there is a small difference in $\dot{Q}$ and $\dot{Q}_e$, and Eqn.(2.13), the term $n\dot{Q} - n\dot{Q}_e$ is magnified by being divided by $\vartheta_d \rho_d$. This leads to convergence problems for the T_d equation. In order to overcome this problem, the source term in Eqn.(2.13) is made zero as soon as T_d reaches the saturation temperature. We check whether saturation temperature has reached by checking if $B_M - B_T <= 0.0001$. If so, we enforce $\dot{Q} - \dot{Q}_e = 0$.

Chapter 4

Results and Discussion

We first check whether the flow solver satisfies the principle of mass conservation. This is not as simple as it looks, for mass conservation has to be *enforced* by the continuity equation for a flow with variable density (caused by evaporation).

4.1 Validation of the Flow Solver from First Principles

We consider a simple channel flow problem for the validation. The domain is shown in the Figure 4.1. We consider a uniform flow of n-heptane droplet-laden air flowing

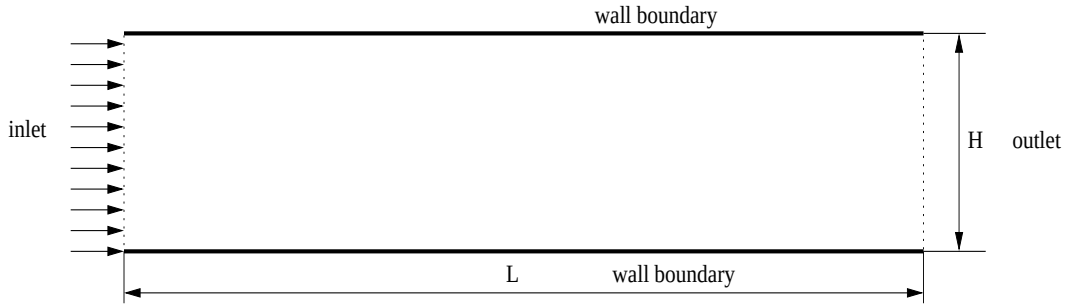

Figure 4.1: The Computational Domain

through the considered domain. We assume a constant rate of evaporation for the droplet phase, the value of $\lambda_{st} = 0.3\, mm^2/s$ which is the steady state evaporation rate for n-heptane. The problem parameters are described below:-

1. $H = 0.1\, m\, , L = 1.0\, m\, ,\, u_{g,in} = u_{d,in} = 1.0\, m/s\, , Re = 100$

2. $\vartheta_d = 0.0005$, $\rho_g = 1.225\, kg/m_3$, $\rho_d = 684.0\, kg/m^3$

At the walls a free-slip condition is specified for the carrier phase velocity and disperse phase velocity. The Reynolds number is based on the channel height. Inorder to get Re=100, the viscosity of carrier phase is considered as $1.225X10^{-3}$.

The check for mass conservation is essentially checking for the mass flow rates of different phases at different sections in the flow direction. Due to the evaporation of droplets the mass flow rate of the droplet phase is gradually reducing in the direction of the flow and the reverse is true for the carrier phase. But the sum of these two should remain close to constant, as the velocity of both phases are nearly identical.

The mass flow rate at any section may be obtained by integration. The mass flow rate for the carrier gas phase is given by

$$\dot{m}_g = \int_0^H \rho_g\, u_g\, dA$$

The mass flow rate for the disperse phase at the same location is given by

$$\dot{m}_d = \int_0^H \rho_d\, \vartheta_d\, u_d\, dA$$

The total mass flow rate at any cross section is $\dot{m}_{total} = \dot{m}_g + \dot{m}_d$ which must be constant along the flow direction under steady state flow conditions. The values of $\dot{m}_g$,$\dot{m}_d$ at the inlet and outlet section are given in the Table**??**.

Table 4.1: Mass Conservation

Mass flow rate	At Inlet	At outlet
Carrier Phase	1.22438750 (kg/s)	1.56599992 (kg/s)
Droplet Phase	0.34200000 (kg/s)	0.00003420 (kg/s)
Total flow rate	1.56638750 (kg/s)	1.56603412 (kg/s)

From the Table, it is observed that mass is conserved with an error of 0.0225%.

4.2 A Few Basic Test Problems

We now move onto a couple of basic problems in order to validate the solver. We use a one-way coupling in these cases, that is to say that the disperse phase is affected by

the fluid phase, but not vice-versa (the discretized equations are modified to achieve this, by removing the appropriate source terms).

We first consider the case of a freely falling droplets in a quiescent medium (which is air in this case). The problem schematic and grid used are shown in the Fig. 4.2 and 4.3 respectively. We consider two cases

1. Non-evaporating droplets (particles) are allowed to fall under gravity in a stationary fluid.

2. Evaporating droplets are allowed to fall under gravity in a stationary fluid.

In both these cases the solution obtained with our solver is compared with the solution of the Lagrangian formulation. The disperse phase droplets are released into quiescent carrier phase at a very low velocity ($0.0001\ m\,s^{-1}$). The droplets are moving under the influence of gravity. Due to drag between the droplet phase and the carrier phase, the velocity of the droplets increases until terminal velocity is reached. The equation of motion for a particle falling freely under gravity in a quiescent fluid in the Lagrangian formulation is

$$\rho_d \frac{du_d}{dt} = F_{drag} + \rho_d\, g$$

The drag force F_{drag} is computed using the relations in our solver that are outlined in Chapter 2. As can be readily seen this is a simple ordinary differential equation which may be solved numerically by the Runge-Kutta method, to provide an "exact" solution for comparing with the solution of the Finite-volume solver.

4.2.1 Freely Falling Particles in a Stationary Fluid

We test the code for non-evaporating fuel (n-Heptane) droplet for two case (a) particle diameter of $100\,\mu\,m$ and (a) particle diameter of $50\,\mu\,m$ with density of $684.0\,kg\,m^{-3}$ freely falling under gravity. The numerical solutions obtained by the solver and from the Runge-Kutta method are compared in Figure 4.4. From Figure 4.4 we observe that the terminal velocity is small for smaller particles. Fig. (4.4) shows a good agreement between our solver and the Lagrangian model, thereby verifying the particle dynamics part of the solver.

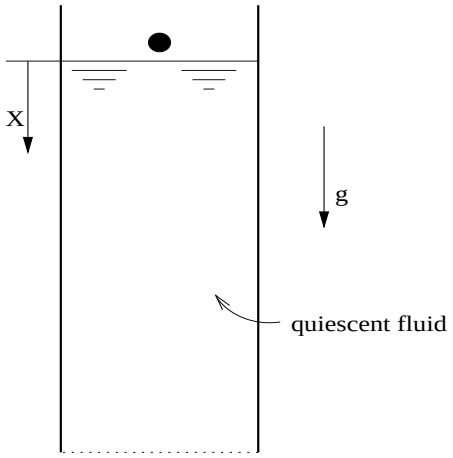

Figure 4.2: Freely Falling Particle in a Stationary Fluid

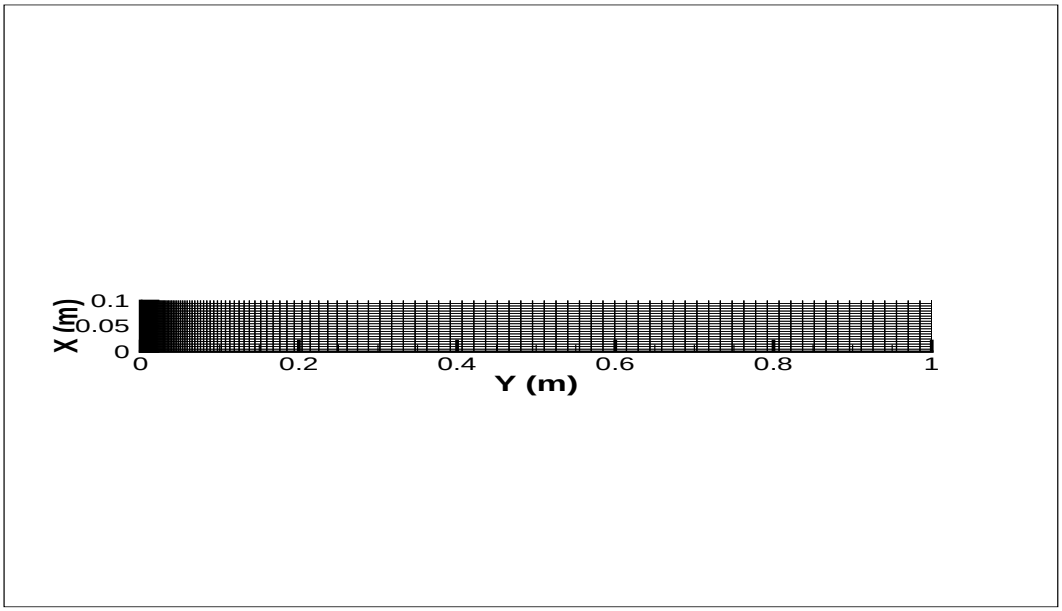

Figure 4.3: Freely Falling Droplets: Grid

4.2.2 Freely Falling Evaporating Droplets in a Stationary Fluid

Freely falling evaporating droplets in a quiescent medium (air) is the next test that we consider. The equation of motion for an evaporating droplet falling freely under gravity is same as discussed in the section 4.2. The grid used is also same as that

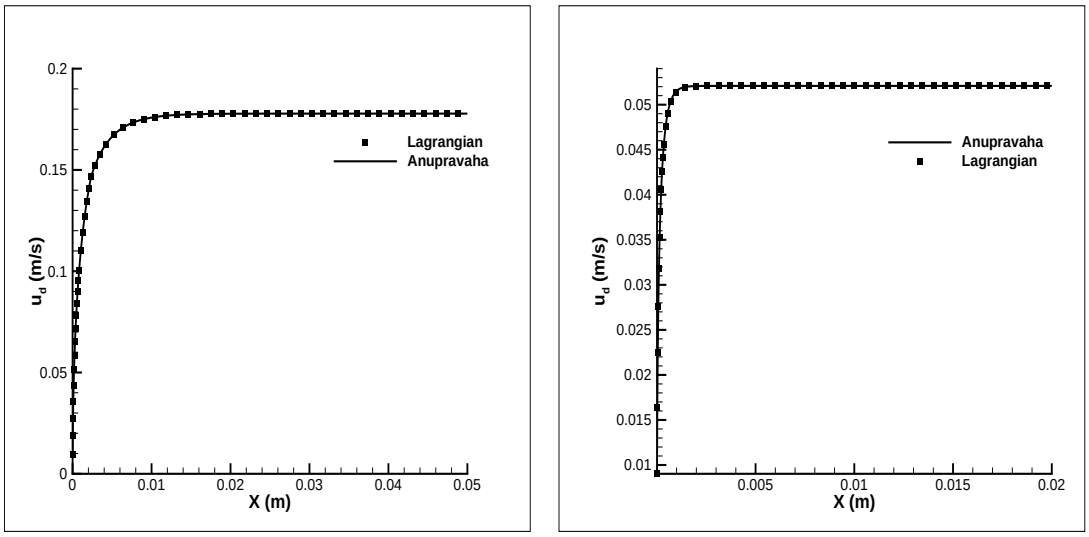

(a) **(b)**

Figure 4.4: Freely Falling non-evaporating particle in a Stationary Fluid for (a)diameter of $100\,\mu\,m$ (b)diameter of $50\,\mu\,m$

for the particle case. For n-heptane liquid fuel droplet, density $\rho_d = 684.0$ and initial droplet diameter is taken as $50\,\mu m$. The droplet has initial velocity of 0.0001 m/s and is evaporating at a constant rate. The evaporation constant for d^2-law (Eqn. **??**) is $\lambda_{st} = 0.2979\,mm^2/s$. Fig. 4.5 shows a good agreement with our solver and the Lagrangian model. These tests confirm that the particle and droplet dynamics are captured accurately by the solver.

4.3 Evaporation Model: Validation

In literature, we find that evaporation characteristics and the flow characteristics are usually dealt with separately. Hence, to validate our evaporation model, we consider one-way coupling in our solver such that only the droplets are affected by the surrounbding gas phase and not vice-versa. Hence, we do not solve for the gas phase temperature and specify a constant value (again by suitable modifications). Four different datasets, pertaining to low pressure, low and moderate evaporation rate conditions are utilized to evaluate and compare our evaporation model with literature results. All results are for a single, isolated droplet evaporating in an infinite, constant temperature and constant velocity/quiescent air environment which is assumed to be unaltered by the droplet presence. Since, all the cases considered are for single droplets, the evaporation

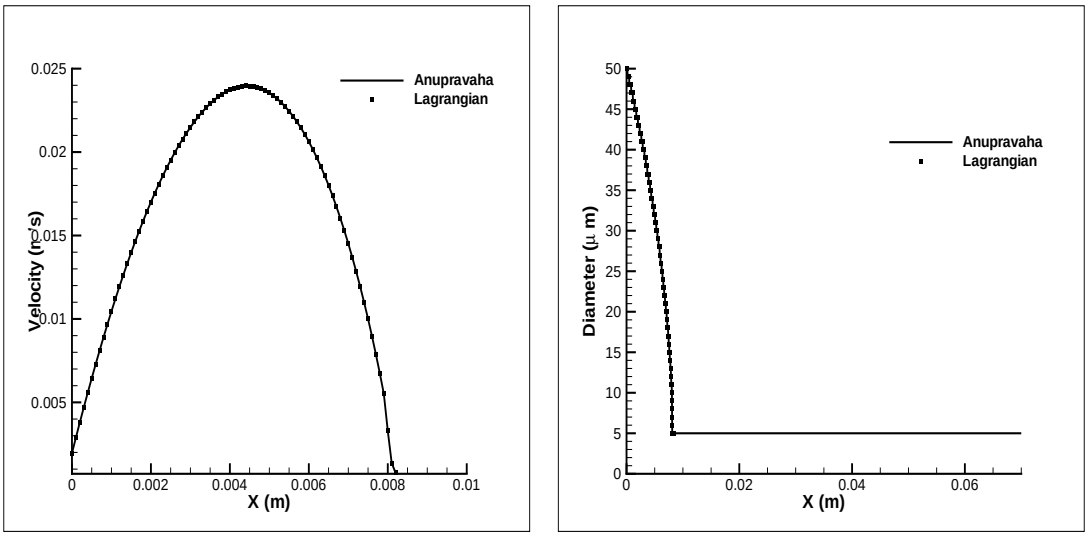

(a) (b)

Figure 4.5: Freely falling evaporating droplet in a stationary fluid (a)velocity profile (b)diameter profile

rate of the droplet depends only on the temperature difference between both the phases apart from the properties of the phases and the initial droplet diameter. Our solver is implemented such that the mass fraction of the evaporated fuel in the surrounding gas-phase plays an important role in determining the evaporation rate. In order to simulate results for a single droplet, we refrain from solving for evaporated fuel mass-fraction and specify it as zero. For the present cases of evaporation of stationary droplets, the definition of Reynolds number is based on the gas phase velocity. Comparisons with experimental results are made for low and moderate evaporation rates as determined by the air temperature relative to the boiling point of the liquid droplets. The liquid species considered in these cases are n-heptane and n-hexane. Property values for the species used are given in A.1.2 and A.1.3 respectively. The different cases are as follows:

4.3.1 Single n-heptane droplet evaporating in quiescent environment

Spalding's classical model of evaporation is implemented in the current solver and hence we test the evporation characteristics predicted by our solver with the results obtained from Chin and Lefbvre[4]. This test is for an n-heptane fuel droplet evaporating in a quiescent atmosphere. The results are obtained for a droplet of $200\,\mu m$ diameter, in

Table 4.2: Heat-Up Period: Comparison

Parameter	Present	Chin and Lefebvre [4]
Heat-Up Period (ms)	38.0	32.8
d_d After Heat-Up (μm)	184.0	187.0
$T_{S\,st}$ (K)	341.91	341.80
λ_{st} (mm^2/s)	0.302	0.300
Total Drop Lifetime (ms)	158.0	138.0

air at normal atmospheric pressure and a temperature of 773 K. The initial drop temperature is 288 K. Chin and Lefebvre[[4] has predicted the evaporation characteristics for n-heptane fuel with an analytical solution obtained from Spalding's model. The variation of drop diameter, drop diameter squared and surface temperature during the heat-up period are compared with the results obtained by that of Chin and Lefebvre[4], who have given only the transient period data. The results are shown in Figures 4.6 and 4.7. Table 4.2 shows the comparison of the values of various parameters. It can be observed that a close match is obtained, thereby verifying the correct implementation of the evaporation module in the solver.

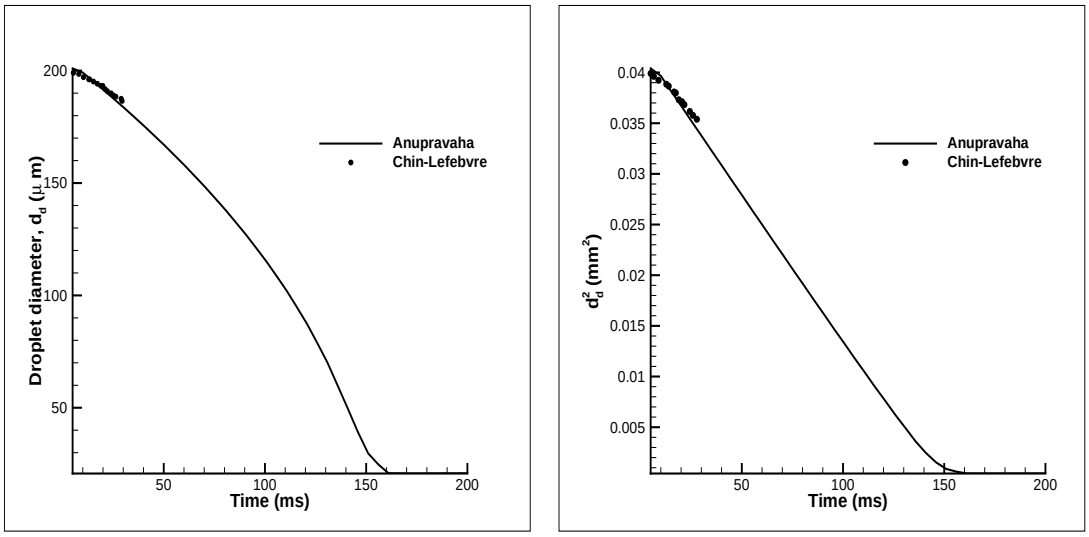

(a) **(b)**

Figure 4.6: Temporal evolution of the (a) droplet diameter (b) droplet diameter square of n-heptane. Conditions are: $T_\infty = 773\,K$, $T_{d0} = 288\,K$, $d_{d0} = 200\mu\,m$.

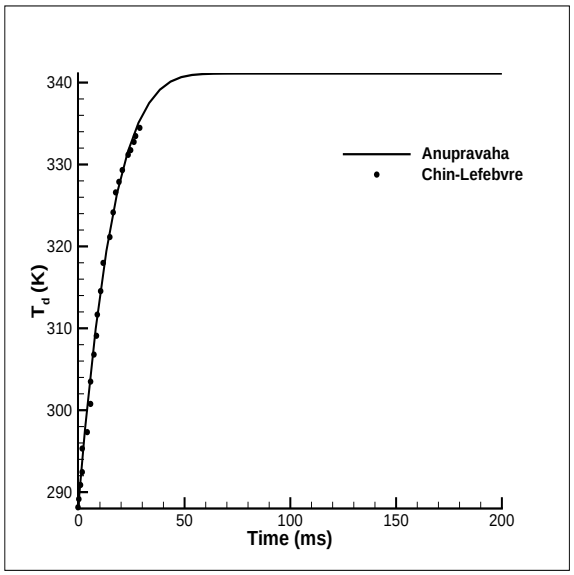

Figure 4.7: Variation of surface temperature during heat-up period for n-heptane

4.3.2 Small n-heptane droplet evaporation in a quiescent environment

In this case, we test the solver's capability for solving gas-droplet flows with smaller droplet sizes. We consider three cases with different diameters and ambient temperatures. In the first case, we consider an n-heptane droplet of initial diameter $d_{d0} = 70\,\mu m$ and temperature $T_{d0} = 293\,K$ evaporating in a quiescent environment and temperature with $T_\infty = 1000\,K$ and pressure, $p = 0.1\,MPa$. We compare the results with the experimental and numerical results given in Frolov et al. [13]. The temporal variation of droplet diameter squared is shown in Fig. 4.8. Experimental results for the droplet temperature are not available, hence we compare our results with theoretical results of Frolov et al. [13] where an analytical solution for the drop temperature based on the thermal conductivity of the droplet liquid was used to predict the mean droplet temperature and surface temperature of the drop. We consider two cases for comparison: droplet diameter of $d_{d0} = 50\,\mu m$ with ambient temperature of (a) $T_g = 1000K$ and (b) $T_g = 1500K$. Since, the model used by Frolov et al. differs from the infinite conductivity model used in our solver, there is some difference between the solutions in Fig. 4.8. But the saturation temperature predicted by the current solver matches with the predicted results of Frolov et al. [13].

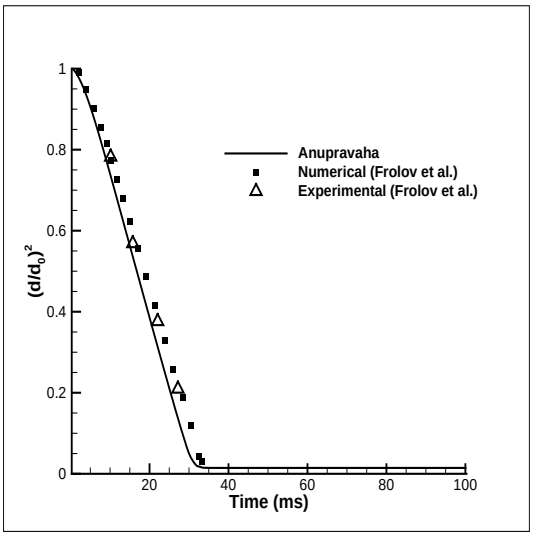

Figure 4.8: Temporal evolution of the droplet diameter squared for n-heptane. Conditions are: $T_\infty = 1000\,K$, $T_{d0} = 293\,K$, $d_{d0} = 70\,\mu m$.

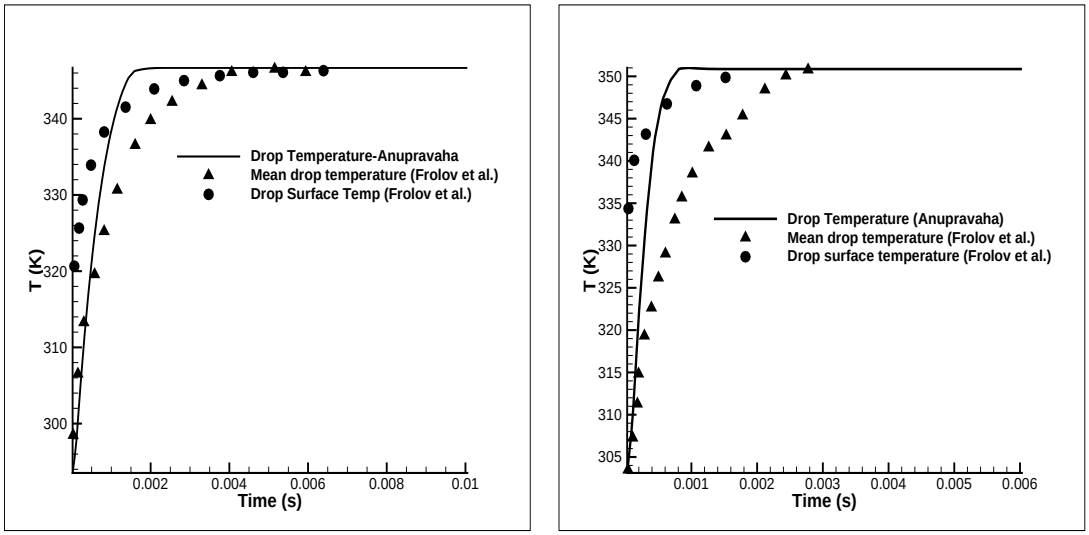

(a) **(b)**

Figure 4.9: Droplet temperature variation with time for: (a) $T_g = 1000\,K$ (b) $T_g = 1500\,K$. Conditions are: $T_{d0} = 293\,K$, $d_{d0} = 50\mu\,m$.

4.3.3 Single n-heptane droplet evaporation in a a gas stream

In this case, we consider the effect of convection on the evaporation of a single droplet. We consider an n-heptane droplet of initial diameter $d_{d0} = 1.052\,mm$ and temperature

$T_{d0} = 300\,K$ evaporating in a air stream of constant velocity $U_\infty = 3.2\,m/s$ and temperature, $T_\infty = 356\,K$, and compare our results with the empirical time evolution of the droplet diameter was recorded by Daif et al. [6] utilizing a CCD camera. Results are also compared with the numerical results of Kolaitis et al. [20]. Figure 4.10 shows the comparison between experimental data and computational predictions for the temporal evolution of the droplet diameter squared. Fig. 4.10 shows that the present solver does an excellent job of predicting the empirical data.

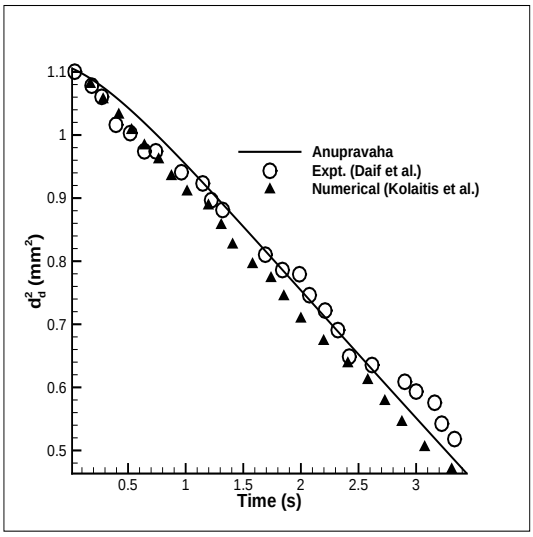

Figure 4.10: Temporal evolution of the droplet diameter squared for n-heptane. Conditions are: $T_\infty = 356\,K$, $T_{d0} = 300\,K$, $d_{d0} = 1.052\,mm$ and $U_\infty = 3.2\,m/s$.

4.3.4 Hexane single droplet evaporation in a gas stream

We consider a hexane droplet with a initial drop size and temperature of $d_{d0} = 1.76\,mm$ and temperature $T_{d0} = 281\,K$, suspended in a convective flow with uniform velocity of $U_\infty = 1.0\,m/s$, for which the gas temperature, $T_\infty = 437\,K$, is nearly one hundred degrees above the liquid boiling point ($T_b = 344.6\,K$) leading to a moderate evaporation rate. The results are compared with the experiments of Downing [8] and numerical results of Miller et al. [24]. From Fig. 4.11(a) shows that the model predicts near linear reduction for d_d^2 with time and matches very well with the results of Miller et al. [24]. Miller et al. have implemented various evaporation models by including the classical equilibrium evaporation models and non-equilibrium Langmuir-Knudsen fromulations. We compare our results with the predicted results of Miller et al. implemented by

using classical Spalding's evaporation model. However, unlike the low evaporation rate predictions, model used in this study and by Miller et al. substantially over-predicts the evaporation rates. The experiments of Downing [8] do not include temperature measurements, therefore, droplet temperature is compared only with the results of Miller et al. [24] in Fig. 4.11. (b)

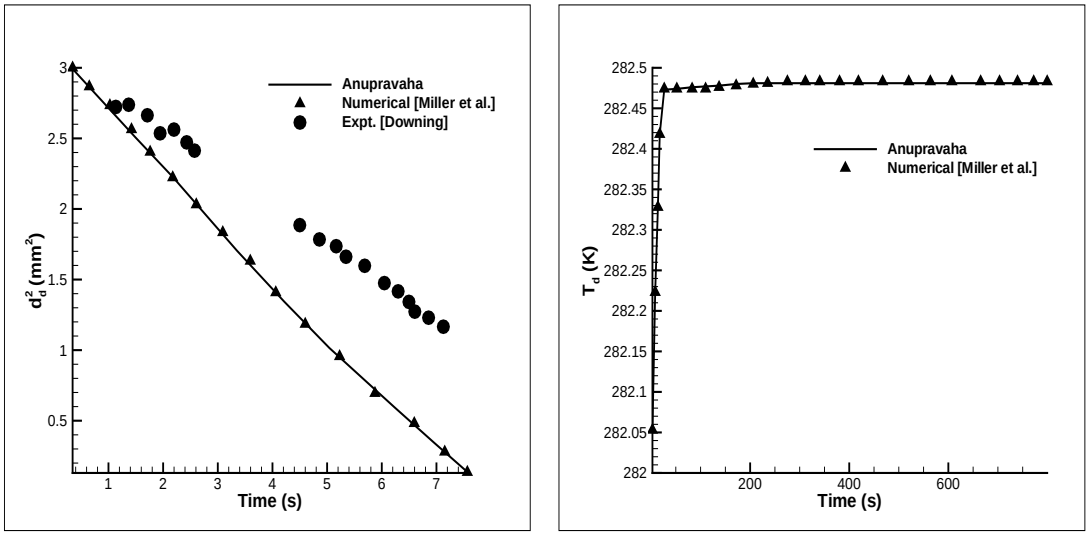

(a) **(b)**

Figure 4.11: Temporal evolution of the (a) droplet diameter (b) Droplet Temperature. Conditions are: $T_\infty = 437.0\,K$, $T_{d0} = 281\,K$, $d_{d0} = 1.76mm$.

4.4 Gas-Particle Flows

We next validate our solver for gas-particle flows for particle diameters of few microns. We consider two cases; flow through a 2D channel flow and flow on a backward facing step. For both the cases, we consider non-evaporating n-heptane particles moving in an air stream.

4.4.1 Gas-Particle Flows Through a 2-D Channel

This problem deals with gas-particle flows in a 2D channel having uniform velocity profiles at inlet for both gas and particle phase. We consider a 2D channel domain of length $L = 5.0m$ and height $H = 0.1m$ as shown in Fig. (4.12). The inlet conditions considered in this case are given in Table 4.3. No slip boundary conditions are applied for the gas phase at the walls. The results are compared with those of commercial software ANSYS FLUENT. Velocity profiles of gas-phase and particle-phase are plotted at three different sections in the channel; (a) at $X = 1.0m$, $X = 2.5m$ and (c) at $X = 4.0m$ and are shown respectively in Fig. 4.13, 4.14 and 4.15. It is observed that near the outlet the velocity profiles lag behind the profiles obtained by FLUENT. This is possibly because we impose a strict coupling between both the phases in terms of drag force, while FLUENT seems to switch the drag force "off" when the particle sizes fall below $10\mu\, m$.

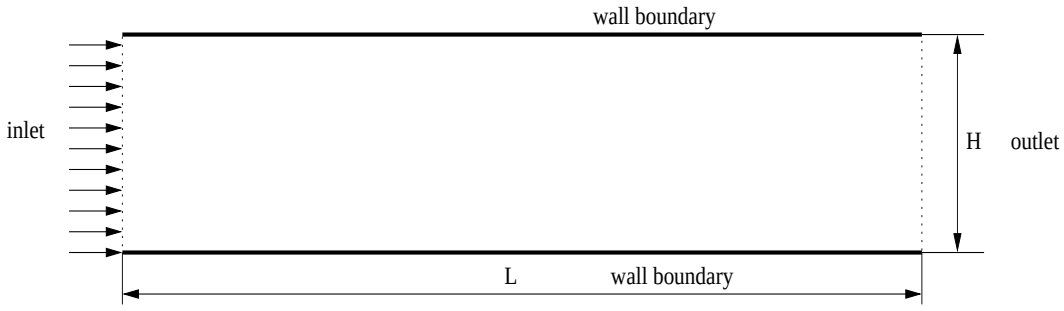

Figure 4.12: The Computational Domain for Gas-Particle flow in a 2D channel

4.4.2 Gas-Particle Flows on a backward facing step

We consider a 2D channel domain of length $L = 7.5m$ with inlet $H = 0.05m$ and step size $= h = 0.05m$ as shown in Fig. (4.16). The inlet conditions considered in this case are given in Table 4.4. The viscosity of air is changed such that $Re = 100$.

Table 4.3: Inlet conditions and property values

Inlet Conditions	
Gas-phase inlet velocity	1.0 m/s
Particle-phase inlet velocity	1.0 m/s
Inlet volume fraction	0.0005
Particle inlet diameter	5μ m
Property Values	
Viscosity of gas	$1.7894e^{-5} Ns/\,m^2$
Gas-phase density	$1.225 kg/\,m^3$
Particle-phase density	$684.0 kg/\,m^3$

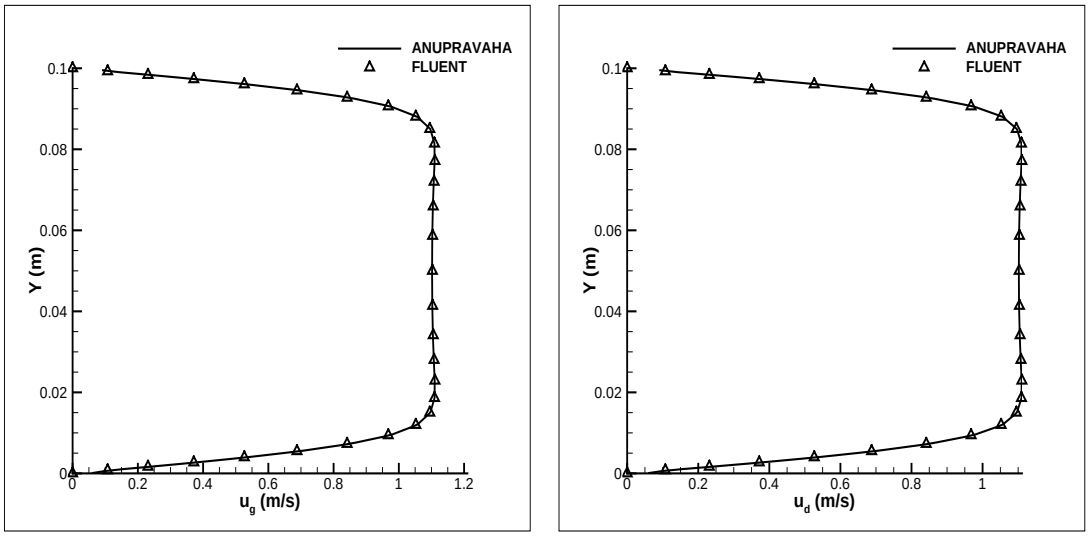

(a) **(b)**

Figure 4.13: Velocity profiles at X=1(a) Gas-phase velocity, u_g (b) Particle-phase velocity, u_d

Here, Re is calculated based on the velocity of the gas phase. Results are compared with the commercial software ANSYS FLUENT. It is seen from Fig. 4.17 that the recirculation-length obtained for Re=100 is same as that of single-phase flows. There is a small difference in the velocity profiles obtained by the present solver and FLUENT owing to the strict drag force coupling considered.

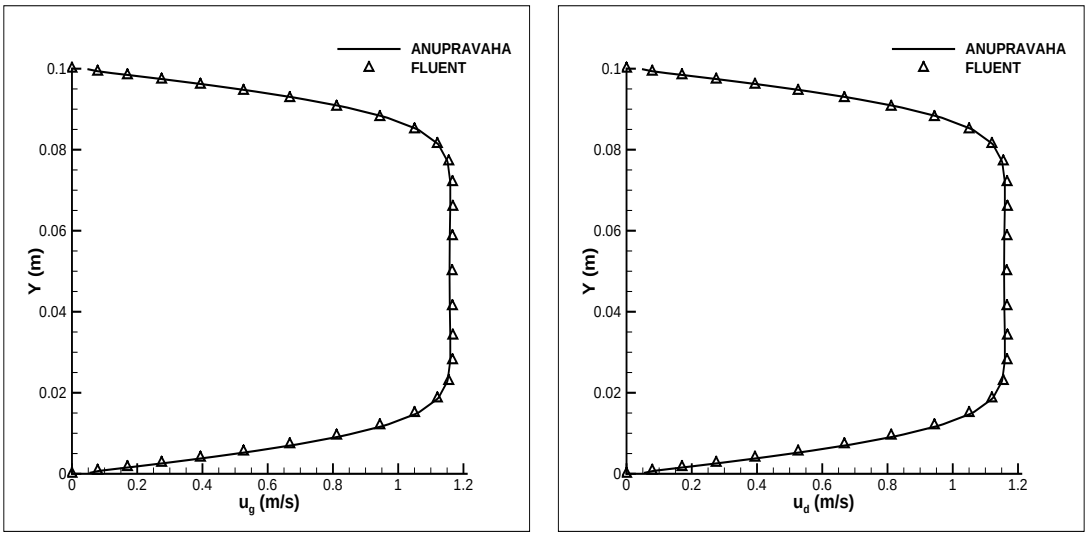

(a) (b)

Figure 4.14: Velocity profiles at X = 2.5 m(a) Gas-phase velocity, u_g (b) Particle-phase velocity, u_d

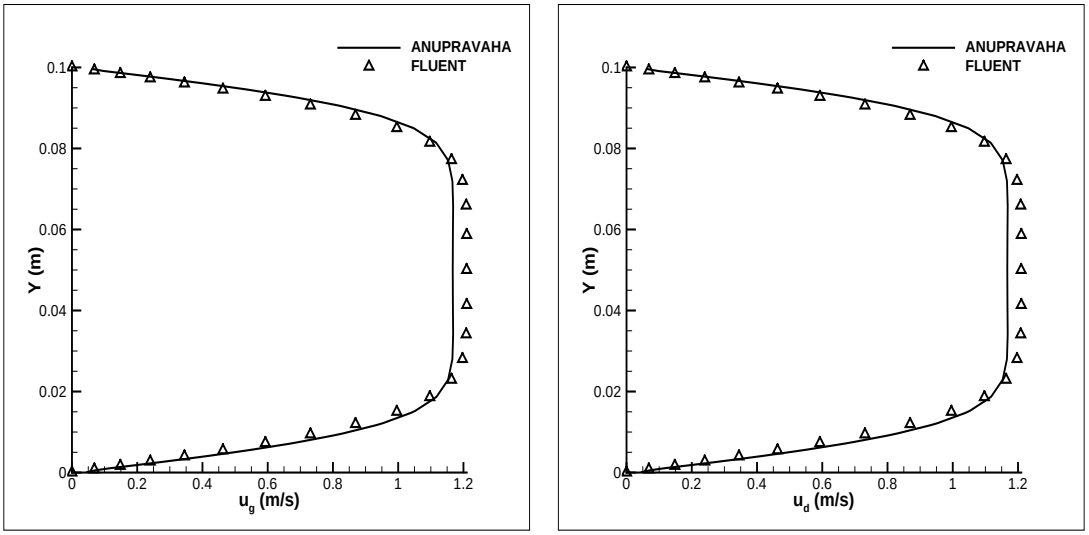

(a) (b)

Figure 4.15: Velocity profiles at X = 4.0 m(a) Gas-phase velocity, u_g (b) Particle-phase velocity, u_d

4.4.3 Points to note

The solver developed in the present work can give converged solution (i.e., convergence of the order of $1e^{-8}$ for all the governing equations) for particle-diameters till 3 $\mu\, m$.

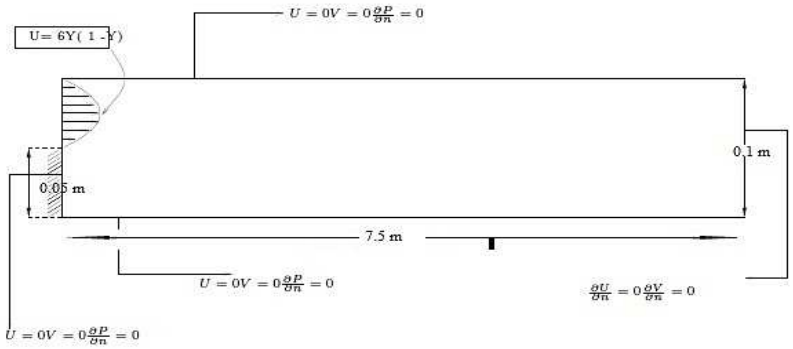

Figure 4.16: Computational domain for flow on a backward-facing step

Table 4.4: Case 2: Inlet conditions and property values

Inlet Conditions	
Gas-phase inlet velocity	1.0 m/s
Particle-phase inlet velocity	1.0 m/s
Inlet volume fraction	0.0005
Particle inlet diameter	20μ m
Property Values	
Viscosity of gas	$0.0003 Ns/\,m^2$
Gas-phase density	$1.225 kg/\,m^3$
Particle-phase density	$684.0 kg/\,m^3$

For gas-particle flows, the momentum equation for gas phase and particle phase are as given in Eqns. (4.1) and (4.2):

$$\frac{\partial\,\mathbf{u}_g}{\partial\,t} + \nabla\cdot(\mathbf{u}_g\,\mathbf{u}_g) - \frac{1}{\rho_g}\,[\,\nabla\cdot(\mu_g\nabla\mathbf{u}_g)\,] = -\frac{1}{\rho_g}\,\nabla P + \mathbf{g} - \frac{\vartheta_d}{\vartheta_g\rho_g}\,\boldsymbol{f}_d + \mathbf{u}_g\,[\,\nabla\cdot\mathbf{u}_g\,] \quad (4.1)$$

$$\frac{\partial\,\mathbf{u}_d}{\partial\,t} + \nabla\cdot(\mathbf{u}_d\mathbf{u}_d) = \mathbf{g} + \frac{1}{\rho_d}\,\boldsymbol{f}_d + \mathbf{u}_d\,[\,\nabla\cdot\mathbf{u}_d\,] \quad (4.2)$$

The convergence of the above two equations depends on the coupling term. The coupling term between both the phases is the drag force term, $\mathbf{F}_d \propto \vartheta_d\,\mathbf{f}_d$. On closer

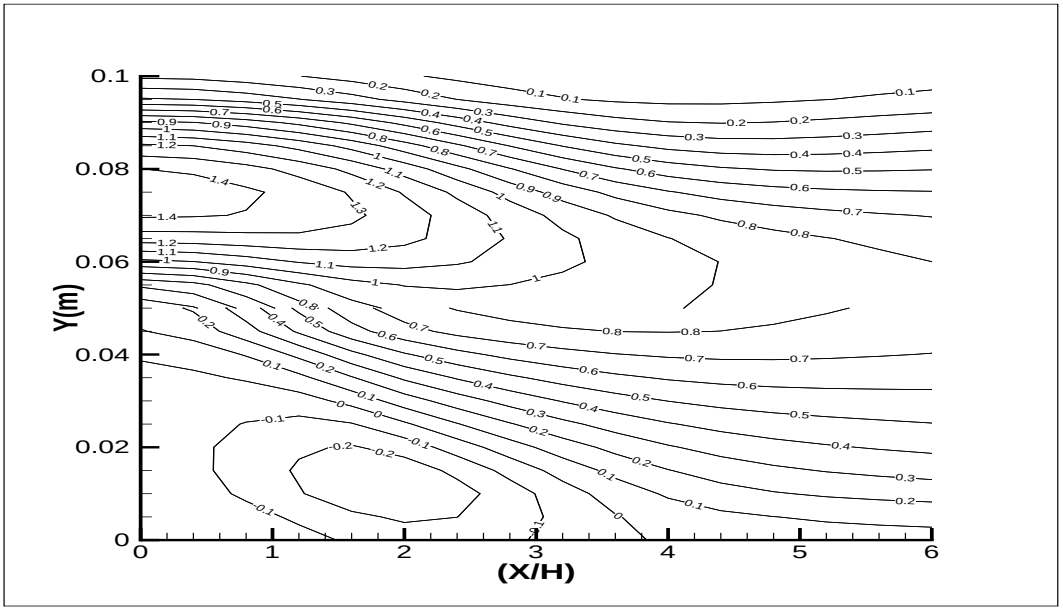

Figure 4.17: Contour plot for flow over a backward-facing step for $Re = 100$

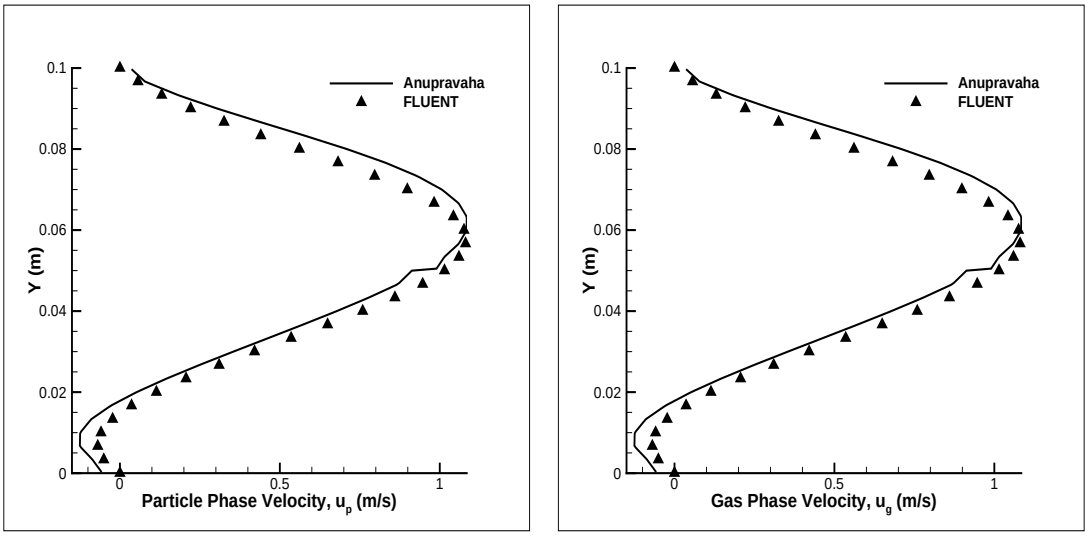

(a) **(b)**

Figure 4.18: Velocity profiles at X = 3.0 m(a) Gas-phase velocity, u_g (b) Particle-phase velocity, u_d

inspection, we find that Drag force, $\mathbf{F}_d \propto \frac{\vartheta_d \mu_g}{d_d^2}$. For smaller particle-diameters, this term becomes quite large and leads to convergence problems. In order to relax the coupling between the phases, the drag force per unit volume , $\mathbf{f}_d$ can be constrained by two methods

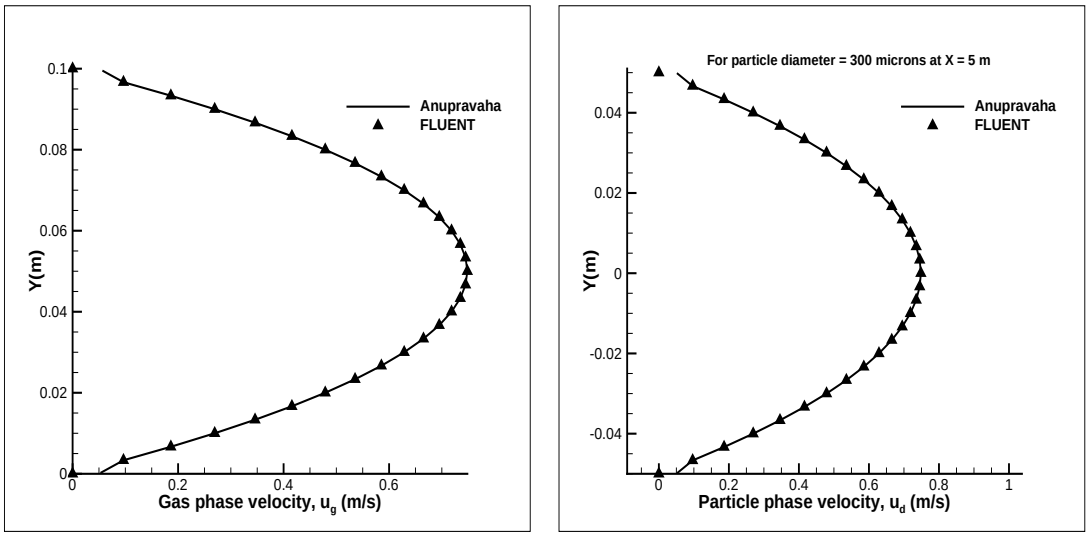

(a) **(b)**

Figure 4.19: Velocity profiles at X = 5.0 m(a) Gas-phase velocity, u_g (b) Particle-phase velocity, u_d

1. by keeping $\mathbf{f}_d$ as a constant for all diameters below a certain nominal diameter, say, $20\mu\, m$.

2. by considering a lower value of viscosity of the gas-phase, μ_g. But, this approach may lead to a small error in the solution.

Another approach to address this issue would be by increasing the central co-efficient of the equation by taking a smaller value of time-step, $\Delta\, t$. This is the approach we follow in the current solver. Table 4.5 gives the time step to be taken for solving gas-particle flows for the considered particle-diameters.

Table 4.5: Time-step values to be considered for air-particle flows

ϑ_d	$\Delta\, t$	converged solution for least particle diameter
0.0005	$1e^{-3}$	$20\mu\, m$
0.0005	$1e^{-4}$	$6\mu\, m$
0.0005	$1e^{-5}$	$2\mu\, m$

4.5 Gas-Droplet Flow Through 2-D Channel

Having validated the flow gas-droplet flow solver against basic cases and the evaporation model against available literature, we now attempt to solve few complete problems of gas-droplet two-phase flows with evaporation. We consider five problems of gas droplet flows varying only in boundary conditions and deal with n-heptane liquid droplets moving in air in a channel having uniform velocity profiles at inlet for the gas-phase as well as for the droplet-phase. For the first four problems, the droplet inlet temperature is assumed to be equal to the saturation temperature. This assumption simplifies the problem as we need not consider the transient liquid droplet heating and the droplet temperature remains at saturation temperature throughout its lifetime. For the fifth problem, the inlet temperature of the droplets is taken to be less than the saturation temperature. Since the above problems also require the use of the energy transport equations for both the phases, we check whether the solver enforces the principle of energy conservation for these test cases.

4.5.1 Energy Conservation:

The principle of energy conservation states that for a steady flow process the total energy entering into the system is equal to the total energy leaving the system when no net work is being done by the system. Considering the gas, liquid droplet and vapour as separate species, for a steady one dimensional gas droplet flow, the energy balance equation can be written as

$$\underbrace{\dot{m}_{gi}\, C_{pgi}\, (T_{go} - T_{gi})}_{A} + \underbrace{\dot{m}_{d}\, C_{ld}\, (T_{s} - T_{di})}_{B} + \underbrace{\dot{m}_{d}\, C_{vd}\, (T_{do} - T_{s})}_{C} + \underbrace{\dot{m}_{d}\, L}_{D} = 0 \tag{4.3}$$

where A denotes the change in energy of the gas-phase, B is the sensible heat for liquid droplets, C stands for the heating of the vapour and the last term D signifies the latent heat of vaporization for the droplet-phase[1]. Subscript i and o denote the values of the parameters at inlet and outlet condition respectively. Rearranging the terms in the Equation 4.3 gives

$$\dot{U}_{out} = \dot{U}_{in} - \dot{m}_{di}\, L - \dot{m}_{di}\, (C_{ld} - C_{vd})\, (T_{s} - T_{di}) \tag{4.4}$$

[1]It is assumed here that the flow work against friction is negligible compared to the enthalpy differences involved, and also that the droplet phase has evaporated totally at the outlet.

where, for the purpose of analysis $\dot{U}_{in}$[2] and $\dot{U}_{out}$ are defined as

$$\dot{U}_{in} \equiv \dot{m}_{gi}\, C_{pgi}\, T_{gi} + \dot{m}_d\, C_{vd}\, T_{di} \tag{4.5}$$

and

$$\dot{U}_{out} \equiv \dot{m}_{go}\, C_{pgo}\, T_{go} \tag{4.6}$$

Note that the above balance rule can be easily modified for two or three dimensional cases where each term has to be obtained by integration over the control surfaces. For example,

$$\dot{U}_{in} = \int_0^H \vartheta_{gi}\rho_{gi}\, u_{gi}\, C_{pgi}\, T_{gi}\, dA + \int_0^H \vartheta_{di}\rho_d\ u_{di}\, C_{vd}\, T_{di}\, dA \tag{4.7}$$

and

$$\dot{U}_{out} = \int_0^H \vartheta_{go}\rho_{go}\, u_{go}\, C_{pgo}\, T_{go}\, dA \tag{4.8}$$

Mass and energy conservation is provided in tabular form for the first and fifth problems given in section (4.5.4) and section (4.5.8) which shows that the laws of conservation are very accurately satisfied by the solver.

4.5.2 Insight into Fluent Multi-phase Solver

A brief overview of the Fluent Multi-phase solver is presented before the results of test cases and their comparison with Fluent are presented in the following sections. Both Eulerian-Lagrangian and Eulerian-Eulerian models are available as a part of Fluent Multi-phase solver. For modeling dilute two-phase flows, Fluent recommends the use of Discrete Phase Model (DPM) which is essentially an Eulerian-Lagrangian formulation. Since, we are using an Eulerian-Eulerian formulation for simulating dilute two-phase flows, we use the Eulerian-Eulerian model of Fluent for comparison. The evaporation model incorporated in Eulerian module of Fluent is a simplistic model in which mass transfer depends solely on the gas-phase temperature and droplet-phase density and volume-fraction. The mass transfer rate as given in Fluent Multiphase documentation is [12] as

If $T_g > T_{sat}$

$$\dot{m}_v = coeff * \vartheta_d\rho_d \frac{(T_g - T_{sat})}{T_{sat}}$$

[2]note C_{vd} is used instead of C_{ld} in the last term of the definition of $\dot{U}_{in}$ below just for accounting convenience.

where, the coefficient *coeff* needs to be specified by the user. This evaporation model is not one of the standard models established in literature, and seems to be chosen to overcome the numerical difficulties associated with small-diameter droplet flows. It does not take into account the effect of the amount of evaporated fuel in the gas-phase and there is no direct dependence of evaporation rate on the diameter of the droplet. All these factors enable Fluent to simulate gas-droplet flows evaporation for droplet sizes of even a few microns.

Other differences between Fluent Solver and Anupravaha

Fluent uses the phase-coupled SIMPLE algorithm (PC-SIMPLE) for solving multi-phase flows in which a pressure correction equation is built based on total volume continuity rather than mass continuity [12]. The pressure-correction equation is given by

$$\sum_{k=1}^{n} \frac{1}{\rho_{rk}} \{ \frac{\delta}{\delta t} \vartheta_k \rho_k + \nabla \cdot (\vartheta_k \, \rho_k \mathbf{u}_k^{'}) + \nabla \cdot (\vartheta_k \, \rho_k \mathbf{u}_k^{*}) - \sum_{l=1}^{n} (\dot{m}_{lk} - \dot{m}_{kl}) \} = 0$$

where, ρ_{rk} is the phase reference density for the k^{th} phase. In the present solver, equation for pressure is obtained by enforcing total mass-conservation (Eqn. 3.39). In the current solver, we solve the continuity equation for the gas-phase to obtain the density of the gas-phase. This gives a more accurate value as the density changes due to the addition of evaporated droplet-vapours is accounted for. But, in Fluent, the continuity equation of each phase is solved for obtaining the volume-fraction of the respective phase by diving the continuity equation of the phase with its respective reference density [12].

$$\frac{1}{\rho_{rq}} \left[\frac{\delta}{\delta t} \vartheta_q \rho_q + \nabla \cdot (\vartheta_q \, \rho_q \mathbf{u}_q^{'}) + \nabla \cdot (\vartheta_q \, \rho_q \mathbf{u}_q^{*}) = \sum_{p=1}^{n} (\dot{m}_{pq} - \dot{m}_{qp}) \right]$$

The density of the gas-phase is calculated separately by either using the ideal-gas law, or volume-weighted average or by using any user-defined function. Hence, the density of the mixture after complete evaporation cannot be determined accurately and depends on the user-choice. This leads to significant difference in the predcted values of gas-phase density, ρ_g. Thermodynamic properties like specific heat of gas-phase, C_{pg} and thermal conductivity of gas-phase k_g are calculated based on volume-weighted or mass-weighted average whereas, in the present solver we use "$1/3^{rd} rule$". This may lead to significant difference in the gas-phase temperature predicted by both the solvers.

This discussion serves to emphasize that the following comparisons of Anupravaha results with those of FLUENT do not take the latter as a 'gold standard' but rather

serve to critically evaluate *both* solvers. In this work, for comparing the present solver's results with FLUENT, a user-defined function is written for mass transfer rate given in [**?**].

4.5.3 Computational Domain and Property Values

The domain considered for all the five cases is shown in the Figure 4.20, where $H = 0.1\,m$ and $L = 0.5\,m$. Expressions for the variation of properties for liquid and vapour phase of n-heptane fuel are given in **??**. The property values of gas-phase(air) and droplet phase(n-heptane) which are common for all the cases are shown in Table 4.6.

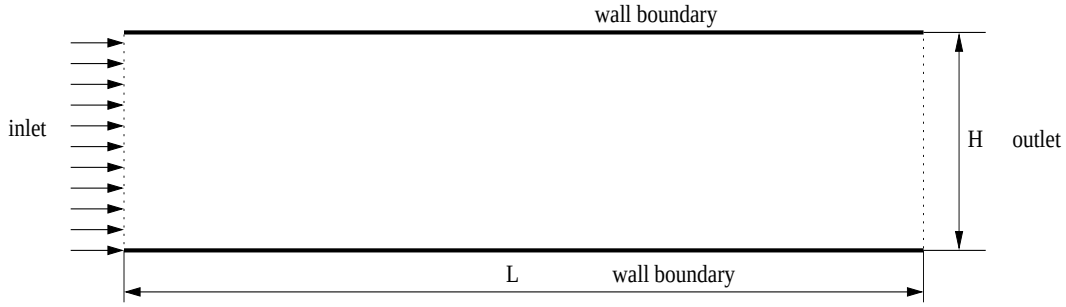

Figure 4.20: The Computational Domain for 2D-Channel Gas-Droplet Flow Problem

Table 4.6: Property values of fluids used

Property values	
Viscosity of gas(at $T = 500K$)	$2.225X10^{-5}\ N\,s/m^2$
Liquid droplet density, ρ_d	$684.0\ kg/m^3$
Specific heat of air, C_{pa}	$1006.43\ J/kg\,K$
Specific heat of fuel vapour, C_{vd}	$2471.0\ J/kg\,K$
Specific heat of liquid droplet, C_{ld}	$2219.0\ J/kg\,K$
Thermal conductivity of air, k_a	$0.0242\ W/m\,K$
Thermal conductivity of fuel vapour, k_v	$0.0128\ W/m\,K$
Latent heat of fuel, L	$320096.0\ J/kg$
Mass diffusivity of vapour in gas, D	$2.26X10^{-5}\ m^2/s$

4.5.4 Gas-droplet channel flow with $T_{di} = T_s$ and $u_{gi} = u_{di}$

In this case, both the gas-phase and droplet phase enter the channel with a velocity of 1m/s when the inlet droplet temperature equal to the saturation temperature of n-heptane ($T_{sat} = 347.2K$ at atmospheric pressure). The inlet properties are given in Table. 4.7. At the wall, the homogeneous Neumann boundary condition is applied for gas-phase velocity and the gas-phase temperature. The latter condition means an insulated boundary condition is applied for temperature while the former implies friction-less ('slip') walls (to avoid friction-work) and ensures a uniform flow profile in the channel. Since, the droplet inlet temperature is equal to the saturation temperature, no transient heating of the droplets takes place and the droplet temperature remains constant at its inlet value while the droplets evaporate due to heating. The conditions are such that the droplets evaporate totally by the end of the channel. The contour plots of the various variables are shown in Fig. 4.21 to Fig. 4.24. The results of both solvers are very close except that Anupravaha stops computing for $\vartheta_d \leq 5 \times 10^{-6}$ due to the difficulties caused by smaller diameter. FLUENT avoids this difficulty by adopting a simplistic evaporation model and by using a constant (inlet) diameter to calculate drag.

The variation of the droplet-phase volume fraction, droplet diameter, gas-phase temperature, fuel mass fraction and gas density along the length of the channel is compared with the results obtained by using the commercial package FLUENT for the same problem. As expected the gas-phase temperature drops off along the length of the channel due to heat transfer from the gas-phase to the droplets. Also the fuel mass fraction and the gas-phase density are seen to increase due to droplet evaporation.

Comparison of the variation of properties along the length of the channel are shown in Fig. 4.25 to Fig. 4.27 (a). It is observed that the predicted values of gas-phase temperature T_g and gas-phase density, ρ_g vary from FLUENT results because of the difference in the method of calculating the concerned properties. It is observed that a constant temperature of droplet ($= T_{sat}$) is maintained through out the channel from Fig. 4.27 (b). The velocity profiles for both gas-phase and droplet-phase are compared with Fluent results at three different sections as shown in Fig. 4.28 to Fig. 4.30. This may be due to the strict coupling enforced by the drag force implemented by the present solver. Within the evaporation zone, the velocity profiles match well with the Fluent results. However, the velocity profiles outside the evaporation zone vary by a small

amount and the fact that Fluent does not update the droplet diameter and hence the changed diameter is not accounted for while calculating drag force. Mass and Energy conservation data are given in Table 4.8 and Table 4.9 and is observed that both are conserved to a high degree of accuracy by the Anupravaha solver.

Table 4.7: Case 1: Inlet conditions

Inlet conditions	
Gas-phase inlet velocity, u_{gi}	1.0 m/s
Droplet-phase inlet velocity, u_{di}	1.0 m/s
Gas-phase inlet temperature, T_{gi}	773.0 K
Droplet-phase inlet temperature, T_{di}	347.8 K
Inlet fuel mass fraction, M_{Fo}	0.0
Gas-phase inlet density, ρ_{gi}	1.225 kg/m^3
Droplet-phase inlet volume fraction, ϑ_{do}	0.0005
Droplet inlet diameter, d_{do}	50 μm

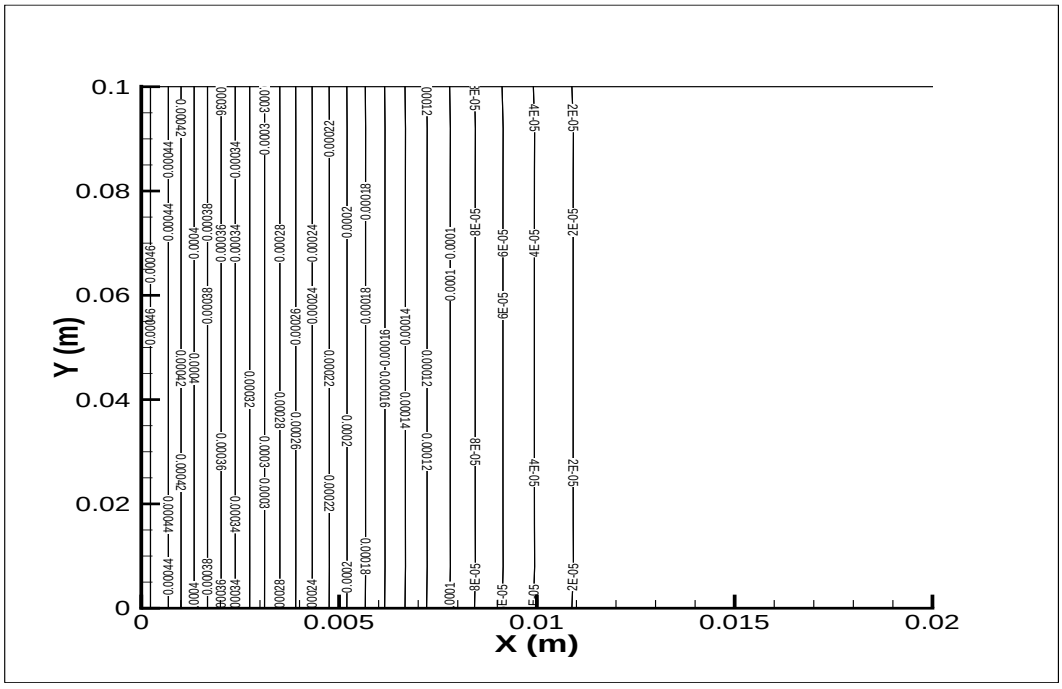

Figure 4.21: Case 1: Uniform flow through 2D Channel. Contour plot for droplet-phase volume fraction

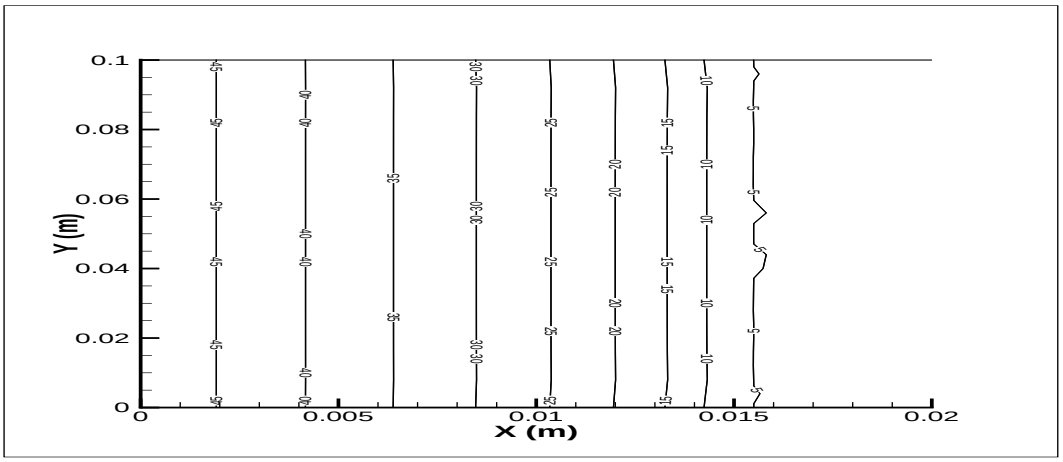

Figure 4.22: Case 1: Uniform flow through 2D Channel. Contour plot for droplet-phase diameter

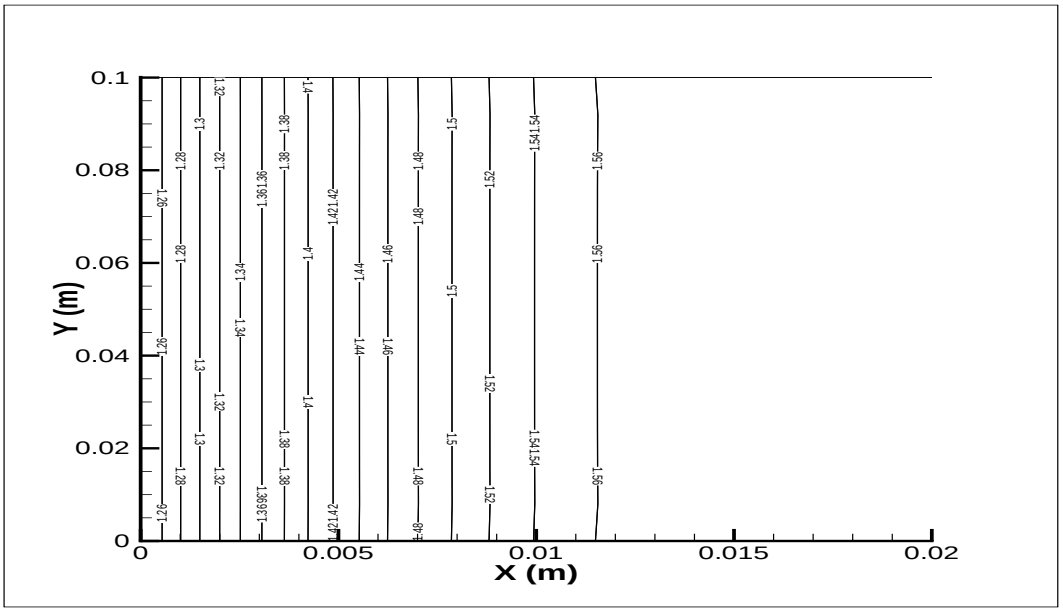

Figure 4.23: Case 1: Uniform flow through 2D Channel. Contour plot for gas-phase density

	$\dot{m}_g$ (kg/s)	$\dot{m}_d$ (kg/s)	Total (kg/s)
Inlet	0.122438	0.034200	0.156638
Outlet	0.156275	0.000343	0.156618

Table 4.8: Case 1: Results for Mass Conservation

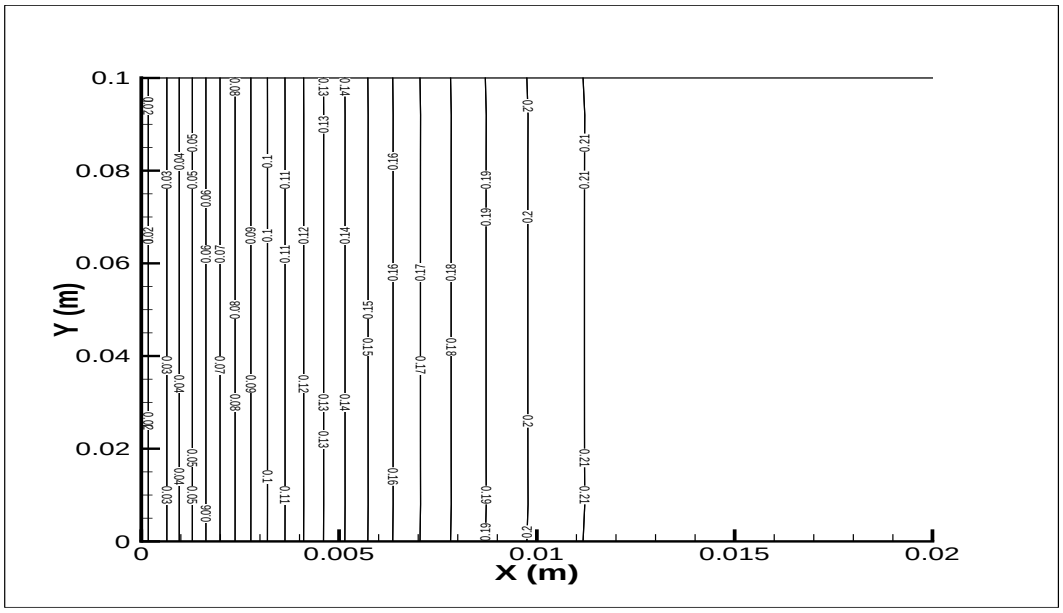

Figure 4.24: Case 1: Uniform flow through 2D Channel. Contour plot for evaporated fuel mass-fraction

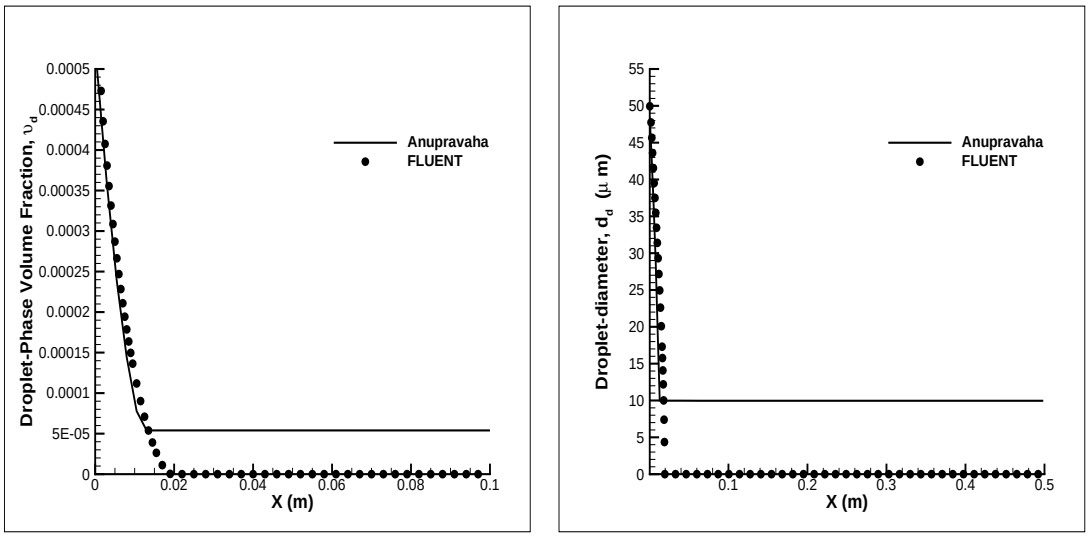

(a) (b)

Figure 4.25: Case 1: Uniform flow through 2D Channel. (a) Variation of droplet-phase volume fraction, ϑ_d along the channel (b) Variation of droplet-diameter, d_d along the channel

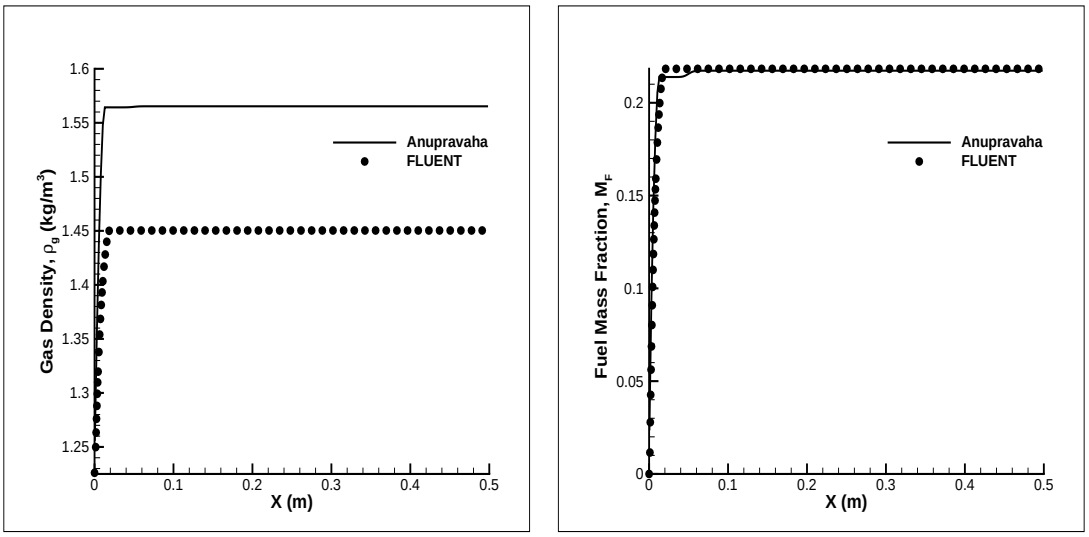

(a) **(b)**

Figure 4.26: Case 1: Uniform flow through 2D Channel. (a) Variation of gas-phase density, ρ_g along the channel (b) Variation of evaporated fuel mass fraction, M_F along the channel

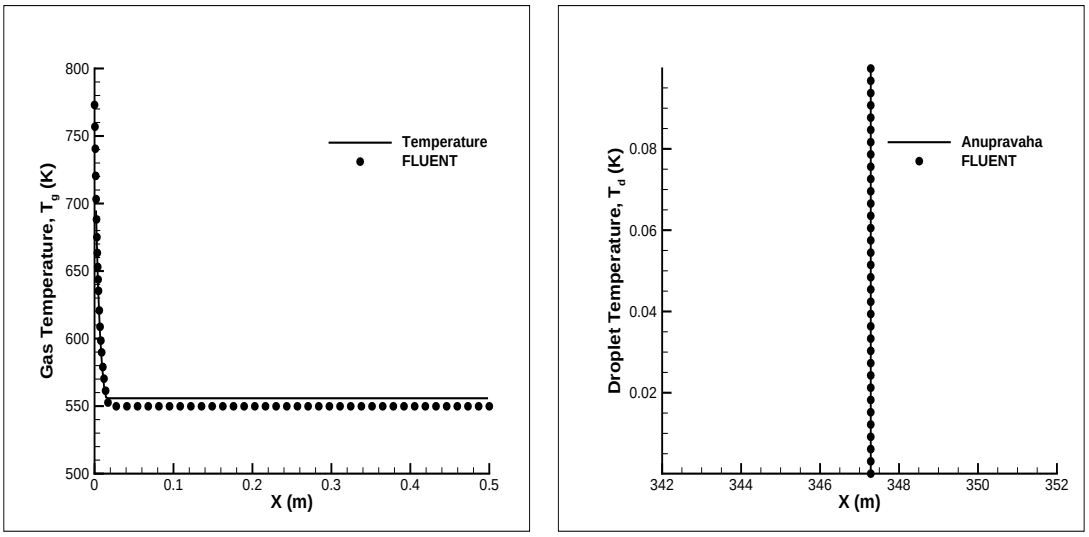

(a) **(b)**

Figure 4.27: Case 1: Uniform flow through 2D Channel. (a) Variation of gas-phase temperature, T_g along the channel (b) Droplet-phase temperature, T_d profile at $X = 0.25m$

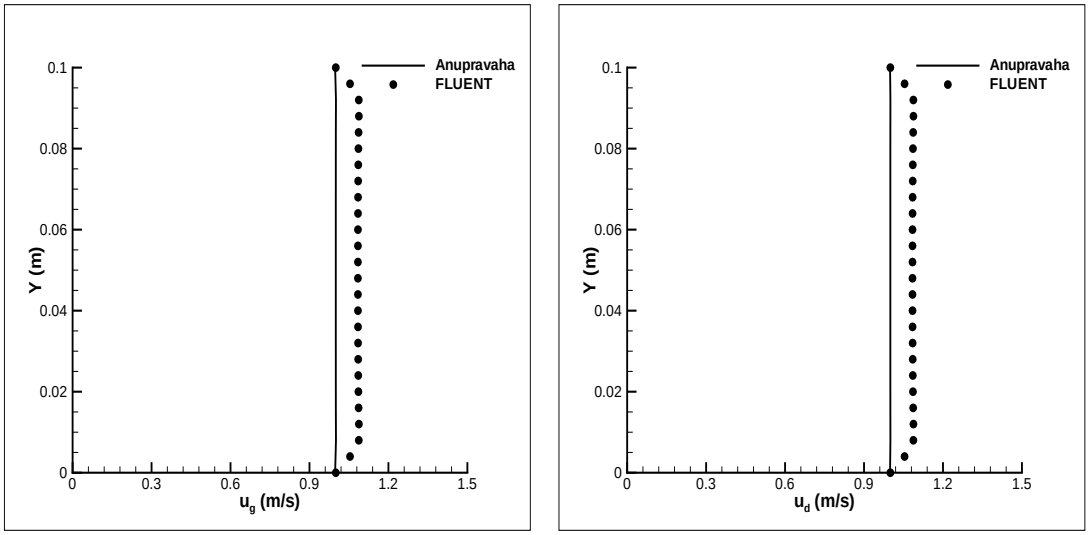

(a) (b)

Figure 4.28: Velocity profiles at X = 0.005 m(a) Gas-phase velocity, u_g (b) Droplet-phase velocity, u_d

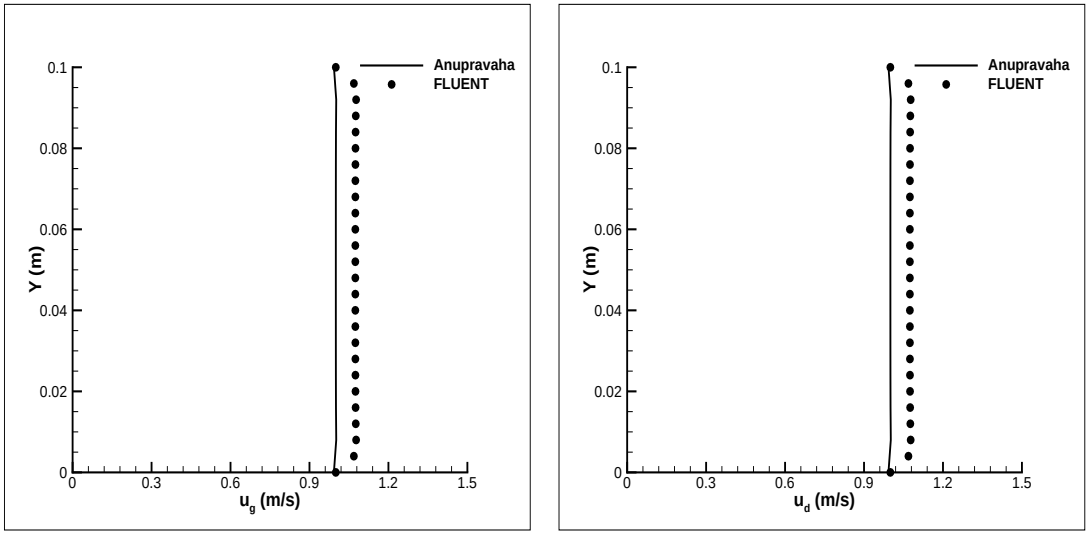

(a) (b)

Figure 4.29: Case 1: Velocity profiles at X = 0.015 m(a) Gas-phase velocity, u_g (b) Droplet-phase velocity, u_d

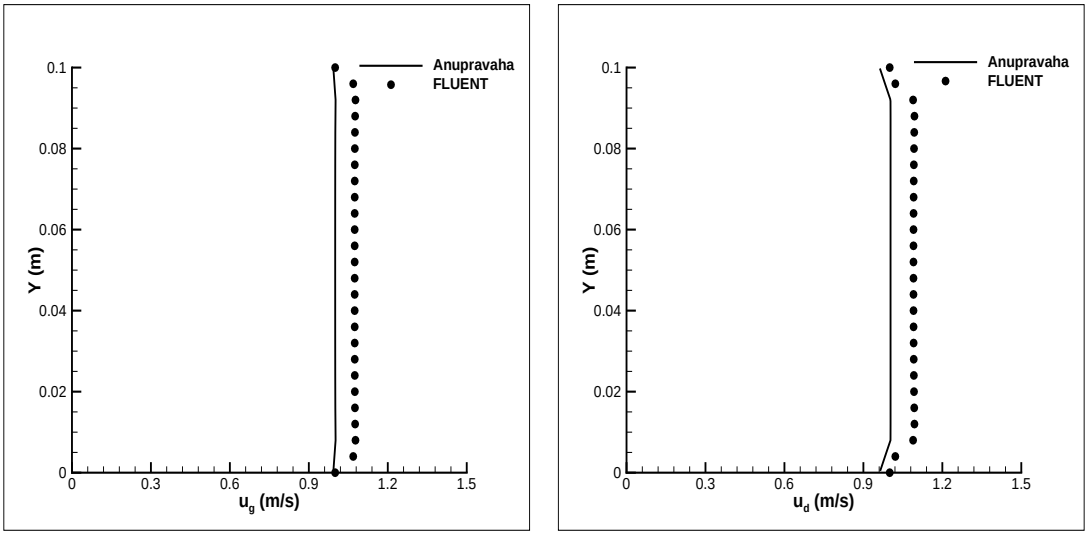

(a) **(b)**

Figure 4.30: Case 1: Velocity profiles at X = 0.1 m(a) Gas-phase velocity, u_g (b) Droplet-phase velocity, u_d

U_{in} (J/s)	126653.9
U_{out} (J/s)	115715.0
Total heat of vaporization (J/s)	10947.3
Total enthalpy spent for heating droplet (J/s)	0.0
% error	0.008 %

Table 4.9: Case 1: Results for Energy Conservation

4.5.5 Gas-droplet channel flow with $T_{di} = T_s$ and $u_{gi} > u_{di}$

In this case, gas-phase velocity is 2m/s and droplet-phase velocity is 1m/s. Inlet droplet temperature equals the saturation temperature of the droplet ($T_{sat} = 347.2K$ at atmospheric pressure). The inlet properties are given in Table. 4.10. All other boundary conditions are same as in section 4.5.4. The contour plots of the various variables are shown in Fig. 4.31 to Fig. 4.35. It is observed from the droplet-phase velocity contour plot, (Fig. 4.33, that the droplets acquire the gas-phase velocity very quickly (of the order of a few milliseconds). Comparison with Fluent results for the variation of properties along the length of the channel are shown in Fig. 4.36 to Fig. 4.37. From Fig. 4.37(a) it is seen that gas-phase temperature variation differs from Case 1 4.5.4 as the flow-rate of gas-phase in this case is half as that of Case 1. As seen in the previous case, there is a small variation between the velocities predicted by the present solver and that obtained from Fluent results as shown in Fig. 4.38 to Fig. 4.40. It is also observed from the contour plots that evaporation occurs for an extended length ($\simeq 0.03m$) compared to the previous case as the residence time of droplets is less due to the increased speed.

Table 4.10: case 2: Inlet conditions

Inlet conditions	
Gas-phase inlet velocity, u_g	2.0 m/s
Droplet-phase inlet velocity, u_{di}	1.0 m/s
Gas-phase inlet temperature, T_{gi}	773.0 K
Droplet-phase inlet temperature, T_{di}	347.8 K
Inlet fuel mass fraction, M_{Fo}	0.0
Gas-phase inlet density, ρ_{gi}	1.225 kg/m^3
Droplet-phase inlet volume fraction, ϑ_{do}	0.0005
Droplet inlet diameter, d_{do}	50 μm

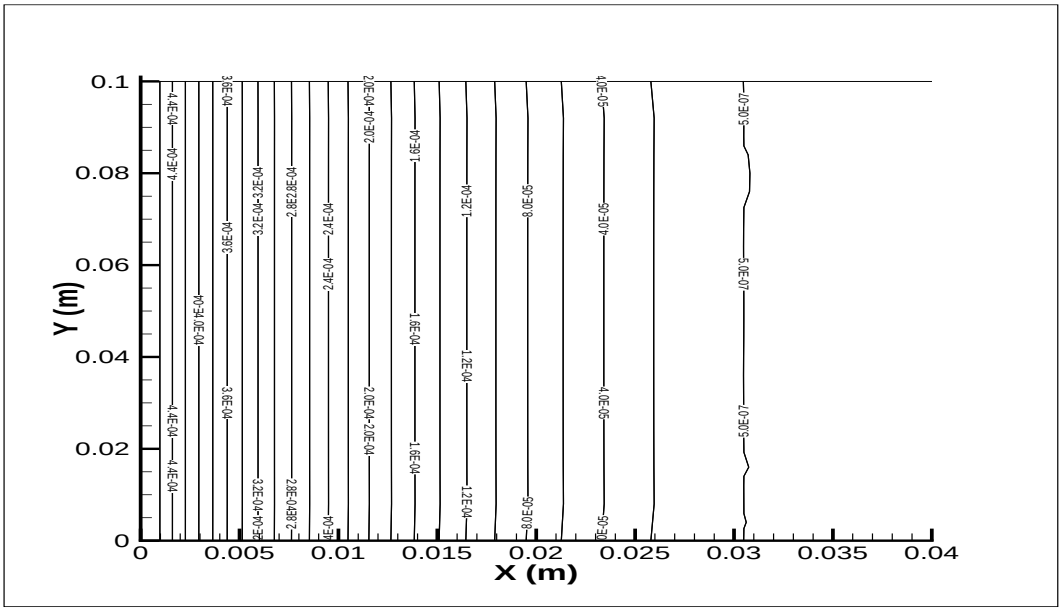

Figure 4.31: Case 2: Uniform flow through 2D Channel. Contour plot for droplet-phase volume fraction, ϑ_d.

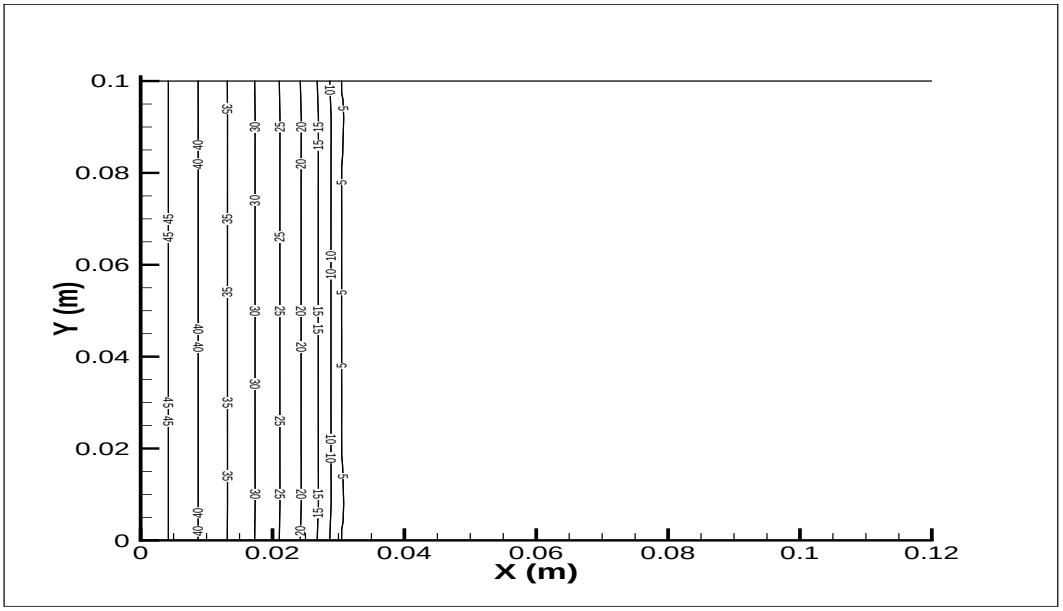

Figure 4.32: Case 2: Uniform flow through 2D Channel. Contour plot for droplet-diameter, d_d.

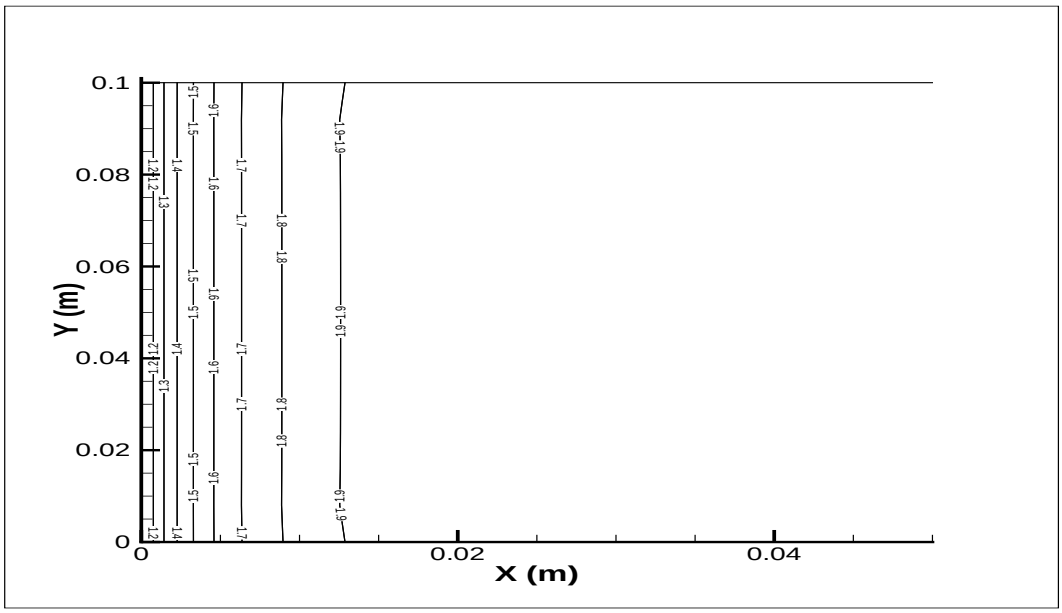

Figure 4.33: Case 2: Uniform flow through 2D Channel. Contour plot for droplet-phase velocity, u_d.

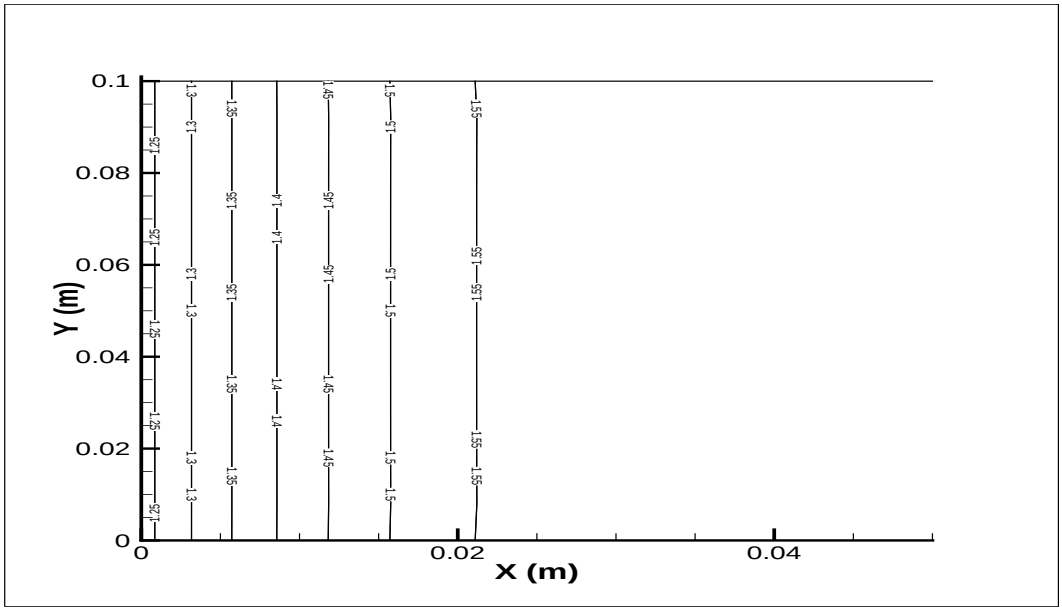

Figure 4.34: Case 1: Uniform flow through 2D Channel. Contour plot for gas-phase density, ρ_g.

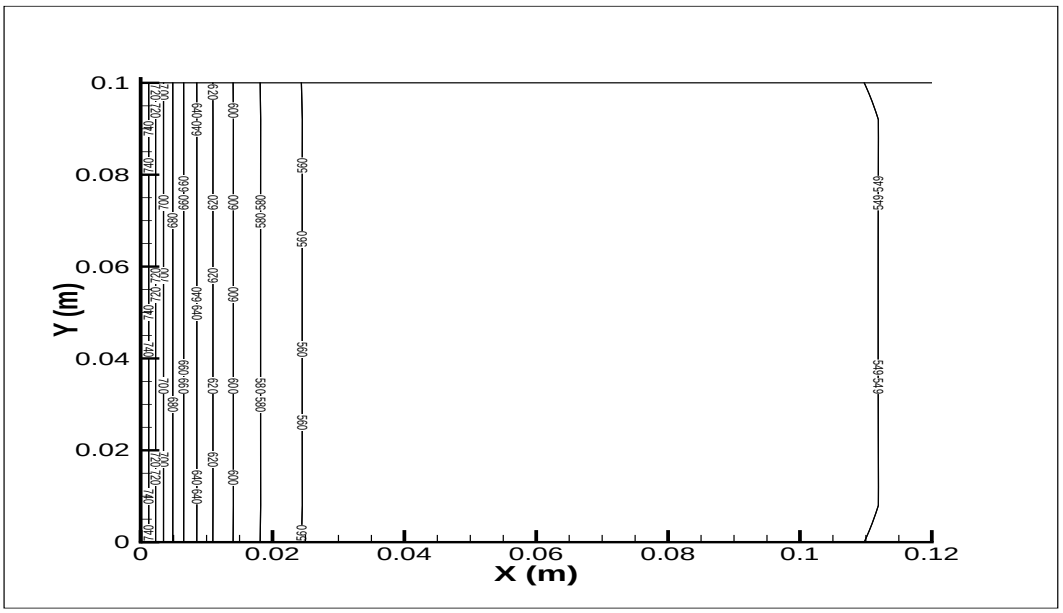

Figure 4.35: Case 2: Uniform flow through 2D Channel. Contour plot for gas-phase temperature, T_g.

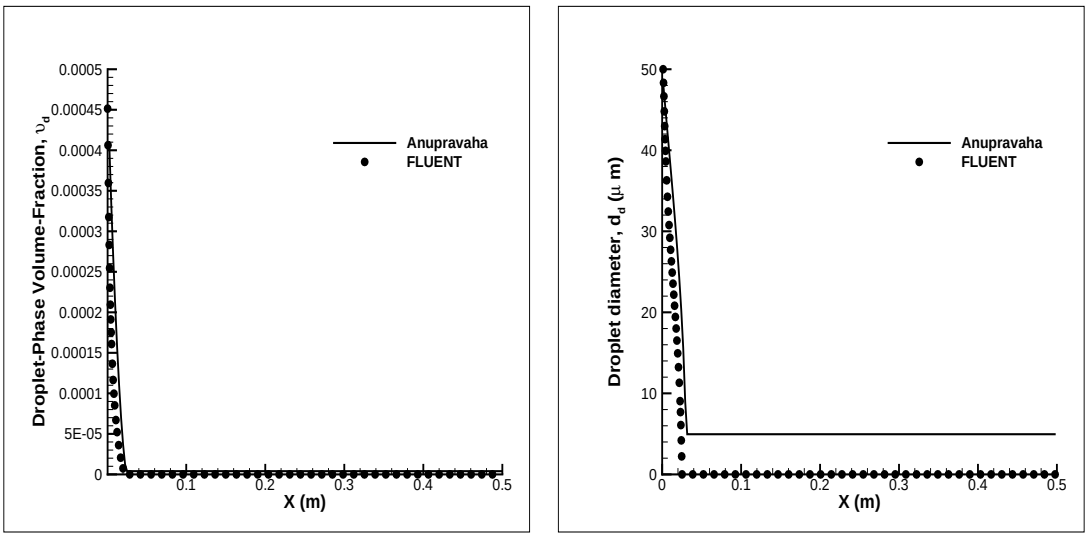

(a) **(b)**

Figure 4.36: Case 2: Uniform flow through 2D Channel. (a) Variation of droplet-phase volume fraction, ϑ_d along the channel (b) Variation of droplet-diameter, d_d along the channel

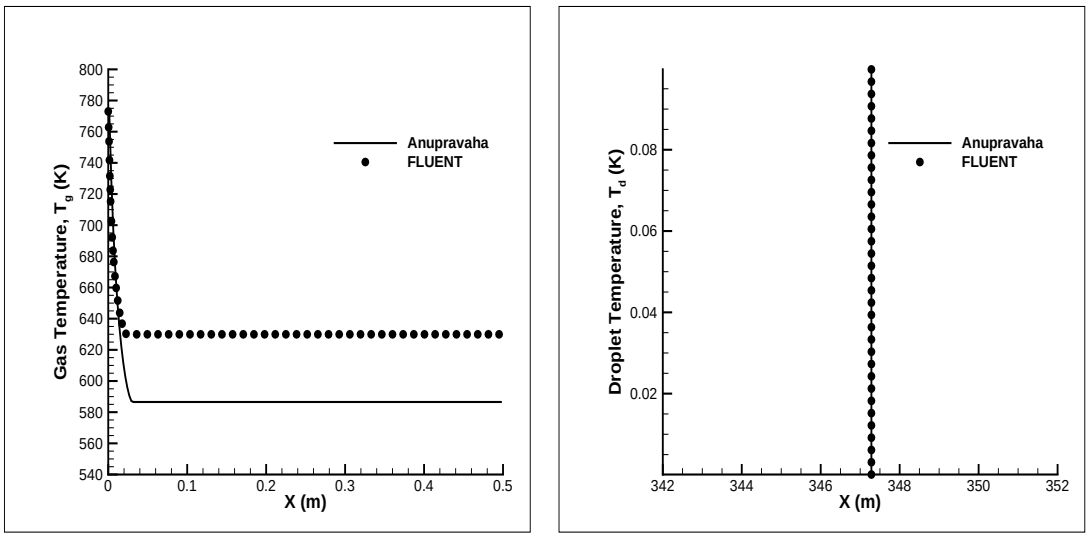

(a) (b)

Figure 4.37: Case 2: Uniform flow through 2D Channel. (a) Variation of gas-phase temperature, T_g along the channel (b) Variation of droplet temperature, T_d across section X = 0.25 m.

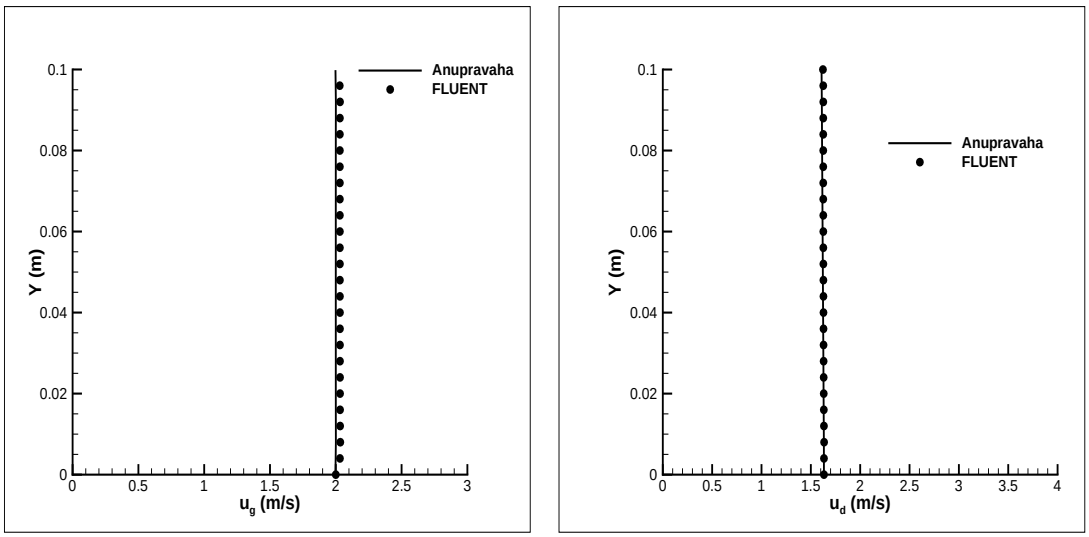

(a) (b)

Figure 4.38: Case 2: Uniform flow through 2D Channel. Velocity profiles at X = 0.005 m(a) Gas-phase velocity, u_g (b) Droplet-phase velocity, u_d

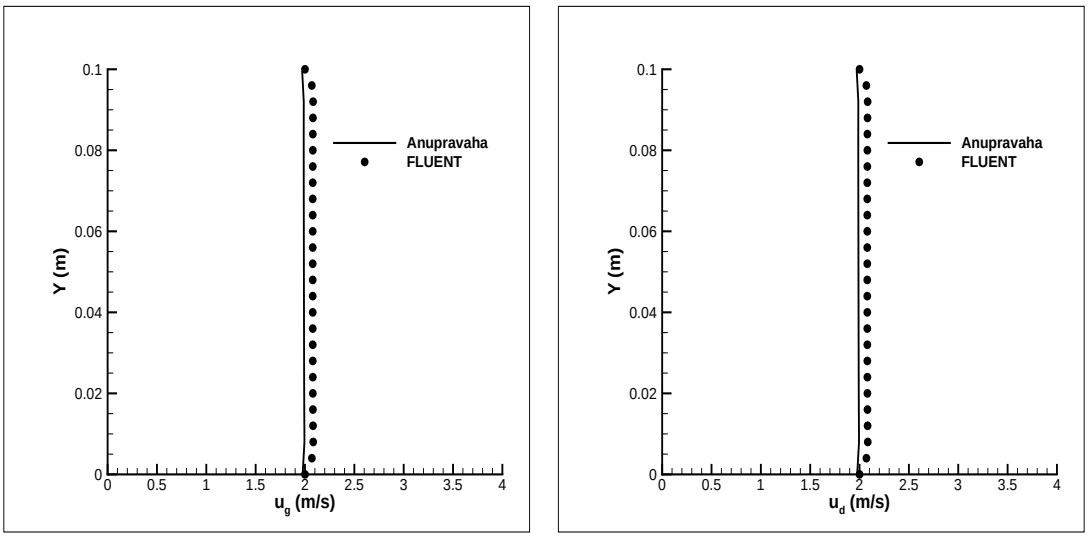

(a) **(b)**

Figure 4.39: Case 2: Uniform flow through 2D Channel. Velocity profiles at X = 0.02 m(a) Gas-phase velocity, u_g (b) Droplet-phase velocity, u_d

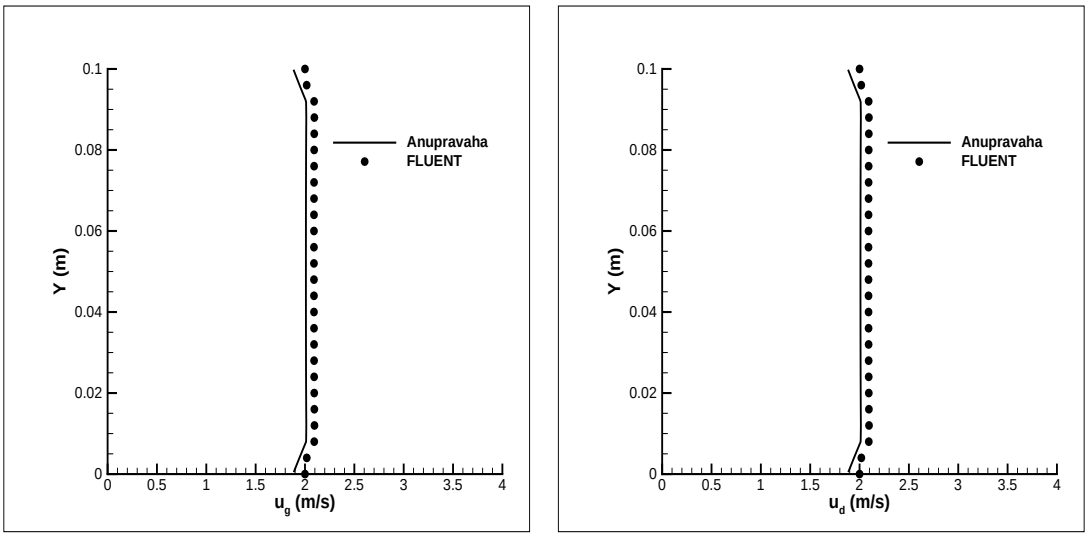

(a) **(b)**

Figure 4.40: Case 2: Uniform flow through 2D Channel. Velocity profiles at X = 0.1 m(a) Gas-phase velocity, u_g (b) Droplet-phase velocity, u_d

4.5.6 Gas-droplet channel flow with $T_{di} = T_s$ and $u_{gi} < u_{di}$

In this case, gas-phase velocity is 0.5 m/s and droplet-phase velocity is 1m/s. Inlet droplet temperature equals the saturation temperature of the droplet ($T_{sat} = 347.8K$ at atmospheric pressure). The inlet properties are given in Table. 4.11. All other boundary conditions are same as in section 4.5.4. Since, the inlet mass-flow rate of the droplet is same as in section 4.5.4 and 4.5.5, the gas-phase density at outlet will be same as observed in the previous cases. The contour plots of the various variables are shown in Fig. 4.41 to Fig. 4.44. It is observed from the droplet-phase velocity contour plot, Fig. **??**, that the droplets decelerate quickly and attain the gas-phase velocity in a few milliseconds. It is also observed from the contour plots that the spray length of evaporation is almost half of what was observed in Case 1 (section 4.5.4) as the residence time of droplets is more due to the decreased speed. As seen in the previous two cases, there is a small variation between the velocities predicted by the present solver and that obtained from Fluent results as shown in Fig. 4.47 to Fig. 4.49.

Table 4.11: Case 3: Inlet conditions

Inlet conditions	
Gas-phase inlet velocity, u_g	0.5 m/s
Droplet-phase inlet velocity, u_{di}	1.0 m/s
Gas-phase inlet temperature, T_{gi}	773.0 K
Droplet-phase inlet temperature, T_{di}	347.8 K
Inlet fuel mass fraction, M_{Fo}	0.0
Gas-phase inlet density, ρ_{gi}	1.225 kg/m^3
Droplet-phase inlet volume fraction, ϑ_{do}	0.0005
Droplet inlet diameter, d_{do}	50 μm

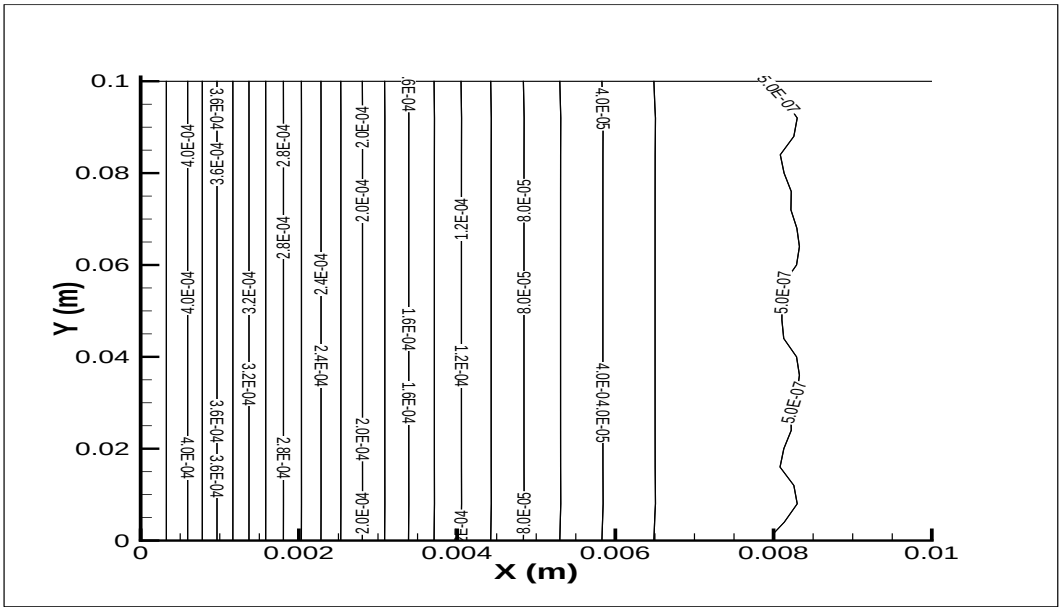

Figure 4.41: Case 3: Uniform flow through 2D Channel. Contour plot for droplet-phase volume fraction, ϑ_d.

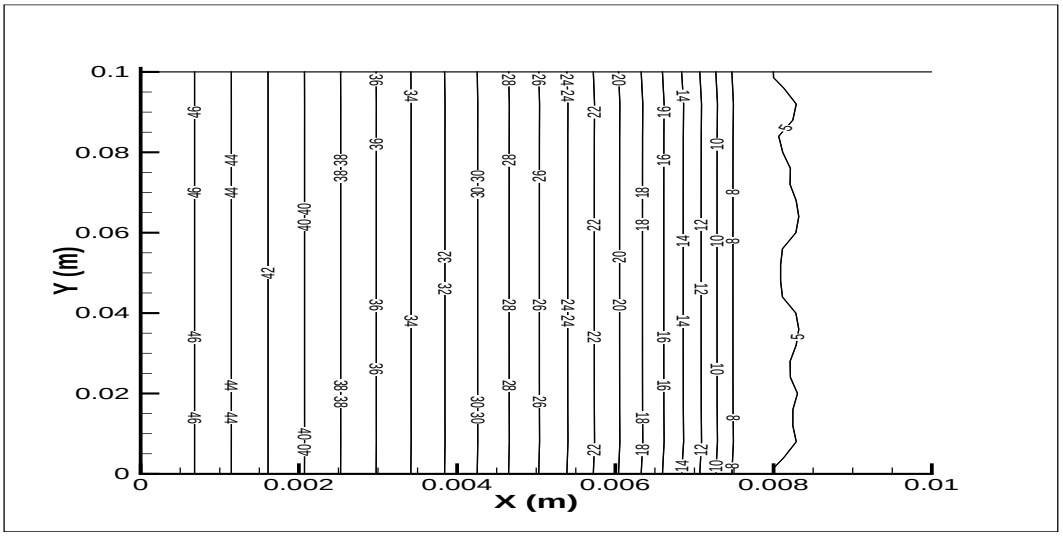

Figure 4.42: Case 3: Uniform flow through 2D Channel. Contour plot for droplet-diameter, d_d.

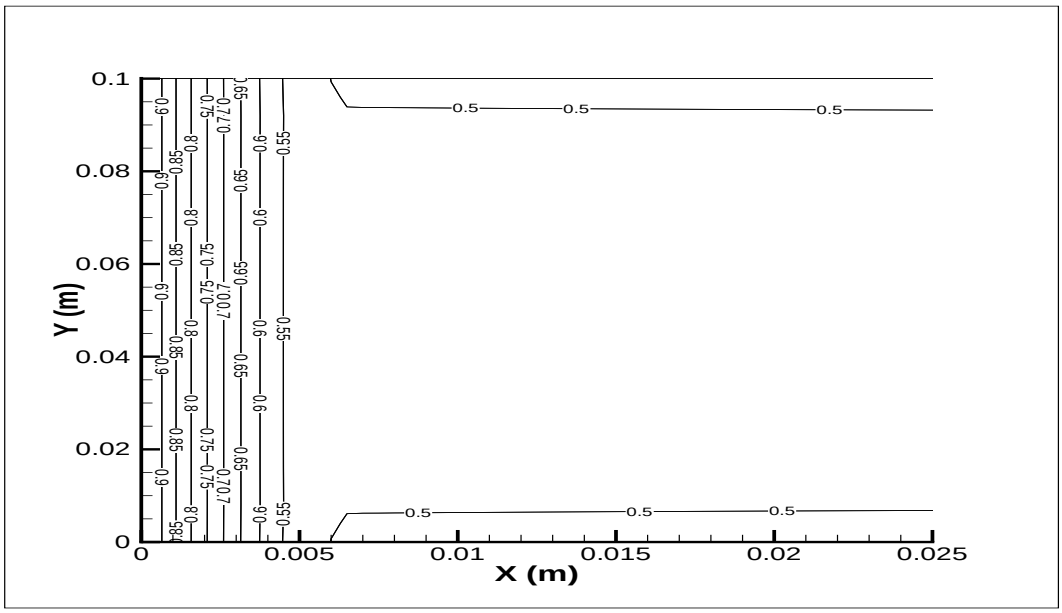

Figure 4.43: Case 3: Uniform flow through 2D Channel. Contour plot for droplet-phase velocity, u_d.

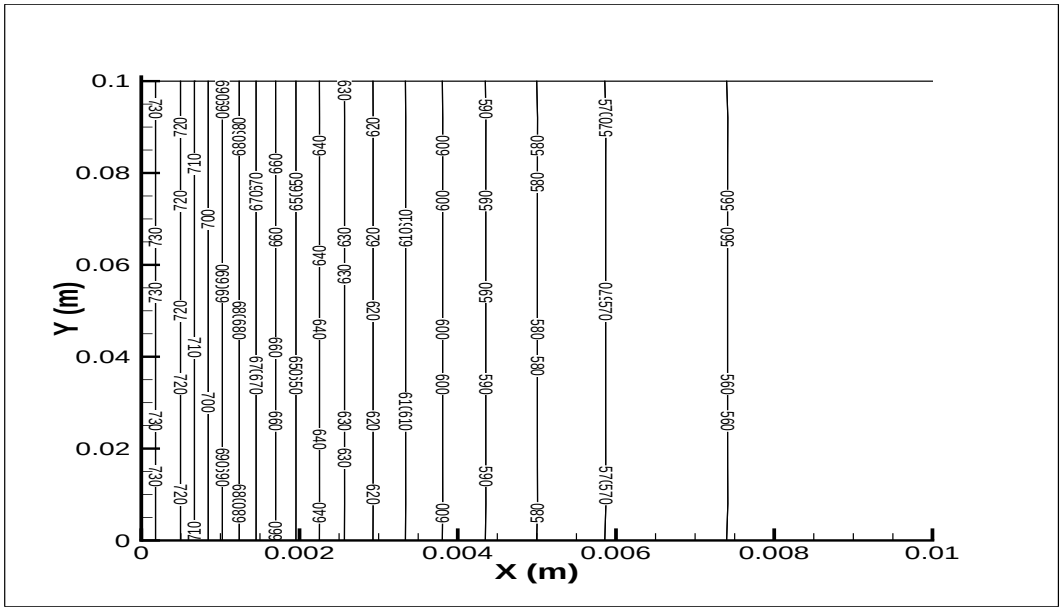

Figure 4.44: Case 3: Uniform flow through 2D Channel. Contour plot for gas-phase temperature, T_g.

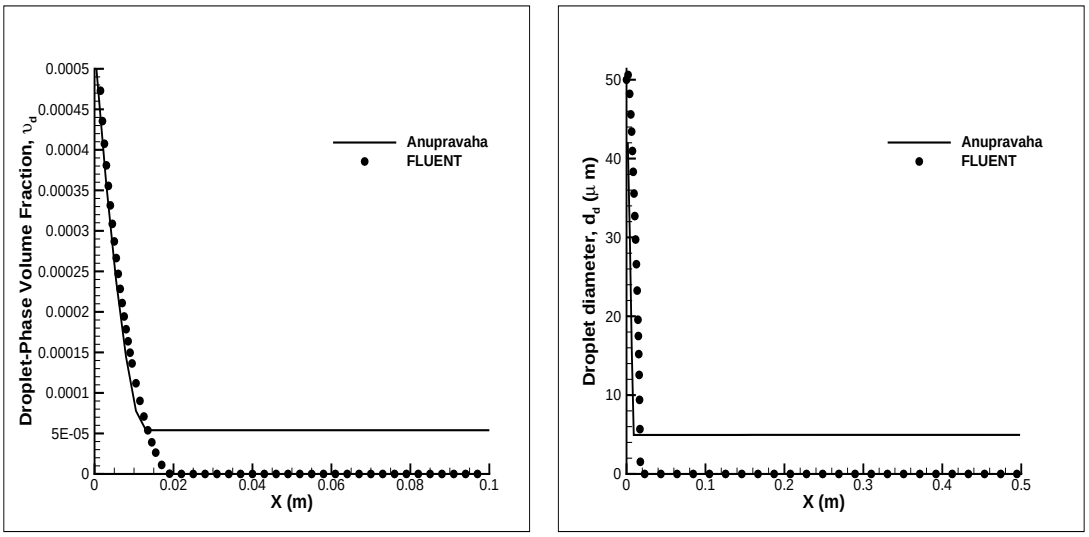

(a) **(b)**

Figure 4.45: Case 3: Uniform flow through 2D Channel. (a) Variation of droplet-phase volume fraction, ϑ_d along the channel (b) Variation of droplet-diameter, d_d along the channel

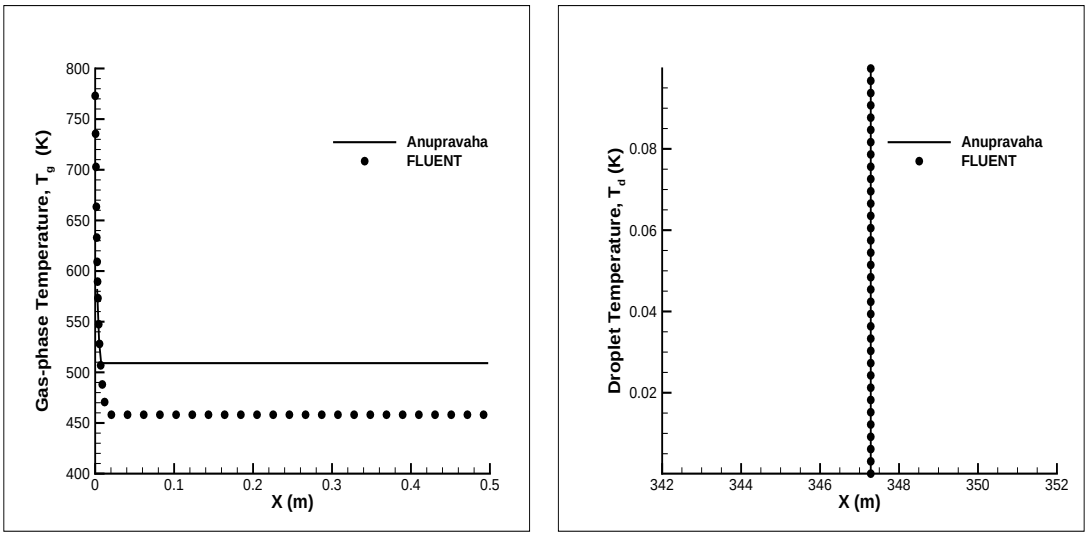

(a) **(b)**

Figure 4.46: Case 2: Uniform flow through 2D Channel. (a) Variation of gas-phase temperature, T_g along the channel (b) Variation of droplet temperature, T_d across section X = 0.25 m.

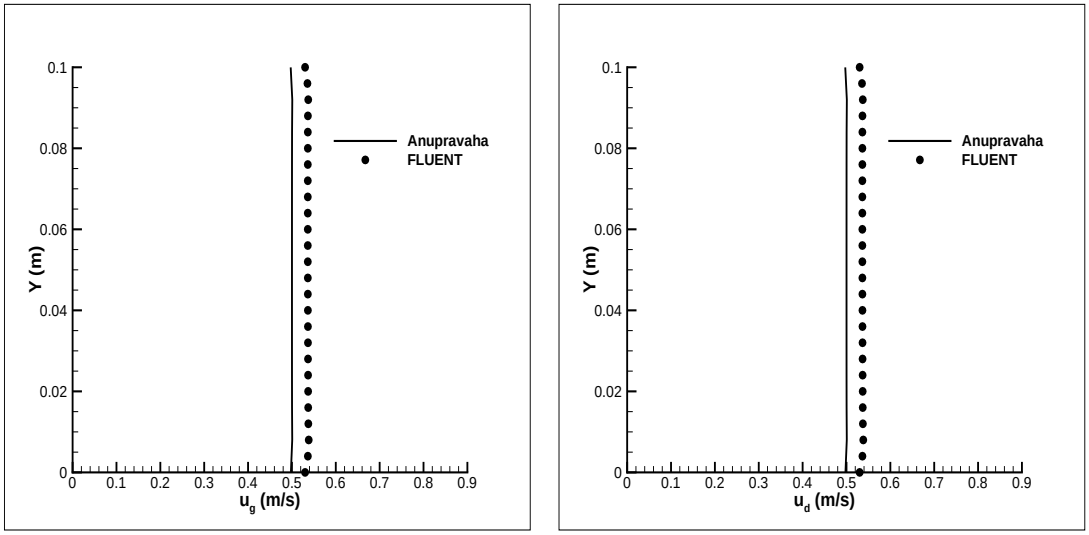

Figure 4.47: Case 3: Uniform flow through 2D Channel. Velocity profiles at X = 0.005 m(a) Gas-phase velocity, u_g (b) Droplet-phase velocity, u_d

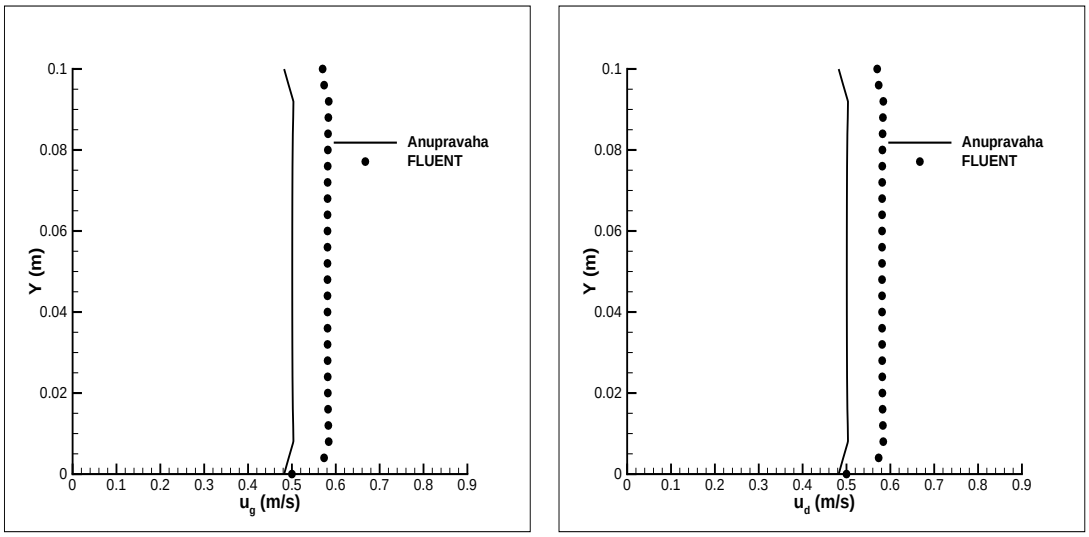

Figure 4.48: Case 3: Uniform flow through 2D Channel. Velocity profiles at X = 0.02 m(a) Gas-phase velocity, u_g (b) Droplet-phase velocity, u_d

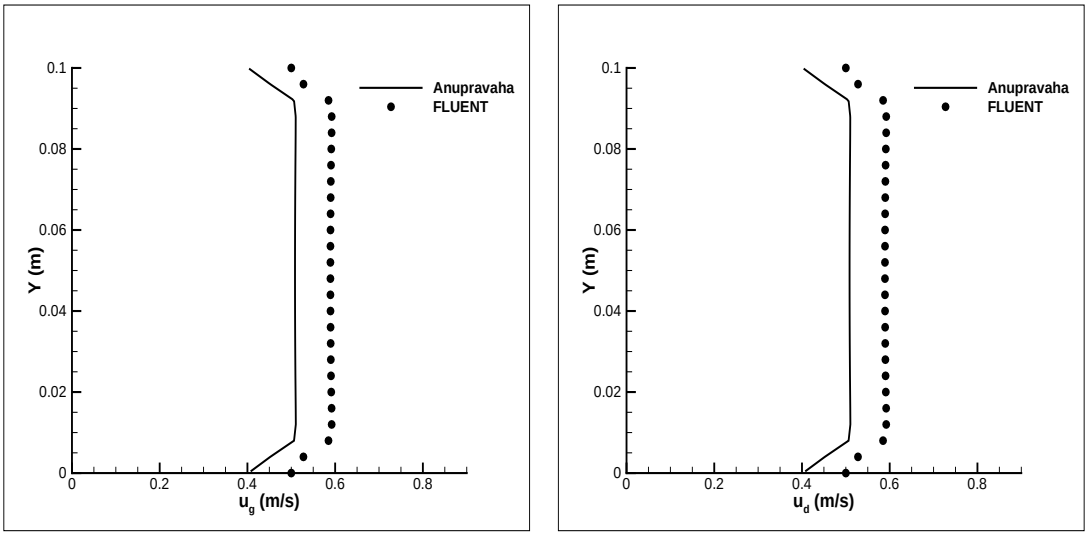

(a) **(b)**

Figure 4.49: Case 3: Uniform flow through 2D Channel. Velocity profiles at X = 0.1 m(a) Gas-phase velocity, u_g (b) Droplet-phase velocity, u_d

4.5.7 Gas-droplet channel flow with isothermal walls

In this case, gas-phase velocity is 0.5 m/s and droplet-phase velocity is 1m/s. Inlet droplet temperature equals the saturation temperature of the droplet ($T_{sat} = 347.8K$ at atmospheric pressure). The inlet properties are given in Table. 4.12. This case differs from Case 1 by the boundary conditions applied at the walls for gas-phase temperature. Dirichlett boundary condition of 1000 K is applied at both the walls for gas-phase temperature. Since, the inlet mass-flow rate of the droplet is same as in section 4.5.4 and 4.5.5, the gas-phase density at outlet, mass-fraction of evaporated fuel vapour will be same as observed in the previous cases. Hence, only the contour profiles of temperature, droplet-diameter and volume-fraction variations along the channel are plotted. The contour plots of the various variables are shown in Fig. 4.50 to 4.52. It is observed from the contour plots that evaporation spray length is shorter compared to Case 1 becaus of the iso-thermal walls boundary condition. Comparison with Fluent results for the variation of droplet-diameter and volume-fraction along the length of the channel are shown in Fig. 4.53 to 4.54.

Table 4.12: Case 4: Inlet conditions

Inlet conditions	
Gas-phase inlet velocity, u_g	1.0 m/s
Droplet-phase inlet velocity, u_{di}	1.0 m/s
Gas-phase inlet temperature, T_{gi}	773.0 K
Droplet-phase inlet temperature, T_{di}	347.8 K
Inlet fuel mass fraction, M_{Fo}	0.0
Gas-phase inlet density, ρ_{gi}	1.225 kg/m^3
Droplet-phase inlet volume fraction, ϑ_{do}	0.0005
Droplet inlet diameter, d_{do}	50 μm

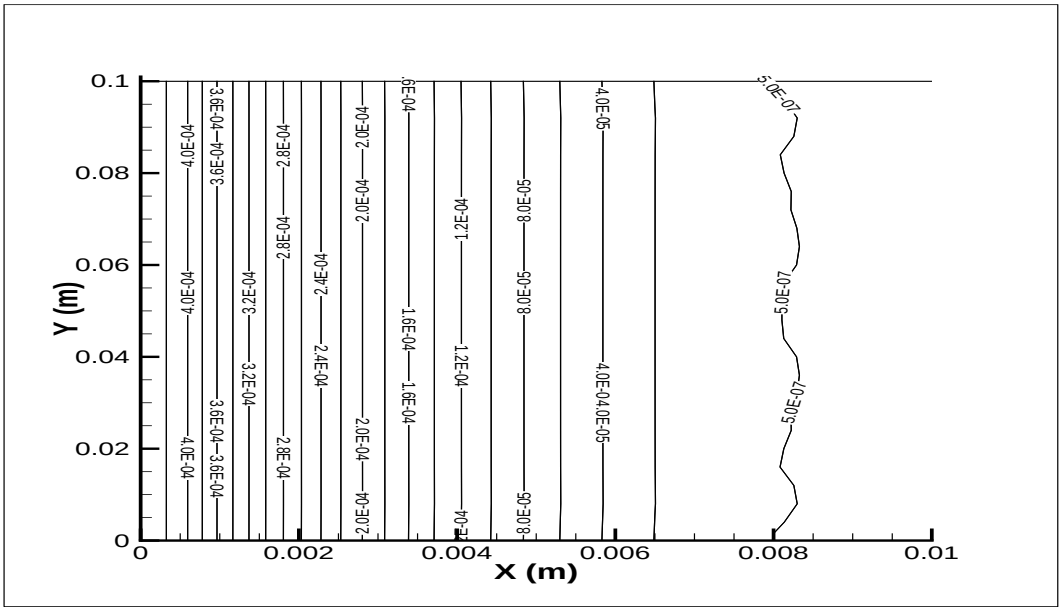

Figure 4.50: Case 4: Uniform flow through 2D Channel. Contour plot for droplet-phase volume fraction, ϑ_d.

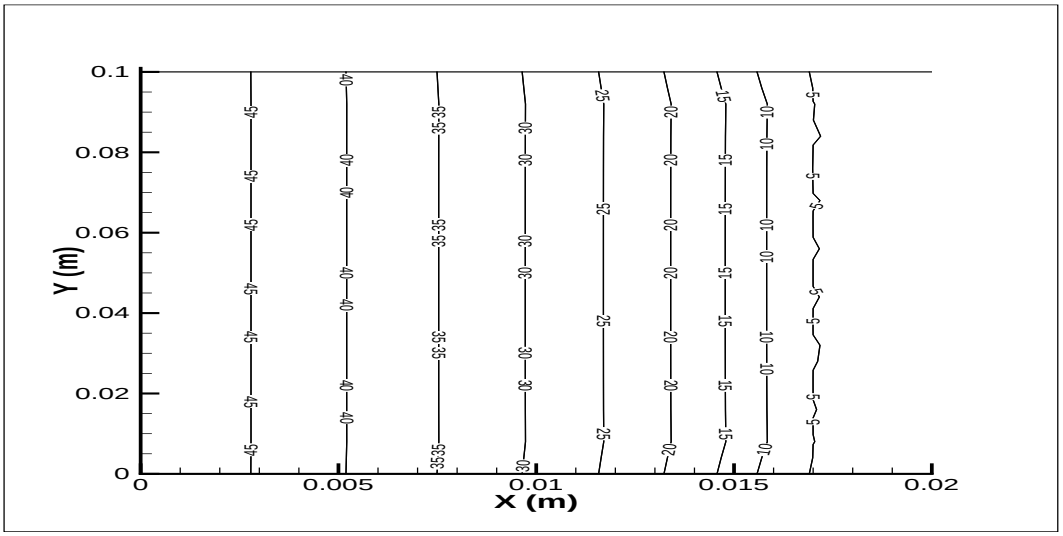

Figure 4.51: Case 4: Uniform flow through 2D Channel with iso-thermal walls. Contour plot for droplet-diameter, d_d.

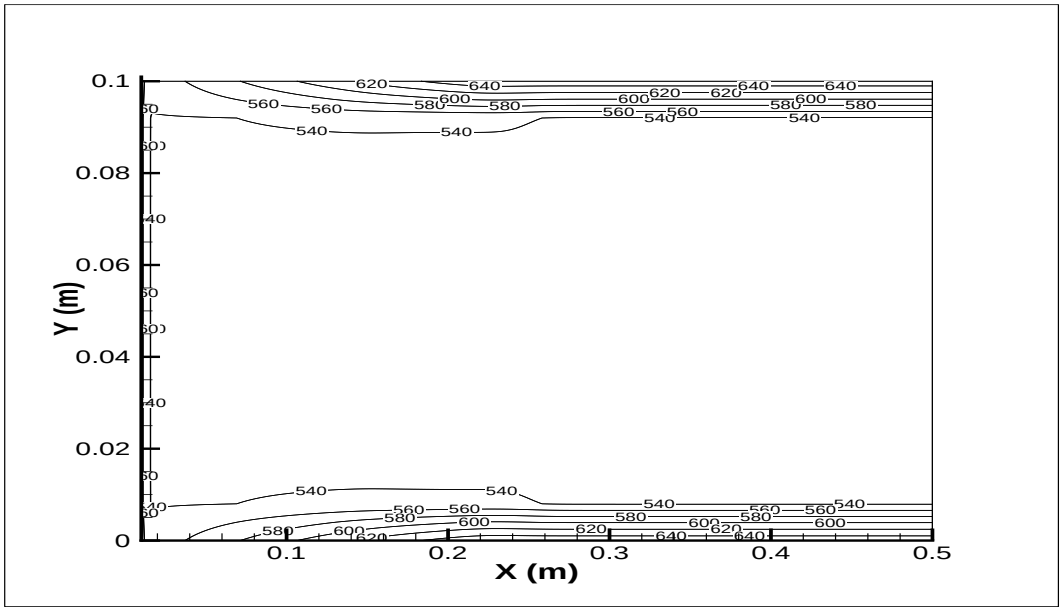

Figure 4.52: Case 4: Uniform flow through 2D Channel with iso-thermal walls. Contour plot for gas-phase temperature, T_g.

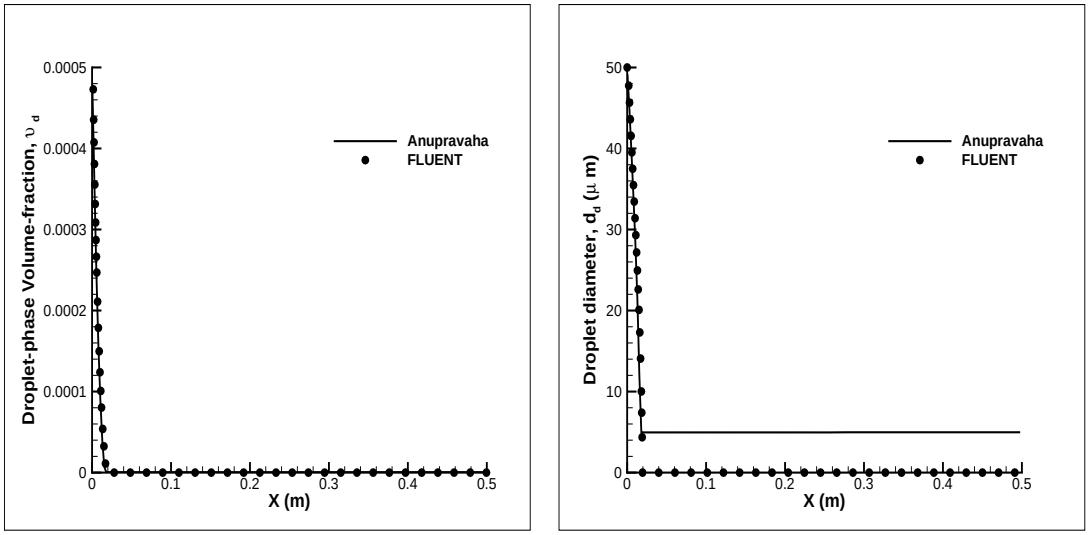

(a) (b)

Figure 4.53: Case 4: Uniform flow through 2D Channel with iso-thermal walls. (a) Variation of droplet-phase volume fraction, ϑ_d along the channel (b) Variation of droplet-diameter, d_d along the channel

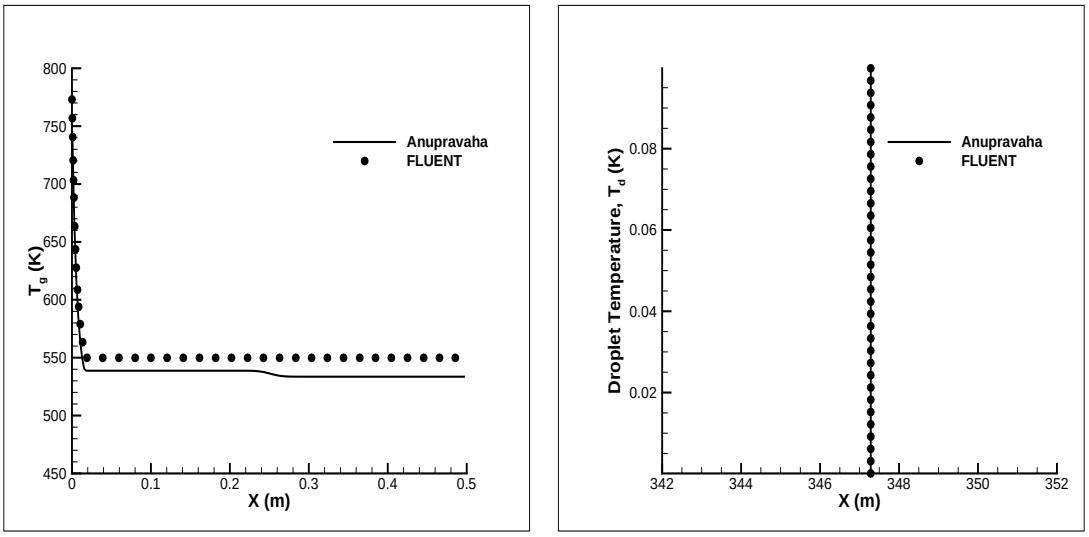

(a) **(b)**

Figure 4.54: Case 4: Uniform flow through 2D Channel with iso-thermal walls. (a) Variation of gas-phase temperature, T_g along the channel (b) Variation of droplet temperature, T_d across section X = 0.25 m.

4.5.8 Gas-droplet channel flow with $T_{di} < T_s$ and $u_{gi} = u_{di}$

In this case, both the gas-phase and droplet phase are entering the channel with a velocity of 1m/s and the inlet droplet temperature is $T_d = 300.0K$. The inlet properties are given in Table. 4.13. At the wall, homogeneous Neumann boundary condition is applied for gas-phase temperature. This means an insulated boundary condition is applied for temperature. The other boundary conditions are same as in Case 1. Since, the droplet inlet temperature is lower than the saturation temperature, transient heating of the droplets takes place. The contour plots for only droplet-phase volume-fraction, droplet-diameter and droplet-temperature are plotted in Fig. 4.55 to Fig. 4.58 as the variation of other variables will be similar to Case 1. It is seen from Fig. 4.56 that evaporation spray length is slightly longer than Case 1 as droplet temperature is lower ($\simeq 0.0m$)than the saturation temperature. Comparison of the variation of properties along the length of the channel with FLUENT are shown in Fig. **??** to **??**. Mass conservation and energy conservation details are given in Table 4.14 and Table 4.15.

Table 4.13: Case 5: Inlet conditions

Inlet conditions	
Gas-phase inlet velocity, u_g	0.5 m/s
Droplet-phase inlet velocity, u_{di}	1.0 m/s
Gas-phase inlet temperature, T_{gi}	773.0 K
Droplet-phase inlet temperature, T_{di}	300.0 K
Inlet fuel mass fraction, M_{Fo}	0.0
Gas-phase inlet density, ρ_{gi}	1.225 kg/m^3
Droplet-phase inlet volume fraction, ϑ_{do}	0.0005
Droplet inlet diameter, d_{do}	50 μm

	$\dot{m}_g$ (kg/s)	$\dot{m}_d$ (kg/s)	Total (kg/s)
Inlet	0.122438	0.034200	0.156638
Outlet	0.156275	0.000343	0.156618

Table 4.14: Case 5: Results for Mass Conservation

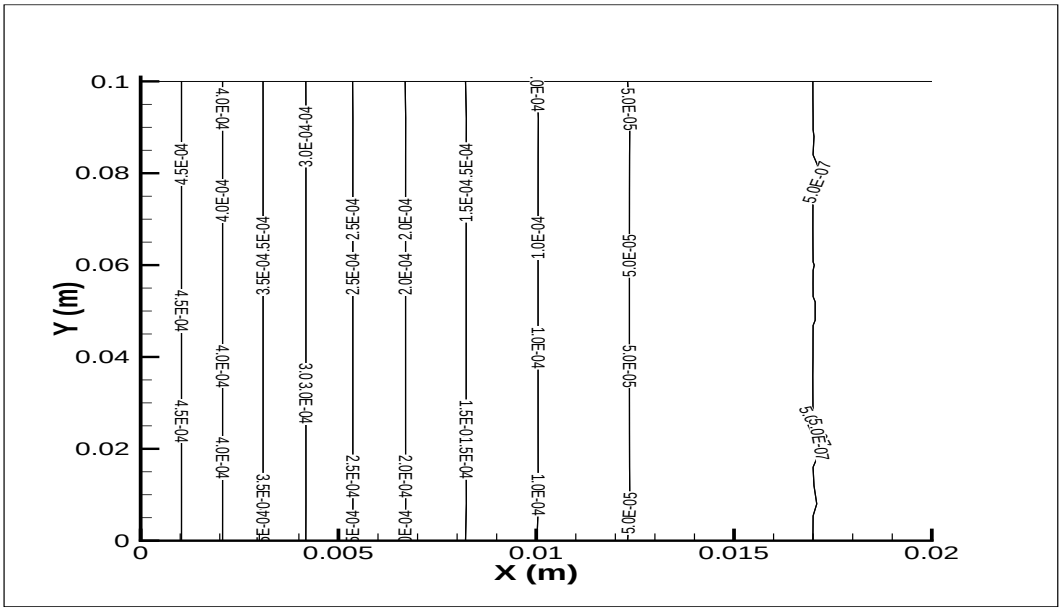

Figure 4.55: Case 5: Uniform flow through 2D Channel with $T_{di} < T_{sat}$. Contour plot for droplet-phase volume fraction

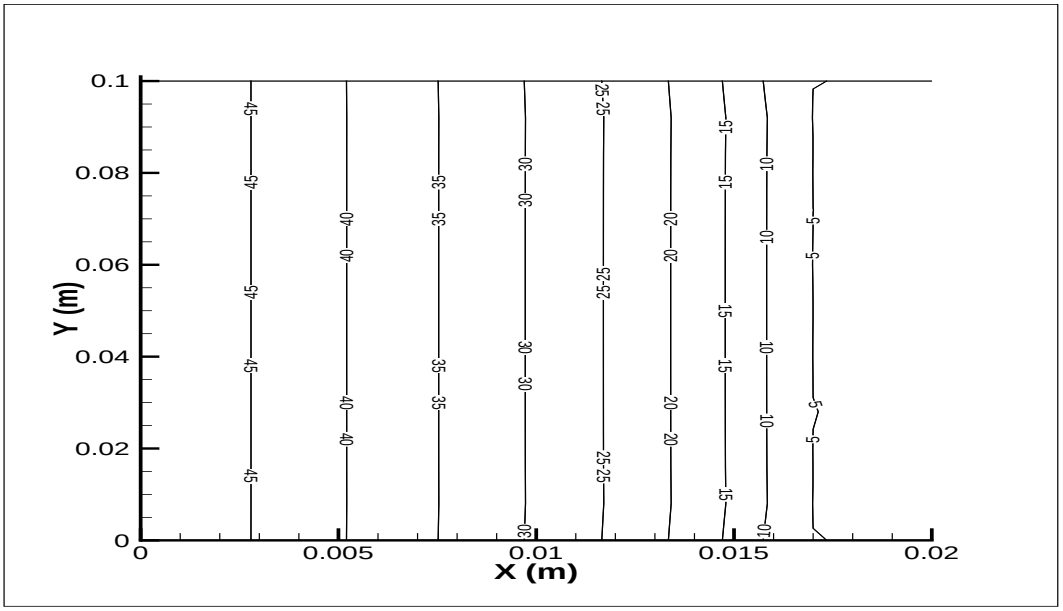

Figure 4.56: Case 5: Uniform flow through 2D Channel with $T_{di} < T_{sat}$. Contour plot for droplet-phase diameter

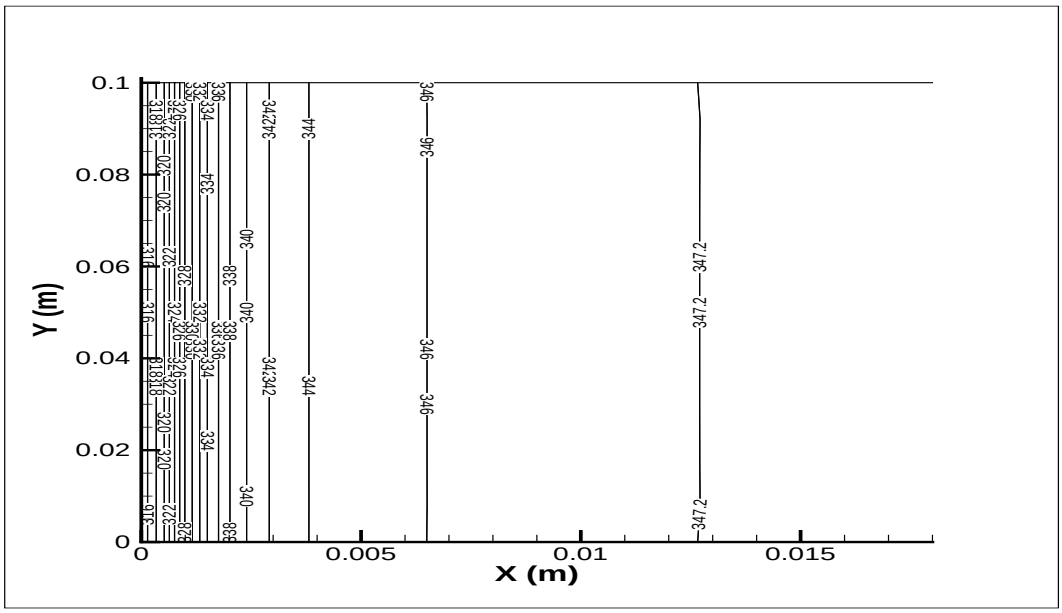

Figure 4.57: Case 5: Uniform flow through 2D Channel with $T_{di} < T_{sat}$. Contour plot for droplet-phase temperature, T_d

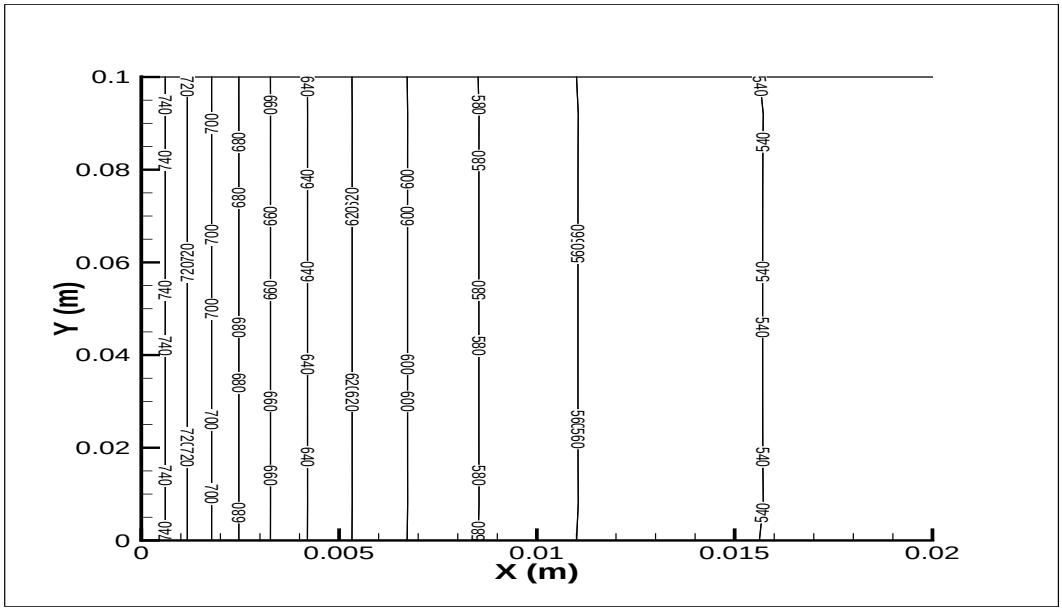

Figure 4.58: Case 5: Uniform flow through 2D Channel with $T_{di} < T_{sat}$. Contour plot for gas-phase temperature, T_g

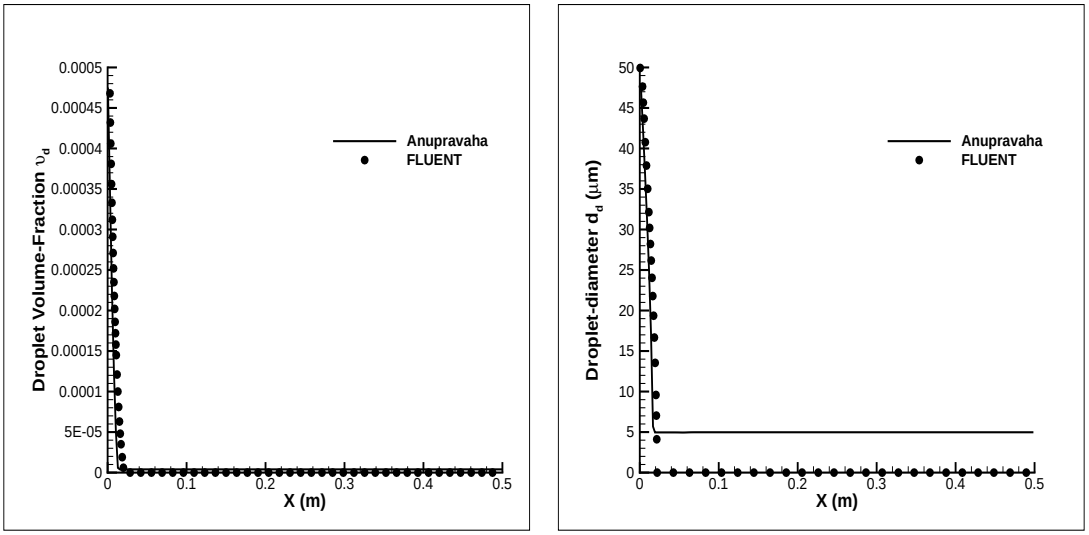

(a) **(b)**

Figure 4.59: Case 5: Uniform flow through 2D Channel with $T_{di} < T_{sat}$. (a) Variation of droplet-phase volume fraction, ϑ_d along the channel (b) Variation of droplet-diameter, d_d along the channel

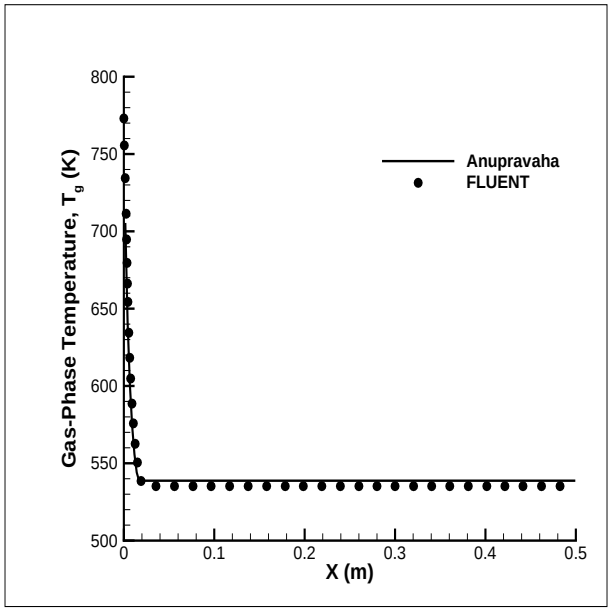

Figure 4.60: Case 5: Uniform flow through 2D Channel with $T_{di} < T_{sat}$. Variation of gas-phase temperature, T_g along the channel

U_{in} (J/s)	120606.18
U_{out} (J/s)	109867.34
Total heat of vaporization (J/s)	10947.28
Total enthalpy spent for heating droplet (J/s)	367.14
% error	0.04 %

Table 4.15: Case 5: Results for Energy Conservation

4.6 Closure

The present solver for gas-particle flows and gas-droplet flows has been extensively validated for different test problems and is found to give satisfactory results. The problem of convergence for lower particle/droplet diameters has been addressed to and is largely overcome by the present solver. Problems with simple 2D geometry have been solved for both gas-particle and gas-droplet flows. Gas-particle flows in 2D channel and backward-facing step problems are solved for using the present solver and is found to give a good match with Fluent results. Similarly, dilute gas-droplet flows with evaporation solver has been used to simulate gas-droplet flows in a 2D channel and is found to work satisfactorily for droplet diameters as small as $50\mu\,m$.

Chapter 5

Conclusion and Scope of the Future Work

Conclusion

An Eulerian-Eulerian model for simulating gas-droplet flows has been successfully implemented as a separate module in a general purpose CFD solver, *IITK-DAE Anupravaha*. The classical model for droplet evaporation developed by Splading [35] with simplifying assumptions has been implemented in the module and was found to give satisfactory results for low and moderate evaporation rates. The evaporation model was thoroughly tested and the results obtained were compared with existing literature. Results showed a very good match between the model predictions and published results.

Scope of the Future work

The module is implemented in a general purpose CFD solver for both 2-D and 3-D problems but has been tested only for 2-D problems. The implementation has to be further verified against 3-D test cases. The module has been implemented only for laminar gas-droplet flows, but many problems which are of practical importance are turbulent. So the next phase of work in future may be the implementation of turbulence both for the gas-phase and the droplet-phase; which may also lead a way for the solver to simulate problems involving droplet combustion.

Sophisticated evaporation models which take into account the non-equilibrium effects and are suitable for high evaporation rate conditions may also need to be implemented. These models are able to simulate complex problems like turbulent evaporating sprays involving high droplet Reynolds number and evaporation rate. Detailed analysis and comparison of such models are found in Faeth [11], Miller [24] and Sirignano [34]. The present evaporation model assumes uniform temperature within the droplet which may prove inaccurate for high evaporation rate conditions. Non-uniformity of the droplet temperature can be modeled by adding extra heat transfer terms in the droplet phase energy equation, as done by Miller [24]. Convergence difficulties were observed for gas-droplet flows with very small values of volume fraction ($\leq 5 \times 10^{-6}$) in the domain. Further investigation is needed in this regard.

The solver considers mono-sized droplets. For problems of practical importance continuous size distribution can be represented by droplets with different sizes which correspond to classes of droplets with each class having its separate set of equations as done by Guo [18]. The present solver deals with flows in the laminar -flow regime only. This can be extended to incorporate turbulence effects on evaporating jet-flows as Elghobashi [10].

The solver considers single component droplets, while many practical applications involving blended fuels require simulation of multi-component droplets. Daif et al.[6] have presented experimental results of vaporization of multi-component droplets in a convective flow. Further development of the present solver to address the vaporization characteristics of multi-component fuel droplets may also be taken up in the future.

Appendix A

Appendix

A.1 Properties of fluids used

For validation of the evaporation model, n-heptane and hexane are used as droplet-phase and air is considered as the carrier-phase. The properties of these fluids used for validation have been given below

A.1.1 Properties of Air

The following relations have been used for calculating the thermodynamic properties of air:

- Specific heat at constant pressure for air

$$C_{pa} = c1 + c2\left(\frac{c3/T_r}{sinh(c3/T_r)}\right)^2 + c4\left(\frac{c5/T_r}{cosh(c5/T_r)}\right)^2 \tag{A.1}$$

  where $c1 = 0.2896 \times 10^5, c2 = 0.09390 \times 10^5, c3 = 3.0120 \times 10^3, c4 = 0.0758 \times 10^5, c5 = 1484$
  In the above expression C_pa is in $J/kmol\,K$

- Thermal conductivity for air in $(W/m\,K)$

$$k\_a = 1.5207\times10^{-11}\,T_r^3 - 4.8574\times10^{-8}\,T_r^2 + 1.0184\times10^{-4}\,T_r - 3.9333\times10^{-4} \tag{A.2}$$

A.1.2 Properties of n-heptane

The following physical properties of n-heptane have been used ([27],[23]).

- Normal boiling Temperature $T_{bn} = 371.6\,K$, Molecular weight $M_F = 100.204$, Critical temperature $T_{cri} = 540.17\,K$, Critical pressure $P_{cri} = 2631.633\,kPa$

- Vapour pressure is obtained by the Clausius-Clapeyron equation as

$$P_{F_S} = \exp\left(14.2146 - \frac{3151.68}{T_d - 43}\right) \text{for}\, T_d >= T_{bn}\ \text{(kPa)} \tag{A.3}$$

$$P_{F_S} = \exp\left(14.3896 - \frac{3209.45}{T_d - 43}\right) \text{for}\, T_d = T_{bn}\ \text{(kPa)} \tag{A.4}$$

  where T_d is the droplet temperature in K and T_bn is the saturation temperature at atmospheric pressure.

- Latent heat of vaporization as a function of droplet temperature is

$$L = 317.8 \times 1000.0 \left(\frac{540.17 - T_d}{540.17 - 371.4}\right)^{0.38}\ (J/kg) \tag{A.5}$$

- Specific heat at constant pressure for fuel vapour

$$C_{vd} = (0.363 + 0.000467\,T_r) \times (5 - 0.001\,\rho_d)\ (J/kg\,K) \tag{A.6}$$

  where $\rho\_d = 684.0\,kg/m^3$

- Thermal conductivity of vapour in $(W/m\,K)$

$$k_v = 10^{-7} \times\ (14.52\,T_{ref} - 5.14)^{2/3} \times (C_{vd}\,M_F/\lambda) \tag{A.7}$$

  where

$$\lambda = T_{cri}^{1/6} \times M_F^{0.5}\ \left(\frac{P_{atm}}{P_{cri}}\right)^{2/3} \tag{A.8}$$

  where $T_{ref} = T_r/T_{cri}$

- Density of liquid fuel, ρ_d in (kg/m^3)
  For $T_d <= 538.0$

$$\rho_d = -941.03 + 19.96181\,T_d - 0.08612051\,T_d^2 + 1.579494 \times 10^{-4}\,T_d^3 - 1.089345 \times 10^{-7}\,T_d^4 \tag{A.9}$$

  Otherwise

$$\rho_d = 4.19528 \times 10^7 - 2.360524 \times 10^5\,T_d + 442.7316\,T_d^2 - 0.2767921\,T_d \tag{A.10}$$

where T_r is the reference temperature obtained by the '1/3' rule.

A.1.3 Physical properties of Hexane ([24])

- Normal boiling temperature $T_{bn} = 344.6\,K$, Molecular weight $M_F = 86.178$, Critical temperature $T_{cri} = 507.6\,K$ and Critical pressure $P_{cri} = 3.04 \times 10^6\,Pa$

- Specific heat of liquid droplet $C_{ld} = 2302.0\,(J/kg\,K)$

- Vapour pressure is obtained by the Clausius-Clapeyron equation as

$$P_{F_S} = \exp\left(14.0932 - \frac{2834.61}{T_d - 43}\right) \text{ for } T_d >= T_{bn} \text{ (kPa)} \tag{A.11}$$

$$P_{F_S} = \exp\left(14.3896 - \frac{3209.45}{T_d - 43}\right) \text{ for } T_d = T_{bn} \text{ (kPa)} \tag{A.12}$$

  where T_d is the droplet temperature in K and T_{bn} is the saturation temperature at atmospheric pressure.

- Latent heat of vaporization

$$L = 5.1478 \times 10^5 \left(1 - \frac{T_d}{512}\right)^{0.3861} \quad (J/kg) \tag{A.13}$$

- Specific heat of vapour

$$C_{vd} = -51.31 + 6.767\,T_r - 3.626 \times 10^{-3}\,T_r^2 \ (J/kg\,K) \tag{A.14}$$

- Thermal conductivity of vapour in $(W/m\,K)$

$$k_{vd} = 1.112 \times 10^{-2} + 3.837 \times 10^{-5}\,T_r + 3.778 \times 10^{-8}\,T_r^2 \tag{A.15}$$

- Density of liquid, $\rho_d = 664.0\,(kg/m^3)$.

- Viscosity of vapour

$$\mu_{vd} = 5.592 \times 10^{-6} + 5.622 \times 10^{-9}\,T_r \ (kg/m\,s) \tag{A.16}$$

where T_r is the reference temperature obtained by the '1/3' rule.

A.2 UDF used in FLUENT calculations

```
/* udf to define evaporation rate */
# include "udf.h"
DEFINE_MASS_TRANSFER(mdg,c,thread,from_phase_index,
from_species_index, to_phase_index,to_species_index)
Thread *droplet = THREAD_SUB_THREAD(thread,from_phase_index);
Thread *gas = THREAD_SUB_THREAD(thread,to_phase_index);

    real Re, Pr, BT, A, B, C;
real mdg, L, T_SAT, Pi;
real var_rho_ratio, vel, diam, n;
mdg = 0.0;
L = 320096.0;
T_SAT = 347.2;
Pi = 22.0/7;
var_rho_ratio = C_VOF(c,droplet)/0.0005;
vel = fabs(C_U(c,gas)- C_U(c,droplet));
diam = C_PHASE_DIAMETER(c,droplet)*pow(var_rho_ratio,0.333);
/*updating the diameter of droplet as Fluent seems not to do it */
n=(6/Pi)*C_VOF(c,droplet)/pow(diam,3);
BT = C_CP(c,gas)*fabs(C_T(c,gas)-C_T(c,droplet))/L;
Re = C_R(c,gas)*vel*diam/C_MU_L(c,gas);
Pr = C_CP(c,gas)*C_MU_L(c,gas)/C_K_L(c,gas);

    A = 2*Pi*diam*(C_K_L(c,gas)/C_CP(c,gas));
B = log(1+BT);
C = (1 + pow(Re,0.5)*pow(Pr,0.33));

    if (C_T(c, droplet) ≥ T_SAT)
mdg = -n*A*B*C;
if (C_T(c, droplet) < T_SAT)
mdg = 0;
return (mdg);
```

References

[1] Abramzon, B.,and Sirignano, W.A., "Droplet vaporization model for spray combustion calculation", *Int. J. of Heat and Mass Transfer*, Vol. 32, pp. 1605-1618, 1989.

[2] Adhiraj Kishore Dasgupta, "Numerical Simulation of Dilute Gas-Particle flows using Eulerian-Eulerian approach in a General Purpose CFD Solver", Thesis for the Degree of Master of Technology, *Department of Mechanical Engineering*, Indian Institute of Technology Kanpur, 2008.

[3] Asano, K., "Mass Transfer from Fundamentals to Modern Industrial Applications" *Wiley publications*, 2006.

[4] Chin, J.S., and Lefebvre, A.H., "The Role of Heat-up Period in Fuel Drop Evaporation", *Int. J. Turbo Jet Engines*, Vol. 2, pp. 315-325, 1985.

[5] Crowe, C.T., Sommerfeld, M. and Tsuji, Y., "Multiphase flows with droplets and particles", *CRC Press: Boca Raton*, 1998.

[6] Daif, A., Bouaziz, M., Chesneau, X. and Cherif, A.A., "Comparison of multicomponent fuel droplet vaporization experiments in forced convection with the Sirignano model", *Exp. Thermal Fluid Sci.*, Vol. 18, pp. 282-290, 1999.

[7] Darwish, M., Moukalled, F. and Sekar, B., "A unified formulation of the segregated class of algorithms for multifluid flow at all speeds", *Numerical Heat Transfer, Part B: Fundamentals*, Vol. 40:2, pp. 99-137, 2001.

[8] Downing, C.G., "The evaporation of drops of pure liquids at elevated temperatures: rates of evaporation and wet-bulb temperatures", *AIChE Journal*, Vol. 12, pp. 760-766, 1966.

[9] Eswaran V. et al., "Development of a General Purpose Robust CFD Solver", Project Report No. 1, *Department of Mechanical Engineering*, Indian Institute of Technology Kanpur, December, 2005.

[10] Elghobashi, S. E. and Mostafa, A. A., "A two-equation turbulence model for jet flows laden with vaporizing droplets", *Int. J. Multiphase flow*, Vol. 11, pp. 515-533, 1985.

[11] Faeth, G.M., "Currect Status of Droplet and Liquid Combustion", *Prog. Energy Combust. Sci.*, Vol. 3, pp. 191-224, 1977.

[12] Fluent Multiphase flows Documentation,*Fluent Inc. Lebanon, NH*

[13] Frolov, S.M., Frolov, F.S., Basara B., "Simple Model of Transient Drop Vaporization", *Journal of Russian Laser Research*, Vol. 27, No. 6, pp. 562-574, 2006.

[14] Frossling, N., "On the Evaporation of Falling Droplets", *Gerlands Beitr. Geophys.*, Vol. 52, pp. 170-216, 1938.

[15] Loth, E.,"Numerical approaches for motion of dispersed particles, droplets and bubbles", *Progress in Energy and Combustion Science*, Vol. 26, pp. 161-223, 2000.

[16] Fuchs, N.A., "Evaporation and droplet growth in gaseous media", *London: Pergamon Press*, 1959.

[17] Godsave, G.A.E., "Studies of the Combustion of Drops in a Fuel Spray-the Burning of Single Drops of Fuel", *Fourth Symposium (International) on the Combustion, Williams and Wilkins, Baltimore*, pp. 818-830, 1953.

[18] Guo, Y.C., Chan, C.K., and Lau, K.S., "A pure Eulerian model for simulating dilute spray combustion", *Fuel*, Vol. 81, pp. 2131-2144, 2002.

[19] Hubbard, G.L., Denny, V. E. and Mills, A.F., *Int. J. Heat Mass Transfer*, Vol. 16, pp. 1003-1008, 1973.

[20] Kolaitis, D.I., Founti, M. A., "A comparative study of numerical models for Eulerian-Lagrangian simulations of turbulent evaporating sprays", *International Journal of Heat and Fluid Flow*, Vol. 27, pp. 424-435, 2006.

[21] Kolev, N.I., "Multiphase flow dynamics", *Springer-Verlag*, Vol. 2, 2005.

[22] Ishii, M. and Hibiki, T., "Thermo-Fluid Dynamics of Two-Phase Flow", *Springer Science+Business Media, Inc.*, 1990.

[23] Lefebvre, A.H., "Atomization and sprays", *Taylor and Francis*, 1989.

[24] Miller, R.S., Harstad, K. and Bellan, J., "Evaluation of equilibrium and non-equilibrium evaporation models for many-droplet gas-liquid flow simulations", *International Journal of Multiphase Flow*, Vol. 24, pp. 1025-1055, 1998.

[25] Mongia, H.C. and Mostafa, A.A., "On the modeling of turbulent evaporating sprays: Eulerian versus Lagrangian approach", *Int. J. Heat Mass Transfer*, Vol. 30, pp. 2583-2593, 1987.

[26] Patankar S.V., "Numerical Heat Transfer and Fluid Flow", *Taylor and Francis*, 2004.

[27] Perry, R H., Green, D.W., "Perry's chemical engineers' handbook", *Mc Graw Hill Publications*, 1997.

[28] Rhie C.M. and Chow W.L., "Numerical Study of the Turbulent Flow Past an Airfoil with Trailing Edge Separation", *AIAA Journal*, Vol. 21, No. 11, pp. 1525-1532, 1983.

[29] Ranz, W.E., and Marshall, W. R., "Evaporation from Drops", *Chem. Eng. Prog.*, Vol. 48, Part I, pp. 141-146, Part II, pp. 173-180, 1952.

[30] Reid, R.C., Prausnitz, J.M. and Poling, B.E., "The properties of gases and liquids", *McGraw-Hill International Editions*, 1988.

[31] Hayder Salman, Marios Soteriou, "Lagrangian simulation of Evaporating Droplet sprays", *Physics of Fluids*, Vol.16, No.12, 4601-4621, 2004.

[32] Sazhin, S., Martynov, S., Shishkova, I., Cruva, C., Karimi, K., Gorokhovski, M., Sazhina E., Heikal, M., "Modelling of Droplet heating, Evaporation and Break-up: Recent Developments", *International Journal of Multiphase*, 2006.

[33] Shashwat Swami Jaiswal, "Numerical Simulation of Dilute Gas-Droplet flows"', Thesis for the Degree of Master of Technology, *Department of Mechanical Engineering*, Indian Institute of Technology Kanpur, 2008.

[34] Sirignano, W.A., "Fluid dynamics and Transport of Droplets and Sprays", *Cambridge University Press*, 1999.

[35] Spalding, D.B., "The combusiton of liquid fuels", *Fourth Symposium (International) on the Combustion, Williams and Wilkins, Baltimore*, pp. 847-864, 1953.